National Défense
Defence nationale

INVESTIGATION OF A MODULAR ANTENNA ARRAY CONFIGURATION AND A FEEDING TECHNIQUE FOR BRICK ARCHITECTURE

by

J. Paul J. Garant, Gilbert A. Morin,
Yahia M.M. Antar and David J. Roscoe

DEFENCE RESEARCH ESTABLISHMENT OTTAWA
REPORT NO. 1315

Canada

September 1997
Ottawa

National Défense
Defence nationale

INVESTIGATION OF A MODULAR ANTENNA ARRAY CONFIGURATION AND A FEEDING TECHNIQUE FOR BRICK ARCHITECTURE

by

J. Paul J. Garant
Department of National Defence
and
Gilbert A. Morin
Milsatcom Group
Space System & Technology Section
and
Yahia M.M. Antar
Royal Military College
and
David J. Roscoe
Communications Research Center

DEFENCE RESEARCH ESTABLISHMENT OTTAWA
REPORT NO. 1315

PROJECT
05CA12

September 1997
Ottawa

ABSTRACT

The satellite communications industry, following the trends seen in personal communications systems, is pursuing the development of smaller and more capable communication terminals. Several antenna technologies and architectures have been studied for a fixed-beam portable communications terminal operating at high frequencies, e.g. 20GHz (receive) and 30GHz (transmit), and capable of providing multiple data links (data, voice, video). However, additional work is required to develop a modular "brick" type of architecture for this application.

This report investigates two aspects of the problem: a modular antenna array configuration, and a suitable feeding scheme involving perpendicular interconnection that is essential to the design of the brick architecture.

An antenna array patterns program was developed within the Matlab environment. This versatile tool can be used to predict planar array radiation patterns for design and general illustration purposes. The program can evaluate, display and analyze two- and three-dimensional radiation patterns, and it can easily be modified to suit specific user requirements. An array configuration suitable for fixed-beam portable satellite applications at 30GHz was developed using this program.

To acquire experience with the design of microstrip patch antennas, and to validate the simulation software that would be used throughout this report, a critical coupling analysis was then conducted for conventional aperture-fed microstrip patch antennas. Simulation results were analyzed to determine the behavior of various parameters for critically coupled antennas, and charts providing a helpful guide for the design of microstrip patch antennas were produced.

The development of the perpendicular interconnection was then initiated with the simulation, fabrication and successful testing of a perpendicular substrate microstrip line-to-line coupler using the proximity feeding technique. A microstrip patch antenna fed from a perpendicular substrate was then designed to operate in the 2GHz range, with excellent results. Following this, a 30GHz perpendicularly fed microstrip patch antenna was developed, generating promising results.

RÉSUMÉ

L'industrie des communications par satellite, suivant la tendance observée dans les systèmes de communications personnelles, est à la recherche de terminaux de plus en plus petits et performants. Plusieurs technologies d'antennes et un grand nombre d'architectures ont été étudiés pour fabriquer des terminaux de communications portatifs à faisceaux fixes pour des fréquences élevées (20 GHz en réception et 30 GHz en transmission) et capable de fournir plusieurs liaisons de donnés (voix, vidéo, données). Cependant, beaucoup de travail reste à faire afin de développer un type d'architecture modulaire en "brique" pour ce genre d'applications.

Ce rapport étudie deux aspects de ce problème: une configuration modulaire du réseau d'antennes et une méthode d'alimentation des éléments d'antennes appropriée à une architecture en brique.

Un logiciel pour étudier les patrons d'antennes réseaux à commande de phase a été dévelopé en utilisant, comme outil, l'environnement de Matlab. Cet outil versatile sert à prédire les diagrammes de rayonnement d'antennes réseaux aussi bien pour la conception que pour des besoins d'illustration. Ce logiciel peut analyser et présenter visuellement des diagrammes d'antennes en 2 et 3 dimensions. Il peut aussi être modifié facilement pour satisfaire les besoins de l'utilisateur. Plusieurs configurations d'antennes réseaux à 30 GHz ont été simulées avec ce logiciel.

Pour acquérir de l'expérience avec la conception d'antennes microrubans et pour valider le logiciel qui sera utilisé dans ce rapport, une analyse de couplage critique a été réalisée avec une antenne microruban à couplage par fente standard. Les résultats de la simulation ont été analysés pour déterminer les effets de différents paramètres sur la performance d'antennes couplées critiquement. Des graphiques ont aussi été créés pour servir de guide à la conception d'antennes microruban.

Le dévelopment d'une interconnexion perpendiculaire a alors été étudié. Un coupleur à fente entre deux lignes microrubans a été simulé, fabriqué, et testé avec succès. Une antenne microruban à plaque alimentée à partir d'un substrat perpendiculaire a ensuite été conçue à 2 GHz avec succès. Enfin, une antenne similaire a été developpée à 30 GHz donnant des résultats prometteurs.

EXECUTIVE SUMMARY

The satellite communications industry is forever pursuing the development of smaller, cheaper, and more capable transmit and receive equipment. In order to increase the mobility and popularity of higher capacity satellite communication terminals, which can be used from virtually anywhere on the planet, all portable system components must be reduced as much as possible in size and weight. Several antenna technologies and architectures have been studied for a fixed-beam portable communications terminal operating at 20GHz (receive) and 30GHz (transmit), and capable of providing multiple data links (data, voice, video). The architectures range from arrays of printed dipoles to deployable reflector systems. The array approach is advantageous because low to medium power amplifiers can be distributed and integrated within the array to yield more efficient antenna structures, when compared to antennas using a single power amplifier. In addition, an integrated antenna array can be low profile, compact, and less obtrusive than a deployable reflector. The ideal array architecture would be made of modular active devices that could easily be removed for repair or replacement when required.

The Array Patterns Program (APP) is a versatile tool that can be used to predict planar array radiation patterns for design and illustration purposes. It inputs calculated or measured radiation pattern cuts from a text file as radiating element data. Two- and three-dimensional radiation patterns can be evaluated, displayed and analyzed in rectangular or polar/spherical format. Being well documented and written in a widely known programming language, the program can easily be upgraded or modified to suit specific user requirements.

An array configuration suitable for fixed-beam portable communication applications at 30GHz was developed using APP. Its small dimension (only 16cm in diameter) makes it ideal for integration in a briefcase size unit. 128 quad electromagnetically coupled (EMC) patch antenna elements arranged in 32 identical linear modules make-up the array.

A critical coupling analysis for aperture-fed microstrip patch antennas where the feedline and patch were on parallel substrates was then conducted. For open-circuited stub lengths varying between 6% and 50% of the feed line's guide wavelength (λ_g) the aperture length was adjusted until critical coupling was achieved. Simulation results were then analyzed to determine various characteristics (impedance bandwidth, frequency variations, directive gain, front-to-back ratio and relative cross-polarization) of the critically coupled antennas. The resulting charts provided a helpful guide for the design of perpendicular substrates microstrip patch antennas at 2GHz and 30GHz.

A microstrip line-to-line coupler, with the two transmission lines on perpendicular substrates, was successfully built and tested to verify the proximity feeding technique. A microstrip patch antenna fed from a perpendicular substrate was then designed to operate in the 2GHz range, and excellent results were achieved. Another perpendicularly fed microstrip patch antenna was designed to operate in the 30GHz range, effectively demonstrating the feasibility of implementing the perpendicular feeding method at higher frequencies.

TABLE OF CONTENTS

LIST OF FIGURES

LIST OF TABLES

CHAPTER 1

INTRODUCTION

1.1 BACKGROUND

The satellite communications industry is forever pursuing the development of smaller, cheaper, and more capable transmit and receive equipment. This follows the trends seen in the personal communications field, where pocketsize cellular phones and pagers enable the establishment of voice and low-speed data connections from/to almost anywhere in urban areas and along major highways. In order to increase the mobility and popularity of higher capacity satellite communication terminals, which can be used from virtually anywhere on the planet, all portable system components must be reduced as much as possible in size and weight.

Several antenna technologies and architectures have been studied for a fixed-beam portable communications terminal operating at 20GHz (receive) and 30GHz (transmit), and capable of providing multiple data links (data, voice, video)[1, 2]. The architectures range from arrays of printed dipoles to deployable reflector systems. The array approach is advantageous because low to medium power amplifiers can be distributed and integrated within the array to yield more efficient antenna structures, when compared to antennas using a single power amplifier. In addition, an integrated antenna array can be low profile, compact, and less obtrusive than a deployable reflector.

Because its overall array architecture is well suited for the portability requirement of the terminal, microstrip has been the preferred antenna technology. However, to minimize the effects of the losses within the microstrip feed network at EHF, and to improve the overall efficiency, medium gain antenna elements (10-15dB) must be used in the array architecture. A smaller number of antenna elements then have to be fed as compared to an array using regular microstrip patches, and amplifiers can be distributed throughout the array.

The ideal array architecture would be made of modular active devices that could easily be removed for repair or replacement when required. Using aperture coupling as the feed mechanism for the antenna elements is advantageous for various reasons; less manual labor is required to assemble the array than for probe feeding, it makes device integration easier, and it provides for separation of the feed circuits and radiating elements. The subject of antenna array architecture has been discussed extensively in

recent literature[4, 5, 6, 7, 8, 9]. Section 1.4 provides a description of the two prevailing types: "brick" and "tile".

The Communications Research Center (CRC) in Ottawa has recently developed a tile architecture that addresses most of these issues. The 30GHz transmit array architecture was designed using a cavity type microstrip antenna element, described in section 1.3.1. The array is made of 64 cavity radiators with 16 integrated power amplifiers. The radiators are disposed on 4 rings of radii of 2, 4.5, 7 and 13cm, containing 4, 8, 16 and 36 elements respectively (Figure 1.1). The array is expected to generate a directivity of approximately 36dB with sidelobe levels smaller than –15dB from the beam peak.

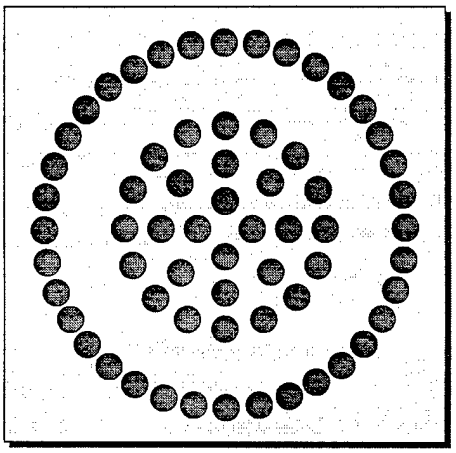

Figure 1.1

CRC 64 Elements Array Configuration

An inherent problem with the construction of this array is that, being made in a single block, it is more difficult to troubleshoot and/or repair than modular constructs where each module can be verified individually. Arrays built along the brick architecture model are usually more amenable to modular construction than their tile counterparts, and could provide a better alternative for the portable satellite communication terminal application.

One of the most difficult engineering challenges of microwave antenna array design is the interconnection and integration of all the required components (feed network, electronic devices, radiating elements, etc...). In the case of brick architectures, efficient interconnections between planar radiating elements (such as microstrip patch antennas) and the remaining system/module components are particularly difficult to achieve. Most of the difficulty is caused by the fact that the radiating element and feed substrates are perpendicular to each other.

1.2 ARRAY CONFIGURATION CONSIDERATIONS

Antenna arrays are used in cases where the system requirements cannot be met by a single radiating element. Radiating elements with low gain (wide beamwidth) can be arranged into arrays in a manner such that the array's performance characteristics meet system requirements. Therefore, in the process of designing a brick architecture that can be modularized the first step is to determine if a suitable array configuration can be developed. This is a crucial step since the shape of the modules, the number of radiating elements fed from each module and the feed network design are closely related to the antenna array configuration.

The first factor that must be considered in the development of an antenna array is the frequency band over which it will operate. In this case the requirement was set to 29.0-30.0 GHz, in the Ka-band. Another key factor is the sidelobe levels, which for this application must be maintained below –15dB. As for the grating lobes, they must be maintained at, or below, the sidelobe level. Normally sidelobe levels can be reduced by tapering the current distribution in the array elements, making the excitation amplitude of the elements in the center of the array at a higher level than for the elements towards the edge of the array. However, in this application the excitation is uniform for all elements in order to reduce the complexity of the problem, both for array configuration and modular design considerations. Because this is a fixed-beam application, the phase of the excitation signal will also be maintained uniform for all radiating elements.

For most mobile personal communication applications the system components must be small enough to fit in a briefcase, therefore the planar array has to be confined to an area of approximately 30x30cm. Its depth is also limited by the size of the carrying case. The Effective Isotropic Radiated Power (EIRP) is expressed by the product of the transmitter output power times the gain of the transmit antenna. In this case, the EIRP of the system is expected to be in the 40-42dBW range in the center of the main radiation beam. To achieve this goal medium power amplifiers will have to be integrated within the array architecture.

It would also be desirable to have the total number of modules making-up the array as a power of *2* (2^n where n is an integer), as this can simplify the design of the array's feed network.

1.3 ANTENNA ELEMENTS

Various types of antenna elements can be used in the design of microwave antenna arrays. The selection of which radiating antenna element should be used for an array depends on the requirements of the system being considered. As stated in section 1.1, medium gain elements (10-15dB) are preferred for this application. No extensive

literature research was conducted to determine all radiating elements that could enter this category. However, two medium gain elements were selected for use in the array configuration study portion of this report: cavity type and quad EMC patch. The following sub-sections will briefly describe these, as well as the basic microstrip patch antenna used in the aperture-fed perpendicular substrates patch antenna development.

1.3.1 MICROSTRIP PATCH ANTENNAS

The basic microstrip patch antenna is made of a thin sheet of metal (the radiating patch) separated from a ground plane by a dielectric substrate, as in Figure 1.2. The radiating element may be a simple resonant patch (rectangular and circular are the most common shapes), a resonant dipole, or an array of patches or dipoles. A variety of methods can be used to excite the radiating elements, including direct microstrip feed, gap feed, probe feeding, suspended line electromagnetically coupled (EMC) feeding and aperture coupling [3].

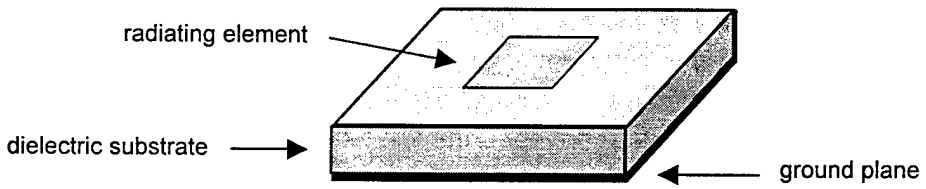

Figure 1.2

Basic Microstrip Antenna

Because they are lightweight and conformable, microstrip patch antennas have been used extensively in aircraft, missile, rocket and satellite applications. Some of their other advantages include low cost, variety of design and ease of integration with other system components. Unfortunately narrow bandwidth performance and conductor losses that increase with frequency are disadvantages inherent of this type of antenna.

1.3.2 CAVITY TYPE ANTENNA ELEMENTS

This is the type of radiating element used in the 64-element array described in section 1.1. The cavity [2] (Figure 1.3) is formed from a thick metallic ground plane, which can be used for fastening modular RF components. An aperture-coupled microstrip patch element is used to feed the cavity. The patch is fed from the feed line through a thin ground plane within the cavity. The circumference of the cavity outlines the effective aperture area of this antenna. The achievable gain is a function of the cavity diameter, typically 13-15 dBi for cavity diameters between 1.5 and $2.0\lambda_0$. A radome is included in the element design to produce a uniform distribution across the cavity aperture, and to function as a matching layer to free space.

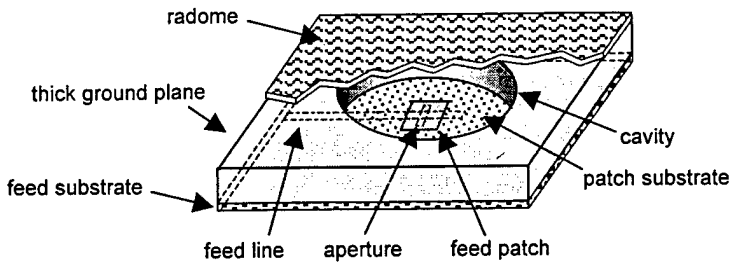

Figure 1.3

Cavity Type Antenna Element

For a 30GHz application the cavity element is approximately 0.5cm high, with a diameter of 2.0cm. Because it provides a thick metallic ground plane that can be used for fastening modular RF components, this antenna element has the advantage of being amenable to device integration.

1.3.3 QUAD EMC PATCH ANTENNA ELEMENTS

The Quad Electromagnetically Coupled (EMC) [2] patch is a multilayer microstrip patch configuration developed to reduce the number of feed points required within a microstrip patch antenna array, a 4:1 reduction has been achieved with this antenna. The element, shown in Figure 1.4, is a three-layer structure where energy is coupled through an aperture from the feed line to the single patch on the first layer of the element. The energy from that patch is then distributed to the four patches on the top layer of the antenna. The quad EMC patch has achieved a gain of approximately 10.75dB.

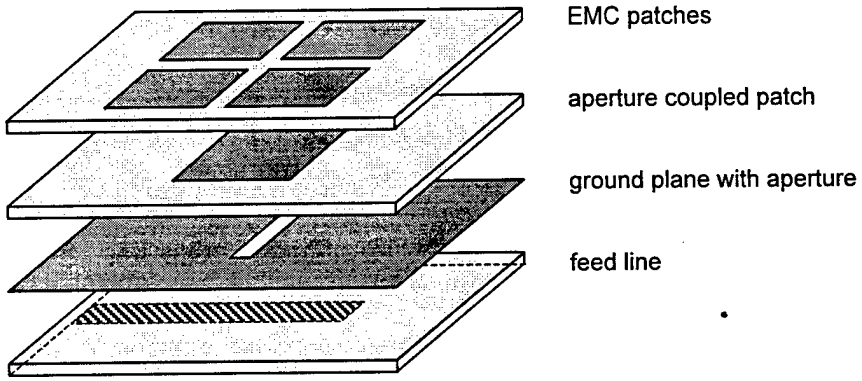

Figure 1.4

Quad EMC Patch Antenna Element

1.4 TILE vs BRICK ARCHITECTURE

Once a configuration amenable to modularization has been found, the array architecture can be developed. Two architectural approaches have been the focus of much attention in recent publications: "tile" and "brick"[4, 5, 6, 7, 8, 9]. The definition and name given to each approach varies from one author to the other, but the following descriptions briefly summarize the general idea. In the tile approach the radiating elements, active devices and signal distribution networks are all mounted on parallel planes (Figure 1.5). For the brick approach the structure supporting the active devices and signal distribution networks is mounted perpendicularly to the array plane containing the antenna elements (Figure 1.6).

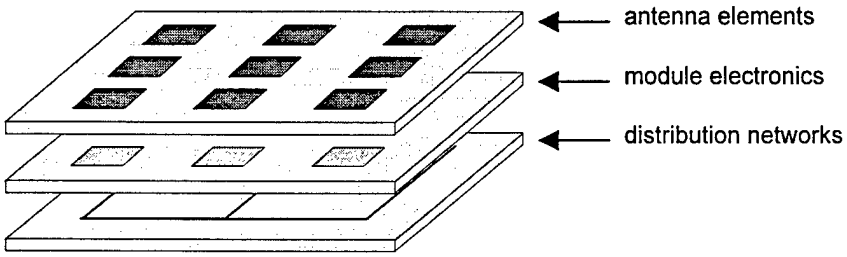

Figure 1.5
Tile Architecture

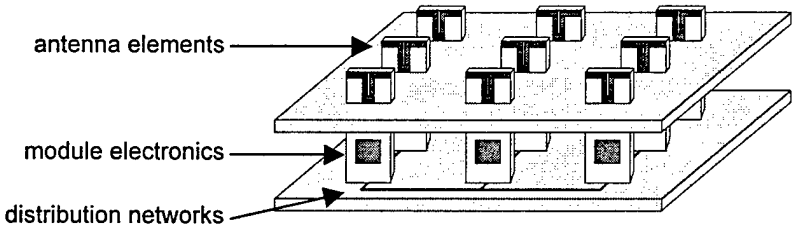

Figure 1.6
Brick Architecture

Each approach has advantages and disadvantages which must be weighted out against the requirements set for the system being designed. The major differences between the two types of architectures center around real-estate and interconnection issues. Brick assemblies provide more real-estate for component layout and heat removal; while in the tile approach real-estate is very limited and cannot easily be increased, but tile arrays are generally more compact.

Both types present interconnection problems. For the tile architecture connections between layers, and between the modules and the signal distribution back plane, can be difficult. As well, in the brick approach efficient perpendicular interconnections at high frequencies represent a significant design challenge.

1.5 OBJECTIVES

For the portable communication transmit array application, as for any other application, the development of a 30GHz brick architecture amenable to modular construction is a very complex undertaking. This is mainly due to the interconnection problems encountered at these frequencies, and feeding the radiating elements from a perpendicular substrate raises the difficulty level even more. Therefore, the scope of this report could not cover the entire problem of designing a brick architecture and had to be limited to the study of certain key aspects of the problem. The next sub-sections explain the three major objectives that were set for this report.

1.5.1 ARRAY CONFIGURATION

The first objective is to develop an antenna array configuration meeting the frequency, sidelobe levels, and directivity parameters required for a portable satellite communication transmit antenna system. Various array configurations will be analyzed, with the cavity and quad EMC patch radiating elements. Computer simulations will be used to evaluate the key parameters that will be required to compare the various configurations. The developed configuration would also have to be amenable to modularization of the antenna system.

1.5.2 DESIGN PARAMETERS OF MICROSTRIP PATCH ANTENNAS

The next objective was to study the effects of varying some microstrip patch antenna design parameters while acquiring experience in the use of the software package that would serve for the simulation of perpendicularly fed microstrip patch antennas. The results of this study can then be used in the design phase of the report. This study will also be used as an evaluation of the software.

1.5.3 PERPENDICULAR FEEDING OF MICROSTRIP PATCH ANTENNAS

The final objective of this report is to design an efficient method of feeding microstrip patch antennas from a perpendicular substrate. Because the basic microstrip patch is easier to design than the cavity type or quad EMC patch elements, it will be used as the radiating element for this portion of the report. This will therefore simplify the analysis of the perpendicular feed mechanism. The development of a perpendicular feed arrangement is necessary for the design of a viable 30GHz brick architecture.

1.6 OUTLINE

The following chapters have been organized along the chronological order in which this work evolved. This section will provide a brief outline of their contents, and the reasons that motivated some of the decisions that were taken along the way.

Because of its circular arrangement, the array developed by CRC (Figure 1.1) could not be modularized. Chapter 2 is a study of possible array configurations that could be modularized. The cavity and quad EMC patch radiating elements were used for this study. To estimate array radiation patterns characteristics the Antenna Radiation Patterns Software (ARPS)[10] was used initially. Using this package became increasingly difficult because of some of its limitations. To resolve this problem, effort was devoted to developing the Array Patterns Program (APP). This Matlab based application permits three-dimensional (3-D) array radiation patterns to be evaluated, displayed and analyzed. APP greatly simplified the completion of the array configuration study. The program is described in detail at Appendix A.

In the next phase (Chapter 3) conventional aperture-fed microstrip patch antennas, with the feed line substrate in a plane parallel to that of the patch, were studied prior to tackling the perpendicular-fed patches. Through computer simulations, some of the experiments from a paper by Sullivan and Schaubert[11] were replicated. The paper contained parameter studies on aperture-fed microstrip patch antennas. This provided some useful experience on the tuning of such antennas, and it helped validate Micro-Stripes simulation results. A parameter study for critical coupling of microstrip patches at various feed line stub lengths for two rectangular patches, at 2GHz and 30 GHz, was then conducted. From this study some valuable tables were compiled.

Chapter 4 covers the design of a 2GHz microstrip line-to-line coupling device where both microstrip lines were on perpendicular substrates. From the literature surveyed, the most promising microstrip patch antenna feed mechanism appeared to be the aperture coupled microstrip antenna with a proximity feed described by Pozar and Jackson[12]. Because this communication contained very little detail on the exact geometry of the perpendicular feed, and to acquire additional experience and confidence with the Micro-Stripes 3-D electromagnetic simulation package, a line-to-line perpendicular coupler was designed, built and tested.

In Chapter 5 the experience gained through the previous chapters simulations and experiments was applied to the perpendicular feeding of microstrip patch antennas, again at 2GHz and 30GHz. The antennas were optimized through simulations, then built and tested. Simulated and measured S-parameters were analyzed to determine the resonant frequency, input impedance and impedance bandwidth of the device. E-plane and H-plane (co-polarized and cross-polarized) radiation patterns were then studied to evaluate the maximum forward cross-polarization, directive co-polarized gain and front-to-back ratio.

Gain measurements were also done, and used to evaluate the efficiency of the perpendicular substrate feeding mechanism.

Chapter 6 is a summary of the work completed. Some possible directions for future research are also included.

CHAPTER 2

ARRAY CONFIGURATION STUDY

2.1 BACKGROUND

This chapter will discuss the development of an antenna array configuration that meets the frequency, sidelobe levels, and directivity parameters required for a portable satellite communication transmit antenna system. Computer simulations of various array configurations will be analyzed to evaluate the key parameters. From this analysis, the most promising array configuration will be selected.

2.2 THEORY

2.2.1 RADIATION PATTERNS

Antenna arrays are groups of similar antennas arranged in various configurations (linear, planar, conformal...) with amplitude and phase distributions designed to produce the desired radiation characteristics. The fields generated by an array are the vector summation of all fields produced by the individual radiating elements. The radiating pattern of an array made of identical elements is the product of the radiating pattern of the individual radiating elements (element factor) by the array factor, which depends on the array geometry and the relative amplitude and phase excitation of the individual elements.

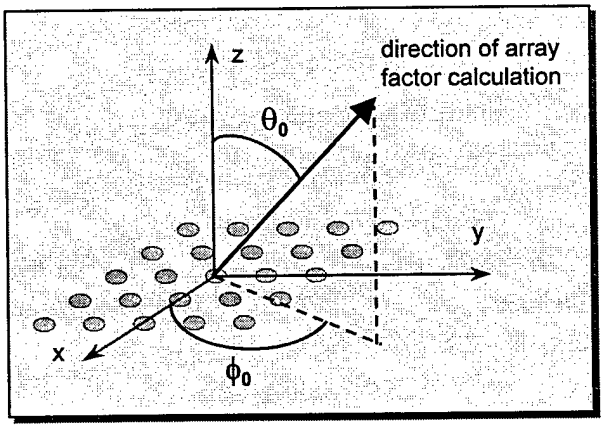

Figure 2.1

Array Factor Geometry

The array factor of a planar array in the direction specified by the (θ_O, ϕ_O) pair as per Figure 2.1, is given by the following equation:

$$array\ factor = \sum_{i=1}^{N} V_i \cdot e^{j\varphi_i}$$

where:

N is the total number of elements
V_i is the voltage amplitude of the element
$\varphi_i = kx_i \sin(\theta_o)\cos(\phi_o) + ky_i \sin(\theta_o)\sin(\phi_o) + \beta_i$
$k = 2\pi/\lambda$ is the wavenumber
(x_i, y_i) is the position of the element in the $z = 0$ plane
β_i is the relative phase of the element

2.2.2 GAIN PARAMETERS[13]

The directive gain (G_d), also called directivity (D), of an antenna system in the (θ_O, ϕ_O) direction is defined as:

$$G_d = \frac{4\pi P(\theta_0, \phi_0)}{\int_0^{2\pi}\int_0^{\pi} P(\theta,\phi)\sin\theta\, d\theta\, d\phi}$$

where $P(\theta,\phi)$ is the power pattern of the antenna.

When a direction is not specified, the maximum value of G_d is called the directive gain of the antenna. The power gain (G) of an antenna is in turn defined as

$$G = \eta_r G_d$$

where η_r is the radiation efficiency, the ratio of the power radiated from the antenna to the power accepted at its input terminal from the source (corresponds to the dissipation loss of the antenna).

The Equivalent Isotropically Radiated Power (EIRP) of an antenna array is then given by the product of its power gain (G_t) in a given direction by the power transmitted by the array from the power source (P_t):

$$EIRP = P_t G_t$$

2.3 RADIATION PATTERN ANALYSIS PROGRAM DEVELOPMENT

In order to estimate array radiation parameters for various configurations, a software package that could evaluate the radiation patterns for arbitrary planar array configurations had to be found. The Antenna Radiation Patterns Software (ARPS)[10] package, by Far Field, met this requirement.

However, using ARPS became increasingly difficult because it could only generate two-dimensional array pattern cuts, which made it laborious to determine the array's highest sidelobe and grating lobe levels. To resolve this problem considerable effort was spent on the development of a Matlab based application that would evaluate, display and analyze three-dimensional radiation patterns, and had no set limit on the number of elements making-up the array.

The Array Patterns Program (APP) provides an easy to use graphical interface, and its efficient handling of three-dimensional radiation patterns has greatly simplified the completion of the array configuration study. It also has the advantage of being easily modifiable because it is written in Matlab, one of the most powerful numeric computation and visualization software packages available, which is widely used throughout the academic and scientific communities. APP can also accept any number of user-defined element pattern cuts, which can make the estimation of array radiation patterns more precise. The application has great potential for design and educational applications. Appendix A to this report contains a detailed description and user's guide for APP.

2.4 ARRAY CONFIGURATION REQUIREMENTS

The aim of this study was to evaluate various antenna array configurations that met the general requirements for a portable satellite communication system. The required parameters detailed in section 1.2 of this report were therefore used for this analysis; they are listed in Table 2.1.

2.5 ELEMENT PATTERNS

The type of radiating element used in an array is of major importance when determining a suitable configuration. The cavity and quad EMC patch elements, described in section 1.3 of this document, were utilized for this configuration study. The following paragraphs provide some information on the radiation patterns used to simulate these radiating elements with the ARPS and APP programs.

Parameter	Stated Requirement
operating frequency	29-30GHz
sidelobe level	less than -15dB
area limitation	30 x 30cm
excitation:	
- phase	same for all elements (no beam steering)
- amplitude	same for all elements (no tapering)
polarization	linear
EIRP	40-42dBW
number of elements	2^n is preferable (n is an integer)

Table 2.1

Array Requirements

2.5.1 CAVITY ELEMENTS

The first element radiation pattern file used in this study was made from measurements, provided by CRC, of a cavity element with a diameter of 2.0cm. Figure 2.2 shows the E-plane and H-plane cuts, along with another pattern identified as $cos(\theta)^n$.

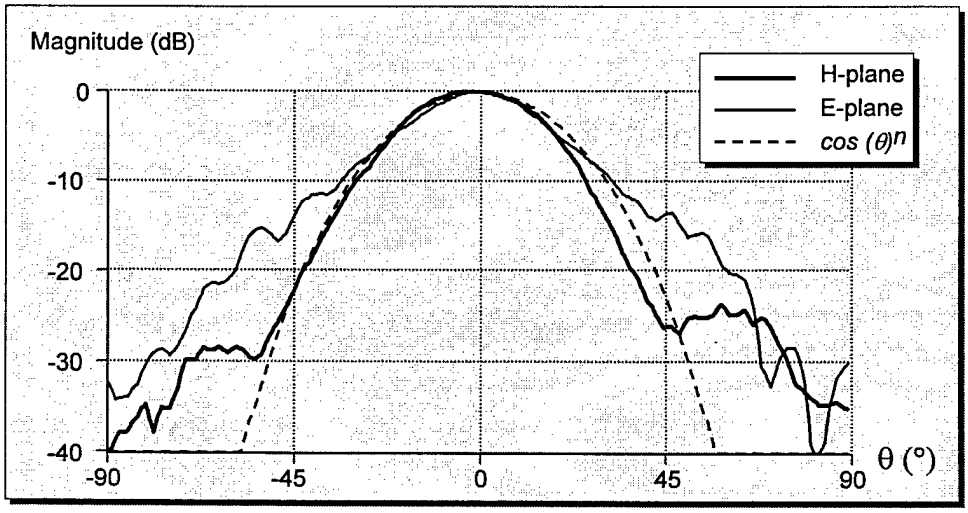

Figure 2.2

2.0cm Cavity Radiation Patterns

The $cos(\theta)^n$ pattern is an approximation used to simulate smaller diameter cavities for which measured data was not available, it is shown in Figure 2.2 for comparison purposes. Using a directivity (D) of 15dB for the 2.0cm cavity, the radiation pattern can be approximated over a sizeable portion of the main lobe by the following $cos(\theta)^n$ function[14]:

$$D = 10\log_{10}\left(2(n+1)\cos(\theta)^n\right).$$

Knowing that the pattern's maximum is located at $\theta = 0°$, and after some simple equation manipulations, we can find the value of n for which the gain at 0° ($cos(\theta)^n = 1$) will be 15dB:

$$n = \frac{10^{G/10}}{2} - 1 = \frac{10^{15/10}}{2} - 1 = 14.81.$$

Using this value of n, and removing the $2(n+1)$ part, we can then evaluate the normalized gain over the required θ range to produce the radiation pattern:

$$G_{normalized} = 10\ \log_{10}\left(\cos(\theta)^n\right).$$

2.5.2 QUAD EMC PATCH ELEMENTS

The patterns of Figure 2.3 were used in all array pattern simulations for the quad EMC patch element. The experimental data files were again provided by CRC.

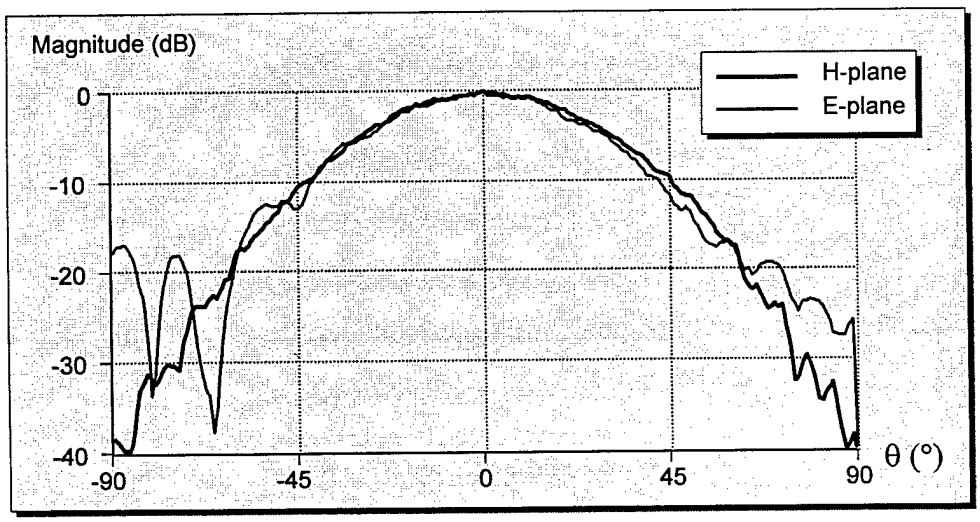

Figure 2.3

Quad EMC Patch Radiation Patterns

2.5.3 CAVITY vs QUAD EMC PATCH

Before getting into the details of the different configurations it is important to note that the cavity element was initially used in this study because of its higher gain characteristic. However, when the center-to-center element spacing is reduced to 15mm the maximum cavity diameter that can be fitted in the array is approximately 14mm, and quad EMC patches have a gain performance comparable to cavities of that size. Furthermore, when the element spacing is less than 15mm quad EMC patches have a better gain performance than suitable cavities.

2.6 ARRAY CONFIGURATION STUDY RESULTS

Because the array must be designed for linear polarization, the apertures feeding the radiating elements must all have the same orientation with regards to the array plane (*x*-*y* plane in Figure 2.1). This must be taken into consideration when searching for array configurations that can be divided into a number of identical sub-arrays, or modules. For this reason, only configurations consisting of modules that can be arranged so they all have the same shape and orientation should be considered. The three types of planar array configurations that were studied using the ARPS and APP software tools are shown in Figure 2.4.

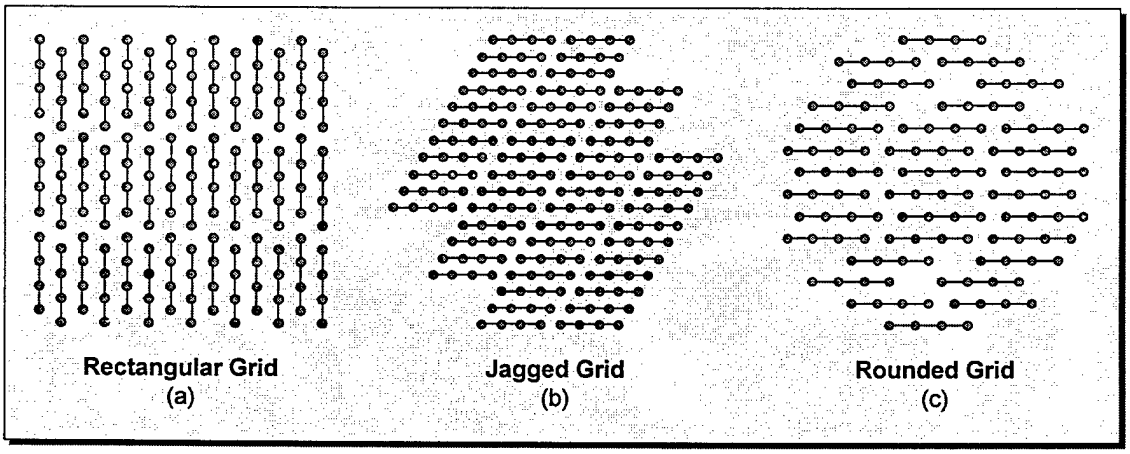

Figure 2.4

Array Configurations

2.6.1 RECTANGULAR GRIDS

Rectangular grids of the type shown in Figure 2.4 (a) provide one of the simplest array element configurations. Evaluated models had 195 elements arranged in a 13 by 15 element grid, this was the largest array that could be fitted within the 30cm x 30cm area.

Theoretical cavity element patterns ($cos(\theta)^n$) for cavity diameters ranging between 1.0cm and 2.0cm were used. The spacing between the cavities was also varied (between 1mm and 4mm), but in all cases the lowest sidelobe and grating lobe results were obtained for the smallest spacing (Figure 2.5 and Table 2.2 show the 1mm cavity spacing results).

The first sidelobe level is almost constant for all cavity diameters and the θ angle where its peak is located increases slightly as the cavity size is reduced. Grating lobe levels are above the sidelobes for all cavities larger than 1.3cm. Notice that the grating lobes increase in level, and get closer to the main lobe as the cavity size is increased. The center-to-center element spacing for the smallest cavity is at 1.1cm. This is close to the free-space wavelength at 30GHz, explaining the great reduction in grating lobe level.

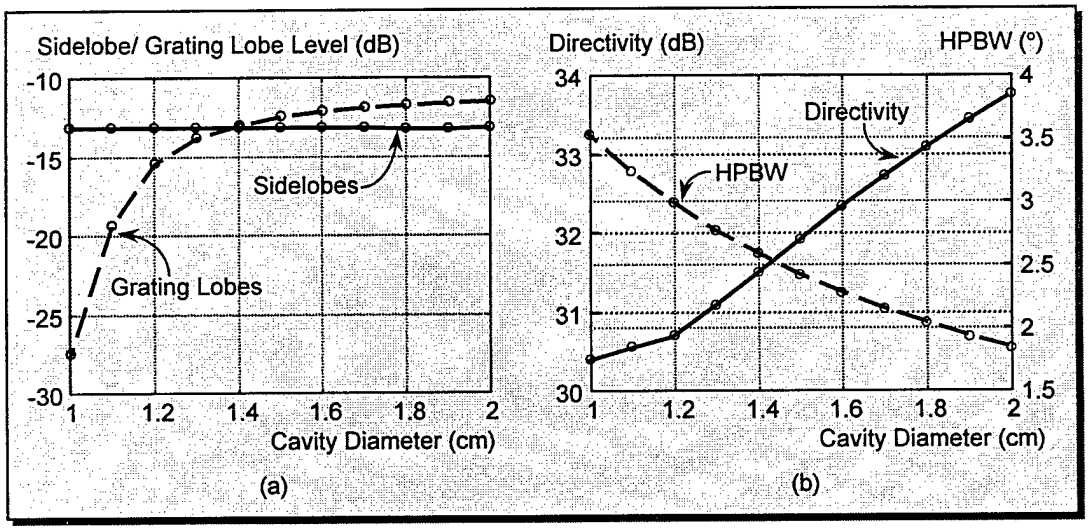

Figure 2.5

Rectangular Grid with Cavity Elements

Cavity Diameter (cm)	Sidelobe Level (dB)	@ θ (°)	Grating Lobe (dB)	@ θ (°)	Array Directivity (dB)	HPBW (°)
2.0	-13.23	3.000	-11.49	33.12	33.74	1.85
1.9	-13.24	3.125	-11.59	35.12	33.42	1.94
1.8	-13.23	3.375	-11.73	37.25	33.07	2.05
1.7	-13.22	3.500	-11.90	39.62	32.71	2.16
1.6	-13.22	3.750	-12.14	42.50	32.32	2.29
1.5	-13.23	3.889	-12.47	45.83	31.91	2.43
1.4	-13.22	4.167	-13.00	49.83	31.49	2.60
1.3	-13.21	4.500	-13.85	55.00	31.07	2.78
1.2	-13.21	4.861	-15.40	61.44	30.69	3.00
1.1	-13.22	5.333	-19.38	70.67	30.54	3.25
1.0	-13.20	5.750	-27.53	70.50	30.39	3.54

Table 2.2

Rectangular Grid with Cavity Elements

Figure 2.6 and Table 2.3 show the results obtained with quad EMC patches, with the first column representing the center-to-center element spacing. Overall the results are fairly similar to those obtained with the cavity elements, except for the grating lobe levels which are slightly better.

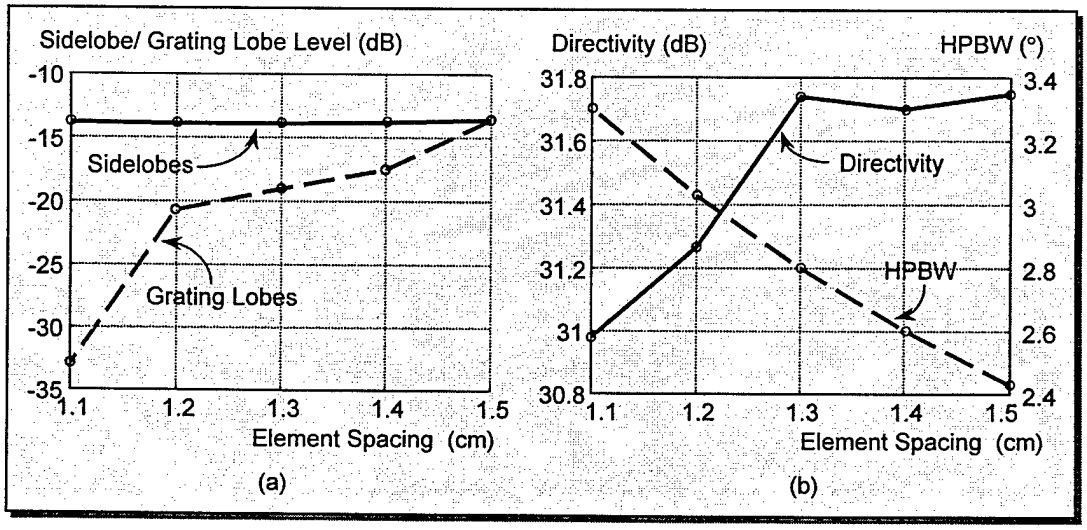

Figure 2.6

Rectangular Grid with Quad EMC Patches

Element Spacing (cm)	Sidelobe Level (dB)	@ θ (°)	Grating Lobe (dB)	@ θ (°)	Array Directivity (dB)	-3dB Main Lobe BW (°)
1.5	-13.59	4.250	-13.64	50.00	31.75	2.43
1.4	-13.75	4.500	-17.49	55.25	31.70	2.60
1.3	-13.86	4.750	-19.03	60.75	31.74	2.80
1.2	-13.85	5.250	-20.67	71.00	31.27	3.03
1.1	-13.81	5.750	-32.90	71.00	30.98	3.30

Table 2.3

Rectangular Grid with Quad EMC Patches

From the above results, it is clear that rectangular grids do not meet the stated sidelobe requirement, regardless of which radiating element is used.

2.6.2 JAGGED GRIDS

Figure 2.4 (b) shows the geometry of a jagged grid configuration made of 208 elements arranged in 52 modules of 4 elements each. Figure 2.7 and Table 2.4 show the analysis results with quad EMC patches used as radiating elements.

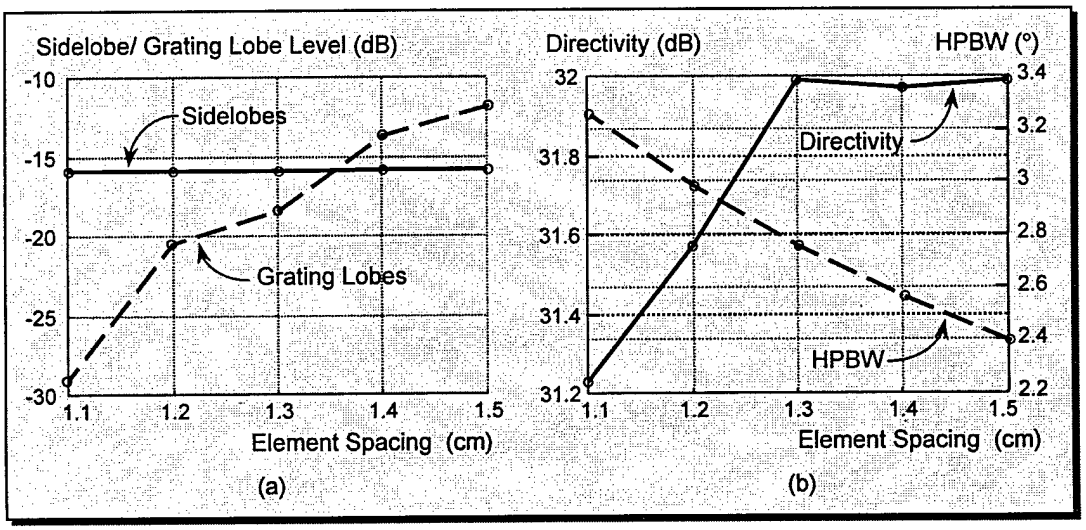

Figure 2.7

Jagged Grid with Quad EMC Patches

Element Spacing (cm)	Sidelobe Level (dB)	@ θ (°)	Grating Lobe (dB)	@ θ (°)	Array Directivity (dB)	HPBW (°)
1.5	-15.88	4.123	-11.86	50.00	31.99	2.39
1.4	-15.89	4.374	-13.69	55.00	31.97	2.56
1.3	-15.91	4.768	-18.40	61.06	31.99	2.75
1.2	-15.84	5.139	-20.47	74.00	31.57	2.98
1.1	-15.83	5.611	-29.03	89.19	31.23	3.25

Table 2.4

Jagged Grid with Quad EMC Patches

These results show that jagged grids performance is similar to that of the rectangular grids, except for the sidelobe levels that are below the –15dB requirement. Jagged grid configurations would therefore be suitable for this application.

2.6.3 ROUNDED GRIDS

Several variations of rounded grids were simulated with quad EMC patch elements, with the best results being obtained with the configuration shown at Figure 2.4 (c). This array is made of 32 modules of 4 elements each, arranged to fit within a

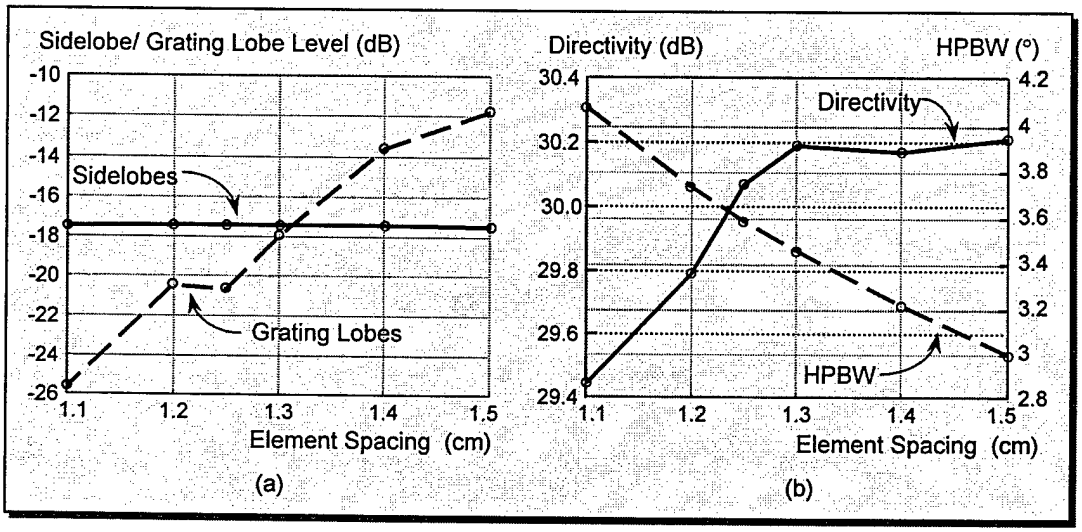

Figure 2.8

Rounded Grid with Quad EMC Patches

circularly shaped area. Results of Figure 2.8 Table 2.5 show better sidelobe performance than the previous configurations but the directivity is not quite as good due to the smaller number of elements, and the resulting smaller area occupied by the array. Rounded grid configurations would therefore be suitable for this portable application.

Element Spacing (cm)	Sidelobe Level (dB)	@ θ (°)	Grating Lobe (dB)	@ θ (°)	Array Directivity (dB)	HPBW (°)
1.5	-17.47	5.142	-11.82	50.00	30.21	2.99
1.4	-17.45	5.532	-13.64	54.89	30.17	3.21
1.3	-17.42	5.967	-18.00	61.03	30.19	3.45
1.25	-17.42	6.146	-20.66	67.33	30.07	3.58
1.2	-17.43	6.403	-20.47	74.00	29.79	3.73
1.1	-17.46	6.986	-25.65	89.00	29.44	4.07

Table 2.5

Rounded Grid with Quad EMC Patch

2.7 PREFERRED ARRAY CONFIGURATION

Of all the array configurations studied, the rounded grid with quad EMC patch elements is the preferred one. Figure 2.9 shows a detailed configuration layout with 1.25cm center-to-center element spacing.

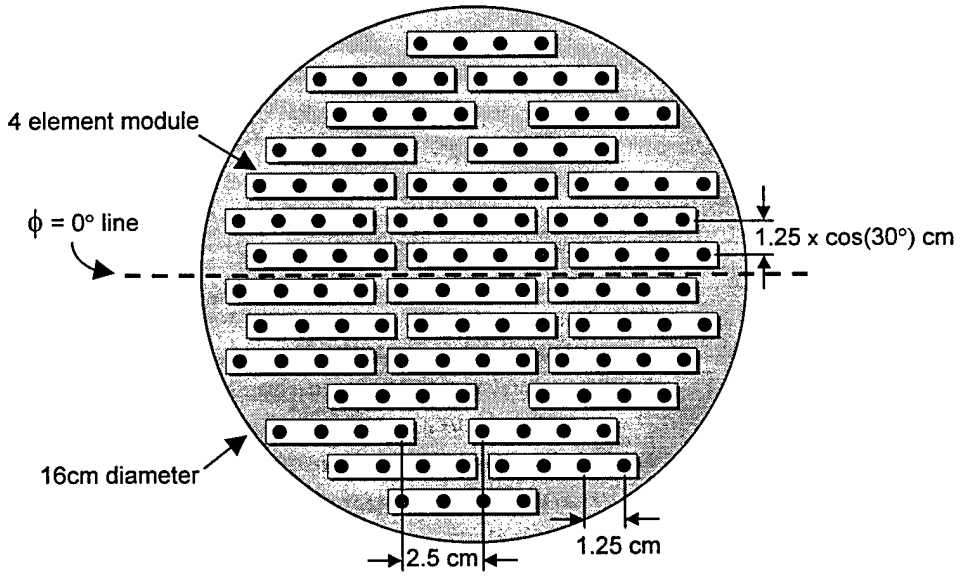

Figure 2.9

Preferred Array Configuration Layout

The sidelobes for this array are approximately 1.6dB lower than the next best configuration. The constant-ϕ radiation pattern cuts for the worst-case sidelobe (-17.42dB) and grating lobe (-20.66dB) levels are shown in Figure 2.10 (a) and (b), respectively. The full 3-dimensional rectangular representation of the array radiation pattern is displayed at Figure 2.11.

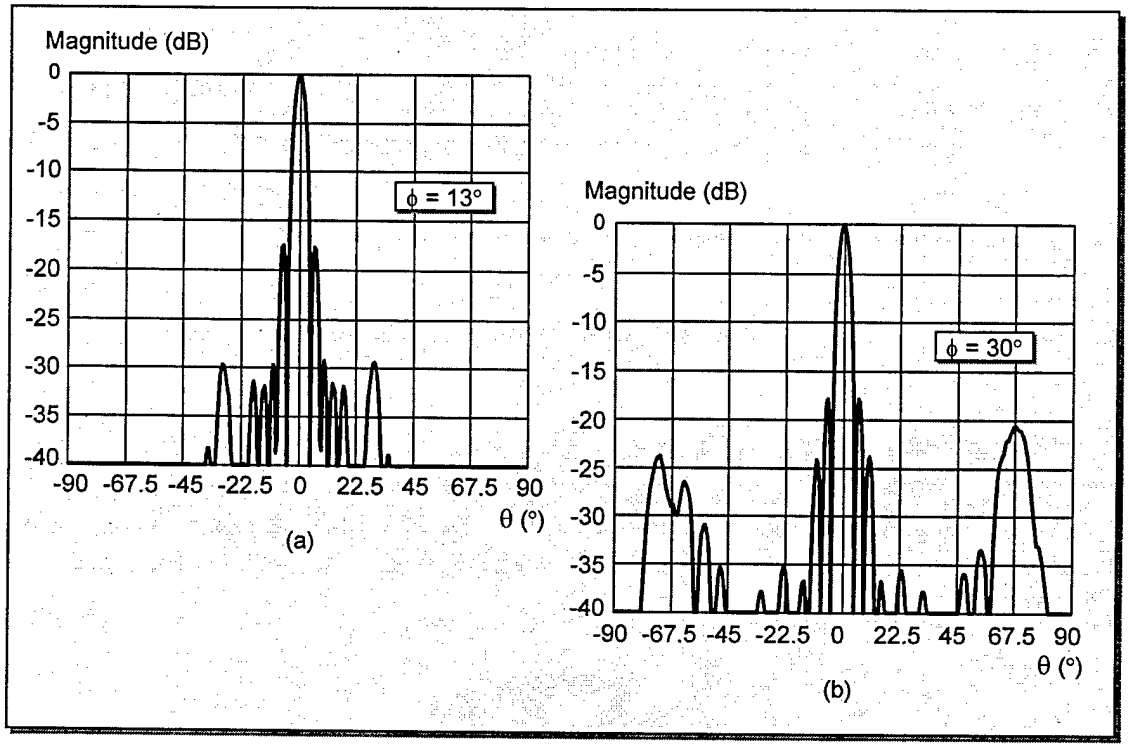

Figure 2.10

Preferred Configuration Constant-ϕ Array Pattern Cuts

Unfortunately, because fewer radiating elements are used, the directivity for this array geometry is slightly lower than that of other configurations. However, this can be compensated by an increase in transmitted power to achieve the required EIRP level. The smaller number of elements is another important consideration since it should make the array cheaper to fabricate and to repair/maintain, a desirable characteristic for any application. Also, the array fits inside a circle measuring only 16cm in diameter, which is another significant advantage for a portable application.

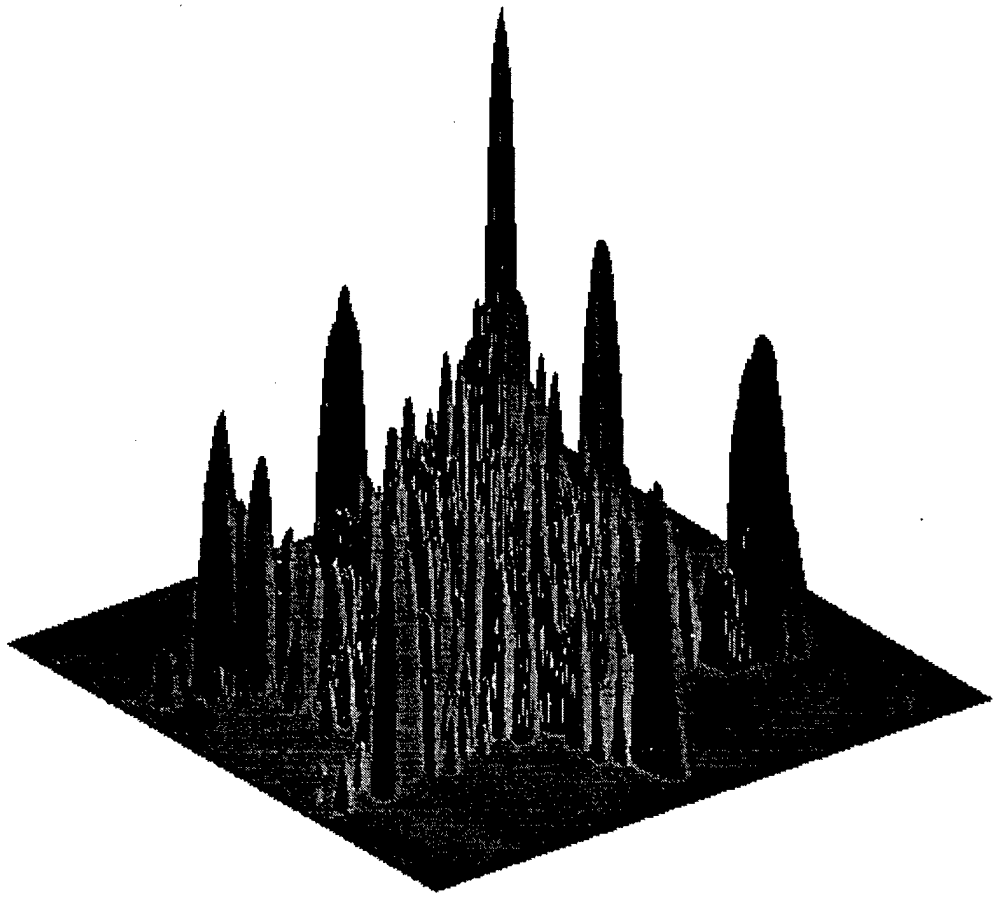

Figure 2.11

Preferred Configuration 3-Dimensional Array Radiation Pattern

2.8 CONCLUSION

In this chapter a 30GHz antenna array configuration meeting the general requirements for a portable satellite communication application was developed. One major advantage of this configuration is that it can easily be implemented with a modularized architecture, as shown in Figure 2.9. The remaining chapters of this report will look into the development of a microstrip patch antenna feed mechanism where the patch and feed line are on substrates that are perpendicular to each other. This type of feed mechanism is essential to the realization of a brick architecture for which this array configuration was developed.

CHAPTER 3

PARALLEL SUBSTRATES APERTURE-FED PATCH ANTENNAS

3.1 BACKGROUND

Now that a suitable array configuration has been developed the next step is to study aperture-fed microstrip patch antennas, while acquiring some experience with the software package used to simulate the antennas and other devices that will be investigated.

Throughout this chapter antennas of the type described in figure 3.1, with the microstrip radiating element and feedline printed on parallel substrates, will be studied. An excellent article written by P.L. Sullivan and D.H. Schaubert[11] in 1986 describes the effects that variations in some design parameters have on the input impedance of aperture-fed patch antennas. The parameters studied are stub length, aperture length, aperture location with regards to the patch, and dielectric constant and thickness of both substrates.

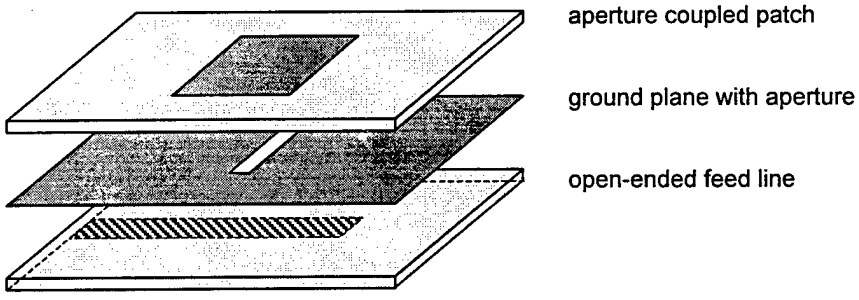

Figure 3. 1

Aperture-Fed Patch Antenna

3.2 MICRO-STRIPES 3-D ELECTROMAGNETIC SIMULATION AND ANALYSIS PACKAGE

An electromagnetic simulation and analysis software package was required to study aperture-fed microstrip patch antennas with parallel and perpendicular feed substrates. Developing such a tool is beyond the scope of this report. Several commercial packages are available that are advertised as capable of doing the required simulation and analysis work.

One such package, called Micro-Stripes, was available at the Royal Military College of Canada (initially version 2.3 for Unix, and later version 3.0 for Windows NT). It uses the Transmission-Line Matrix (TLM) technique in the time domain for the analysis of full three-dimensional structures and antennas. First, Micro-Stripes obtains the time-domain impulse response for a given structure, then it extracts high-resolution frequency-domain results and S-parameter data[15].

The following is a brief description of the Micro-Stripes analysis method:

- the workspace is divided into elemental cells modeled as the intersection of orthogonal, three-dimensional transmission lines;
- voltage pulses are absorbed, transmitted and scattered at each cell and the simulation propagates in time from arbitrary initial field/voltage conditions (all simulations within this report used an impulse voltage at the excitation port in the fundamental mode distribution (quasi-TEM) as the initial condition);
- the fields are stored for selected output points at each time step and post-processing is done to obtain fields, S-parameters, far-field radiation patterns and other required outputs; and
- FFT then provides frequency data points.

Some of the advantages gained by using TLM as opposed to other numerical methods are:

- *Memory*. The relationship between the number of cells in the workspace and the required computer memory is linear. Other methods, such as the finite-element method typically drive computer requirements to grow at the rate of N-cubed as N (the number of elemental volume cells) grows. Therefore, with the same amount of memory, Micro-Stripes can have more cells, a more faithful reproduction of the actual geometry, and provide simulation results closer to reality. For a fixed time step, analysis time increases linearly with problem complexity.

- *Unconditionally stable mathematics*. The TLM method is inherently stable, has no unstable matrices, and the use of increased spatial resolution will always converge to reality.

Overall Micro-Stripes is a very flexible package and, once the initial learning phase had been completed, it became fairly easy to use.

3.3 MICRO-STRIPES VALIDATION

Some of the models used in reference [11] were replicated with Micro-Stripes to evaluate its ability to simulate aperture-fed patch antennas. Specifically, the stub length and aperture length variation experiments were reproduced.

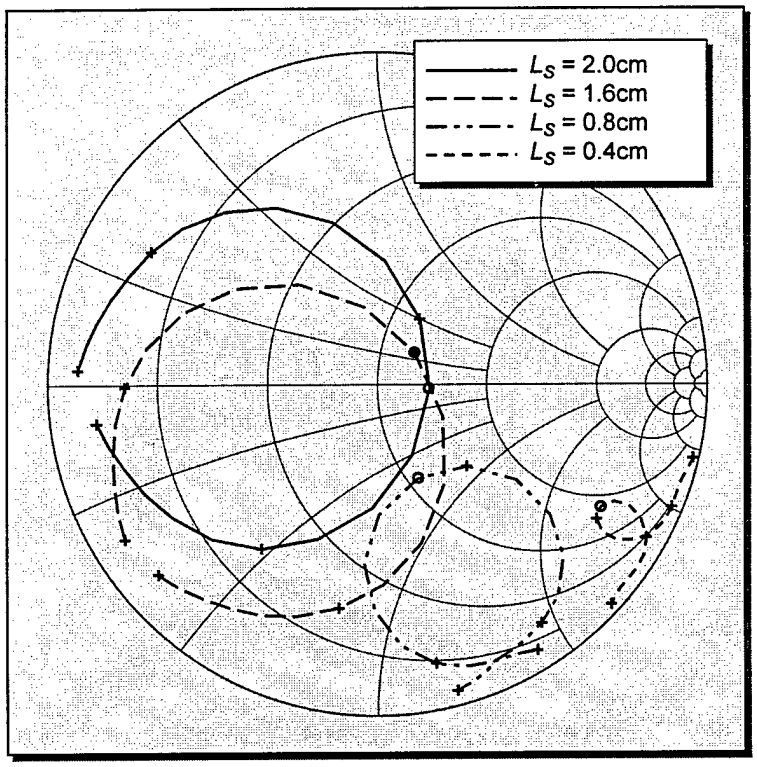

Figure 3. 2

Stub Length (L_S) Variation (2.05-2.25GHz)

Stub Length Variation. The length of the portion of the microstrip feedline that extends beyond the center of the aperture represents the feedline stub. Figure 3.2 displays the results obtained with Micro-Stripes simulations for the parameters given in figure 4 of [11], and using the same stub lengths (L_S). The Micro-Stripes values are very close to the reference's calculated and measured results, but lower in frequency by an average of

about 2.75%. The "+" markers indicate the data points with frequencies closest to 2.05, 2.10, 2.15, 2.20 and 2.25GHz, and the "O" markers indicate where $|S_{11}|$ minimum was attained. Figure 3.2 clearly indicates that the impedance loci of the antennas are rotating clockwise around the Smith chart as the stub is lengthened. It can also be noted that for a given frequency the points corresponding to the various stub lengths approximately follow a constant resistance contour, indicating that the aperture and antenna appear as a series load along an open circuited transmission line.

Aperture Length Variation. In figure 3.3 the input impedance is plotted as a function of the frequency for various aperture lengths using the parameters of [11]. Results demonstrate that the radius of the impedance circle decreases with the aperture length. Also, the center of the circle moves left toward the short circuit point as the aperture length is reduced, showing a decrease in the coupling between the feed line and the patch. The resonant frequency, although primarily determined by the patch dimension along the feed line, increases as the aperture length is decreased. Figure 3.3 results are similar to those of [11], and they are again lower in frequency (by an average 2.47%). Frequency points closest to 2.05, 2.10, 2.15, 2.20 and 2.25GHz are indicated by the "+" markers, the "O" markers indicating the data points where $|S_{11}|$ minimum was attained.

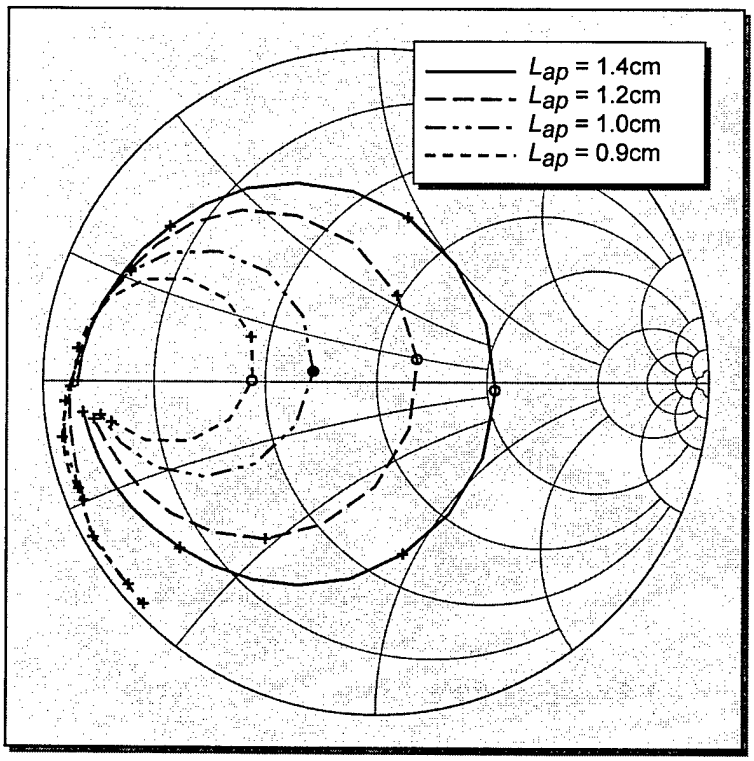

Figure 3. 3

Aperture Length (L_{ap}) Variation (2.0-2.25GHz)

Overall, this section's simulation results show excellent correlation with [11]. The fact that the results are on average only 2.75% and 2.47% lower in frequency than the reference, but otherwise similar, indicates that Micro-Stripes can correctly simulate and analyze aperture-fed microstrip patch antennas.

3.4 CRITICAL COUPLING ANALYSIS

Critical coupling is achieved when all energy from the feed microstrip line is transferred to the patch, indicating a perfect match. This can easily be seen on a Smith chart, when the loop formed by the impedance locus near resonance crosses the center of the chart. When the locus extends beyond the center of the chart it indicates that more than the optimum amount of coupling is taking place, this is referred to as overcoupling. The opposite case, when the locus does not reach the center of the Smith chart, is called undercoupling.

This section will provide details of a study conducted with Micro-Stripes where the aperture length required for critical coupling of an aperture-fed microstrip patch antenna was determined for various stub lengths.

Parameter	2GHz Model	30GHz Model
Feed Substrate:		
- dielectric constant (ε_r)	2.54	2.2
- thickness	1.6mm (1.70% of λ_d)	0.254mm (3.77% of λ_d)
- feedline characteristic impedance	50Ω	50Ω
- microstrip feedline width	4.42mm	0.735mm
- feedline guide wavelength (λ_g)	103.43mm (at 2GHz)	7.324mm (at 30GHz)
Ground Plane:		
- foil thickness	0.01778mm	0.0254mm
- aperture width	1.55mm	0.4mm
- aperture dielectric wavelength (λ_d)	94.12mm (at 2GHz)	6.742mm (at 30GHz)
Patch Substrate:		
- dielectric constant (ε_r)	2.54	2.2
- thickness	1.6mm (1.70% of λ_d)	0.787mm (11.67% of λ_d)
- patch length (resonant dimension)	40mm	2.74mm
- patch width	30mm	3.426mm

Table 3.1
Critical Coupling Analysis Design Details

3.4.1 DESIGN PARAMETERS

Two cases were analyzed: one with the same substrate thickness for the feedline and antenna dielectrics at 2 GHz, and the other at 30GHz where the thickness of the patch antenna substrate was approximately three times that of the feedline dielectric. Table 3.1 gives more details about the models.

3.4.2 RELATIVE DIMENSIONS

For the remainder of this analysis the open-circuited stub length, from the center of the aperture, will be given in percentage of the guide wavelength (λ_g) of the microstrip feedline (see table 3.1). It was calculated by first evaluating the effective dielectric constant of the feedline (ε_e) using[17]:

$$\varepsilon_e = \frac{\varepsilon_r + 1}{2} + \frac{\varepsilon_r - 1}{2} \frac{1}{\sqrt{1 + 12\,d/W}}$$

where:

ε_r is the relative dielectric constant of the feed substrate
d is the thickness of the feed substrate
W is the width of the feed transmission line

The guide wavelength (λ_g) was then calculated with:

$$\lambda_g = \frac{c}{f\sqrt{\varepsilon_e}}$$

where:

c is the speed of light in free space
f is the frequency

Similarly, the aperture length will be given in percentage of the wavelength in the dielectric medium (λ_d). Table 3.1 values were calculated using:

$$\lambda_d = \frac{c}{f\sqrt{\varepsilon_r}}$$

3.4.3 CRITICAL COUPLING ANALYSIS RESULTS

The complete simulation results, in table format, are listed in Appendix B.

3.4.3.1 SLOT LENGTH vs STUB LENGTH

Figure 3.4 shows the slot length versus stub length curves for critical coupling of the 2GHz and 30GHz cases. Both curves have the same shape, with the 30GHz case requiring a much greater aperture length to achieve critical coupling. This is caused by the overall dielectric thickness (feed and patch substrates thickness = 15.44% of λ_d) which is much larger than for the 2GHz case (3.40%). The increased distance reduces the coupling between the feedline and the patch, which is in agreement with [11].

It is interesting to note that in both cases the slot length could not be increased enough to achieve critical coupling for stub lengths shorter than 6%, therefore imposing a lower limit on the practical length of the open-circuited stub.

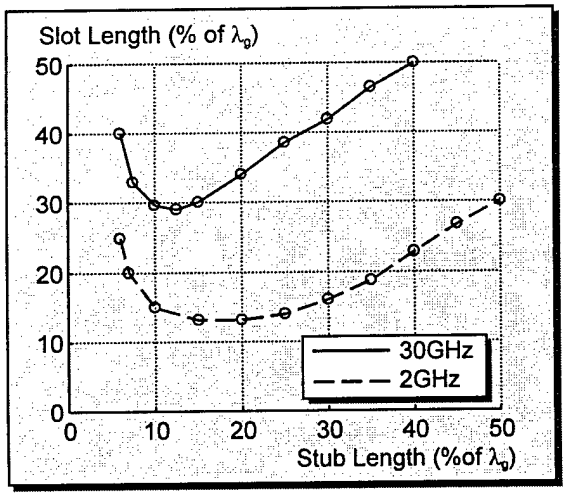

Figure 3. 4

Slot Length vs Stub Length

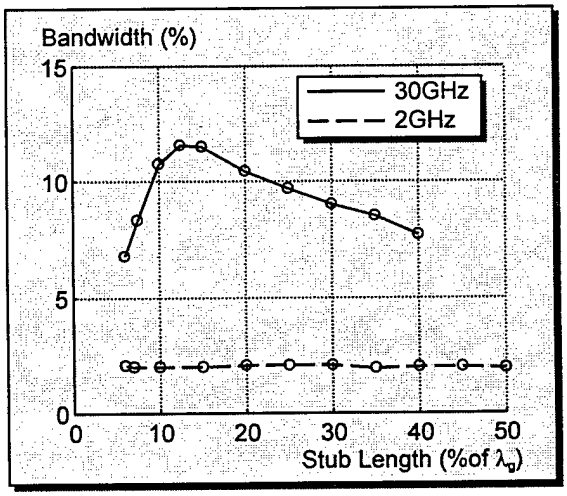

Figure 3. 5

Bandwidth

3.4.3.2 BANDWIDTH

Figure 3.5 shows the bandwidth curves at critical coupling for both cases. Results for the 2GHz case are fairly constant around 2% of the center frequency. The curve is also much lower than for the other case, which was expected because of the difference in microstrip patch substrate thickness. For the 30GHz case, however, there is a significant bandwidth variation with values ranging between 6.77% and 11.57%. It is interesting to note that the maximum bandwidth value occurs for the same stub length (12.5%) as the point in figure 3.4 where the shortest aperture length was required for critical coupling.

3.4.3.3 FREQUENCY VARIATIONS

Figures 3.6 and 3.7 show the variations in percentage of each case's base frequency (2GHz and 30 GHz), versus the stub and slot lengths. The curves show general correlation between the aperture length and the device's resonant frequency. However, in some cases, higher resonant frequencies were obtained with longer apertures. It is also interesting to note that in both cases the highest resonant frequency occurs for a stub length of 20%, regardless of the slot length.

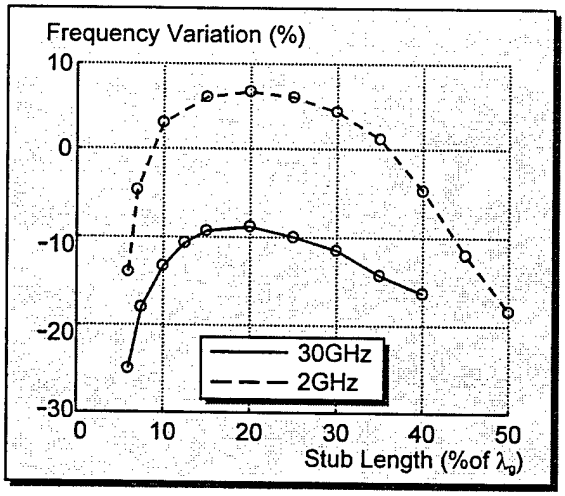

Figure 3. 6

Frequency vs Stub Length

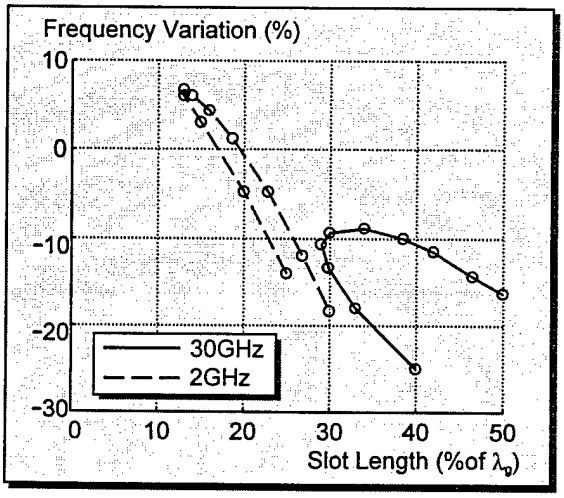

Figure 3. 7

Frequency vs Slot Length

3.4.3.4 DIRECTIVE GAIN

The directive gain (G_d) values used in this section were obtained from Micro-Stripes' *Far-Field Plot* module. The module calculates gain with reference to the overall maximum for all directions and all polarizations. Figure 3.8 shows similar G_d results for both cases, with the 30GHz curve being approximately 0.27 dB above the 2GHz curve. At 30GHz the gain is fairly stable in the 10-30% stub length range with a very sharp drop for shorter stub lengths, the decrease in gain for longer stubs is more gradual. The 2GHz curve does not have the same plateau, but the gain decreases very slowly over the 15-35% stub length range.

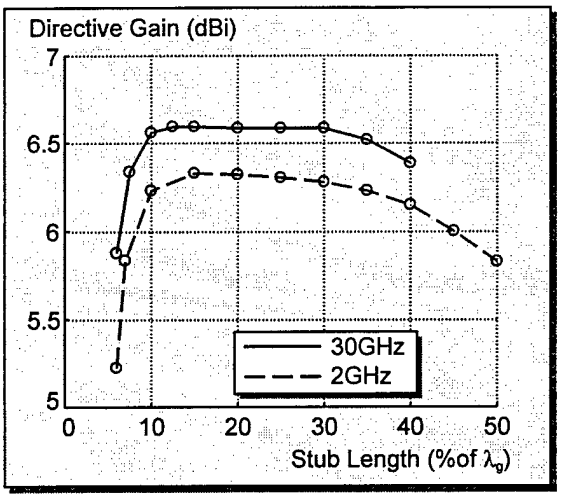

Figure 3. 8

Directive Gain

3.4.3.5 FRONT-TO-BACK RATIO

The front-to-back ratio was evaluated with a Matlab routine that:

- adds-up the co-polarization and cross-polarization cuts;
- evaluates the power surface integrals of the front ($-90° \leq \theta \leq 90°$, where $\theta = 0°$ represents boresight) and back hemispheres, as described in appendix A, section A.2.5.2.3; then
- calculates the $\frac{\text{front radiated power}}{\text{back radiated power}}$ ratio.

Figure 3.9 shows the resulting plots. Notice that in the 2GHz case the curve has a shape similar to the directive gain results, but the 30GHz curve shows a steady increase up to the 35% stub length point.

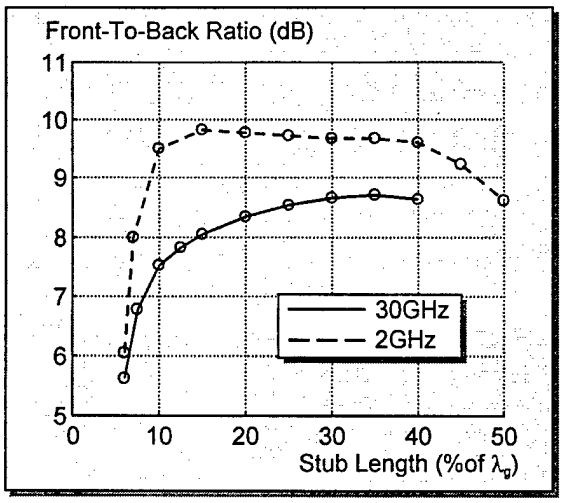

Figure 3. 9

Front-To-Back Ratio

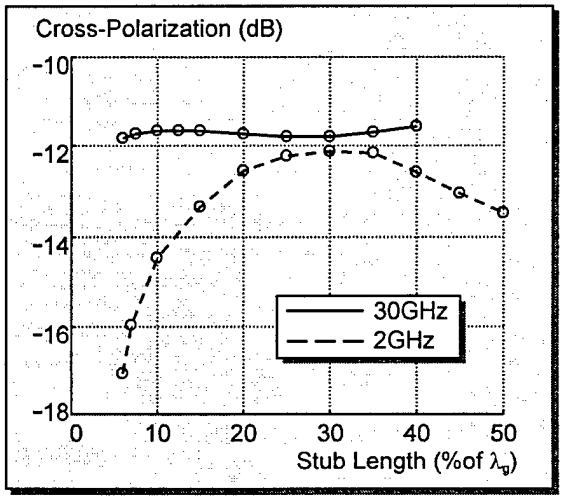

Figure 3. 10

Relative Cross-Polarization

3.4.3.6 RELATIVE CROSS-POLARIZATION

Figure 3.10 shows the highest cross-polarization levels for the normalized patterns in the forward hemisphere ($-90° \leq \theta \leq 90°$, where $\theta = 0°$ represents boresight). Cross-polarization levels are fairly stable around -11.75dB for the 30GHz case, but they vary from -17.06dB to -12.14dB for the 2GHz case.

3.4.3.7 CRITICAL COUPLING ANALYSIS CONCLUSION

This analysis demonstrates that critical coupling of an aperture-fed microstrip patch antenna can be obtained for a variety of different aperture length/stub length combinations. Simulation results also indicate that critical coupling cannot be achieved if the stub length is too short ($< .06\lambda_g$). It is interesting to note that, depending on which of the studied parameters the antenna designer wants to optimize, the optimum critical coupling aperture/stub combination will vary.

CHAPTER 4

PERPENDICULAR SUBSTRATES APERTURE COUPLING

4.1 PERPENDICULAR FEEDING TECHNIQUES

As discussed in chapter 1, in order to develop a brick architecture for the array it is necessary to design a feeding mechanism to efficiently transfer the energy between two perpendicular substrates so the antenna element can be fed. A thorough search of the available literature revealed only two relevant articles. The first is *Aperture Coupled Microstrip Antenna with a Perpendicular Feed*[16], by A.C. Buck and D.M. Pozar (figure 4.1). In this feeding technique the top edge of the slot is connected to the feed line and the bottom edge of the slot is connected to the ground plane of the feed substrate. The patch is therefore fed from the end of the microstrip line, through the slot.

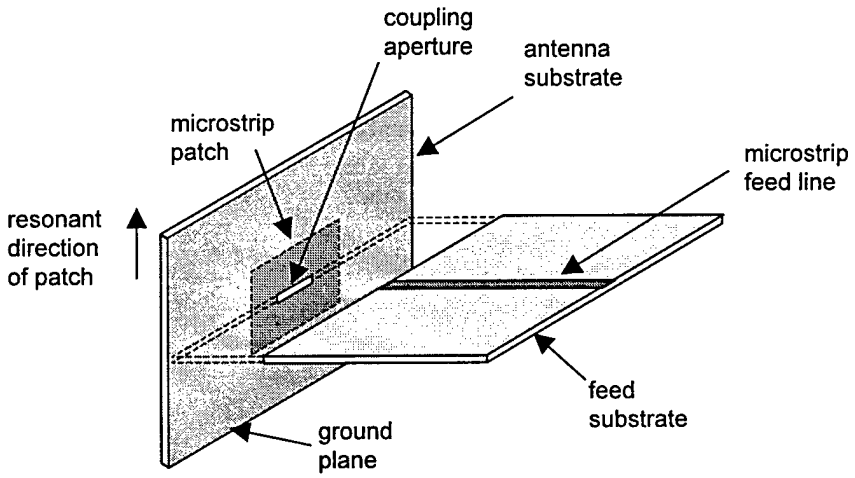

Figure 4. 1

End-Feed Perpendicular Coupling

The second article on perpendicular feeding was *An Aperture Coupled Microstrip Antenna with a Proximity Feed on a Perpendicular Substrate* [12], by D.M. Pozar and R.W. Jackson (figure 4.2). In this case the patch is excited through an aperture in the ground plane by proximity coupling to the microstrip feedline. The feed line is terminated in an open-circuited stub, which is used for tuning. The two ground planes are connected at their junction, except for an area around the slot where the ground plane has been partially removed underneath the feed line. This allows the fields to bend from the feed line to the ground plane of the vertical substrate, and prevents the aperture from being shorted by the feed substrate ground plane.

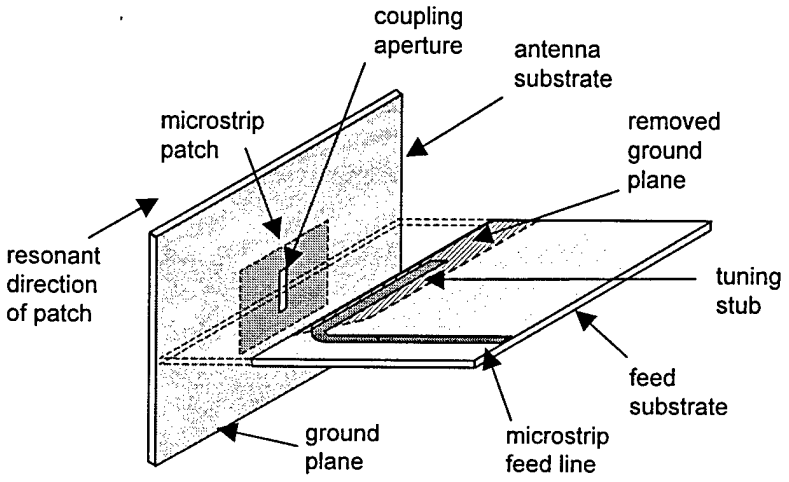

Figure 4. 2

Proximity-Feed Perpendicular Coupling

Unfortunately, neither or the two references ([16] and [12]) provide enough information to readily design a perpendicularly-fed microstrip patch antenna, and before proceeding with either of those feed mechanisms a significant amount of simulation and experimental work is required.

The proximity-feeding technique was selected over the end-feeding mechanism because it seemed easier to fabricate. The end-feed requires physical connections at the slot between the feed line and the perpendicular ground plane, and between the two ground planes; at 30GHz this would be extremely difficult to implement. There seemed to be more "tolerance" to slight fabrication inaccuracies with the proximity-feed, reference [12] even states that a small air gap between the two substrates did not seem to adversely affect the feed mechanism's performance.

4.2 2GHz PERPENDICULAR LINE-TO-LINE COUPLER

The first task undertaken was to design and build a line-to-line coupler using the proximity-feeding method. The first reason for this decision was to gain experience with the coupling mechanism; this was essential since [12] gave no geometry details about the area of the feed substrate ground plane that was removed. The second reason was to acquire additional experience with Micro-Stripes, and to determine how simulation results compared with experimental data on a perpendicularly-fed device that was easy to characterize.

4.2.1 COUPLER GEOMETRY

Figure 4.3 shows the geometry of the line-to-line coupler with its two perpendicular substrates. Detailed coupler design data, along with the Micro-Stripes geometry (*.geom) file listing are included in Appendix C. Note that the operating frequency (around 2GHz) was selected as the line-to-line coupler is an intermediate step towards a perpendicularly fed patch, which was to be compared to the results of [12].

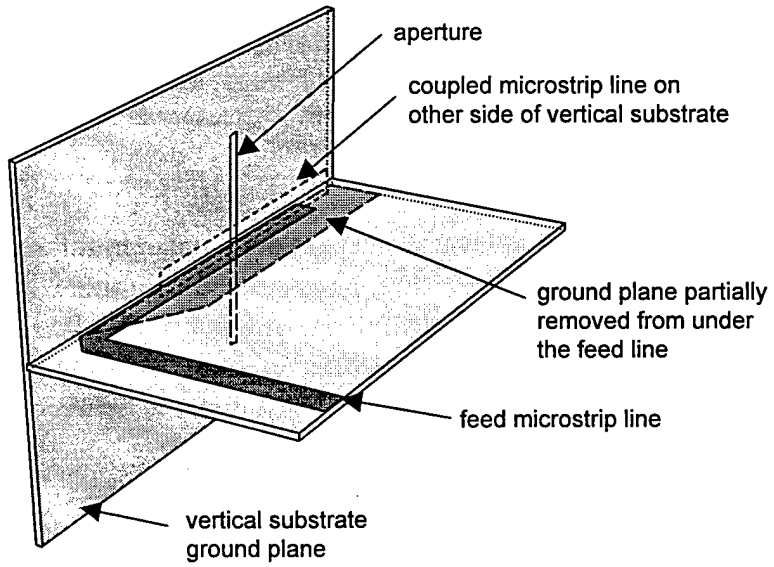

Figure 4. 3

2GHz Perpendicular Line-to-Line Coupler

To study the effect that the ground removal angle (Figure 4.4) had on the return loss simulations were conducted. For those simulations, the ground plane was removed at various angles from under a straight microstrip line running close to a perpendicular metallic wall, with no aperture. The results indicated a better return loss performance for smaller ground plane removal angles. Therefore, the angle was made as small as possible (approximately 21.8°).

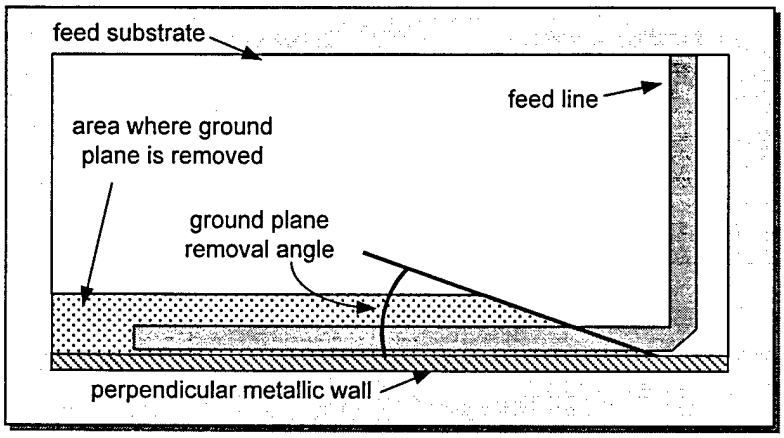

Figure 4. 4

Feed Substrate Ground Plane Removal Angle

Note: Similar ground removal angle tests were later done with an aperture on the perpendicular ground plane feeding a microstrip patch antenna. They produced the opposite results: return loss performance was better for larger angles, with the smallest return loss obtained for a 90° discontinuity located right at the edge of the slot. It therefore seems that the sharper discontinuity increases the amount of coupling through the aperture.

Both open-circuited stub lengths were set at one-quarter of the wavelength in the transmission line ($\lambda_g/4$). For the microstrip line on the slot substrate, λ_g (109.58mm) was evaluated using formulas from Microwave Engineering, by D.M. Pozar[17]. For the portion of the feed line where the ground plane has been removed λ_g (120mm) was evaluated by analysis of the simulations' surface current data (the distance between two successive nulls being equal to $\lambda_g/2$ for the given frequency).

The characteristic impedance for that portion of the feed line was also evaluated; it is approximately *81-j7.5Ω*. Micro-Stripes' *Field plot* module was used to obtain the complex voltages and currents (magnitude and phase) at various points of the line, using the path integration function. From these, the impedance of each point was calculated and plotted on a Smith chart using an arbitrary characteristic impedance(Z_O) value. Z_O was then adjusted, and the points re-plotted, until the *best-fit* circle passing through the reflection coefficient points was centered on the center of the chart. A Matlab routine was

written to speed-up this process. Figure 4.5 shows the resulting plot with 81-j7.5Ω as the line's characteristic impedance.

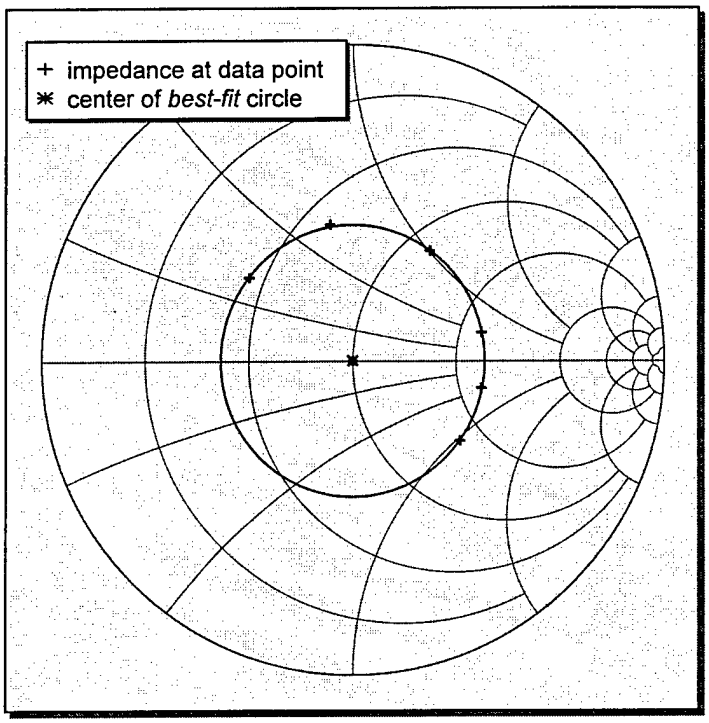

Figure 4. 5

Characteristic Impedance Evaluation

4.2.2 SIMULATION vs EXPERIMENTAL RESULTS

Figures 4.6 and 4.7 show measured and simulated S-parameter performance of the coupler. The purpose of this experiment was not to design an efficient coupler, but to compare simulation and experimental results. Therefore, the actual performance of the coupler will not be analyzed in detail.

Looking at the $|S_{11}|$ performance it can be seen that both results are very similar, except that the experimental data is shifted up in frequency by approximately 5.6 percent. The experimental $|S_{11}|$ minimum of –13.82dB is at 2.278GHz with a 0.37% impedance bandwidth at –8dB, while the simulation gave –18.62dB at 2.156GHz with a bandwidth of 0.48%.

$|S_{21}|$ results are also very similar, with approximately the same shift in frequency. Both experimental and simulated $|S_{21}|$ results at the resonant frequency (–1.56dB and –1.85dB respectively) show that most of the power (65% and 70%) is coupling through the aperture. The sudden drop in $|S_{21}|$ around 3.3GHz is probably caused by the aperture's

resonance (at 3.7GHz the wavelength in the dielectric ($\varepsilon_r = 2.2$) corresponds to the length of the slot).

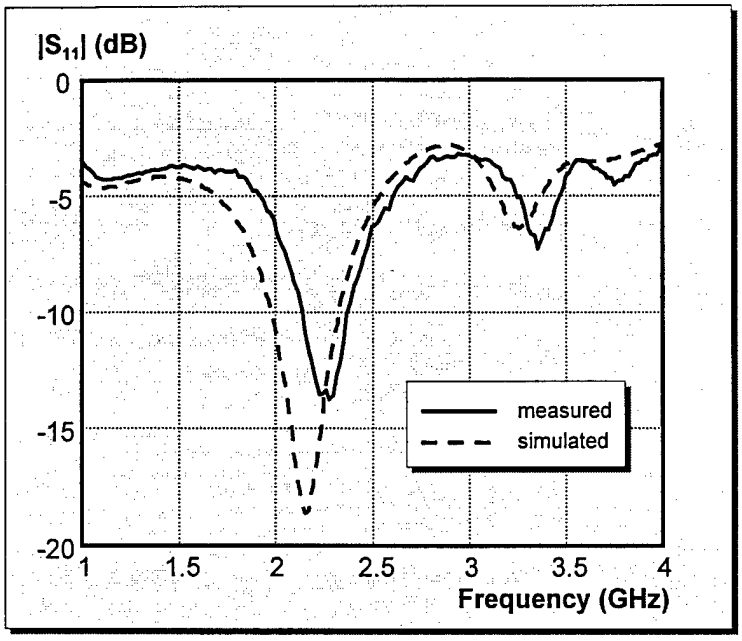

Figure 4. 6

2GHz Perpendicular Coupler $|S_{11}|$ Results

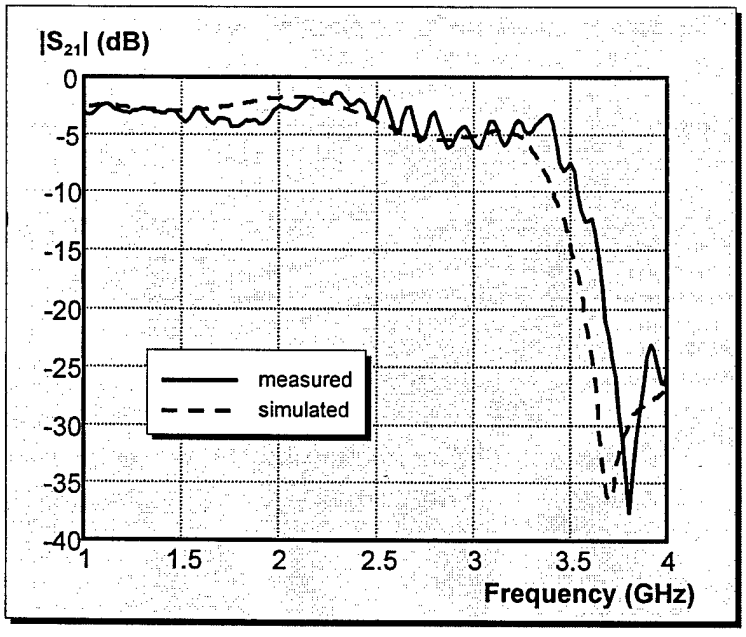

Figure 4. 7

2GHz Perpendicular Coupler $|S_{21}|$ Results

The Smith Chart plot of the simulated and measured data (figure 4.8) shows overcoupling for both cases, with the coupling being greater for measured than simulated data.

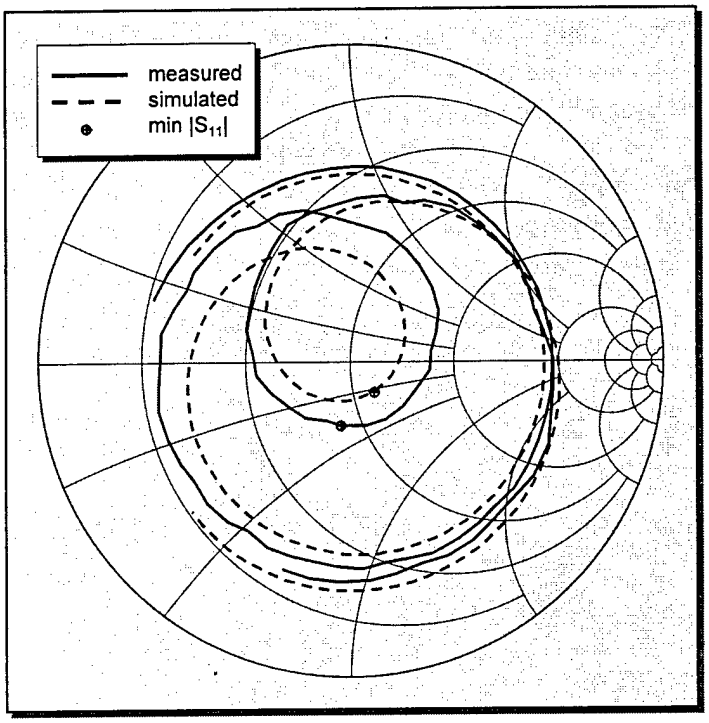

Figure 4. 8

2GHz Perpendicular Coupler S_{11} Smith Chart

4.2.3 3-D PERFORMANCE ASSESSMENT OF MICRO-STRIPES

Micro-Stripes proved to be a very good 3-D design tool for this problem. Predicted S-parameters were close to measured data and, if the frequency shift and coupling increase are taken into consideration when designing devices, the desired operating frequency and coupling characteristics can be achieved with reasonable accuracy.

4.3 2GHz PERPENDICULAR COUPLER CONCLUSION

Results of section 4.2 indicate that the proximity-feeding technique of [12] for coupling energy between two perpendicular substrates actually works. If the coupler was optimized to achieve critical coupling, it could provide an efficient way to effect perpendicular line-to-line interconnections where more traditional methods cannot be applied, as long as the narrow impedance bandwidth of the device is acceptable.

With the proximity-feeding technique confirmed by the perpendicular line-to-line coupler results, and after gaining additional simulation experience with Micro-Stripes, the perpendicular feeding of microstrip patch antennas will be addressed in the next chapter.

CHAPTER 5

PERPENDICULAR SUBSTRATES APERTURE-FED PATCH ANTENNAS

5.1 BACKGROUND

Having studied parallel aperture-fed microstrip patch antennas (chapter 3) and substrates aperture coupling (chapter 4), the next step is to combine these two technologies to design an aperture-fed patch antenna having a feed substrate perpendicular to the patch substrate, hereafter called a perpendicular patch. Figure 5.1 shows the geometry of a perpendicular patch. Two such antennas were simulated, built and tested. The first one, designed to operate around 2GHz, was built to provide a proof of concept. The design presented in [12] did not provide much information with respect to the removal of the ground plane, and some important performance characteristics (such as antenna gain or coupling mechanism efficiency).

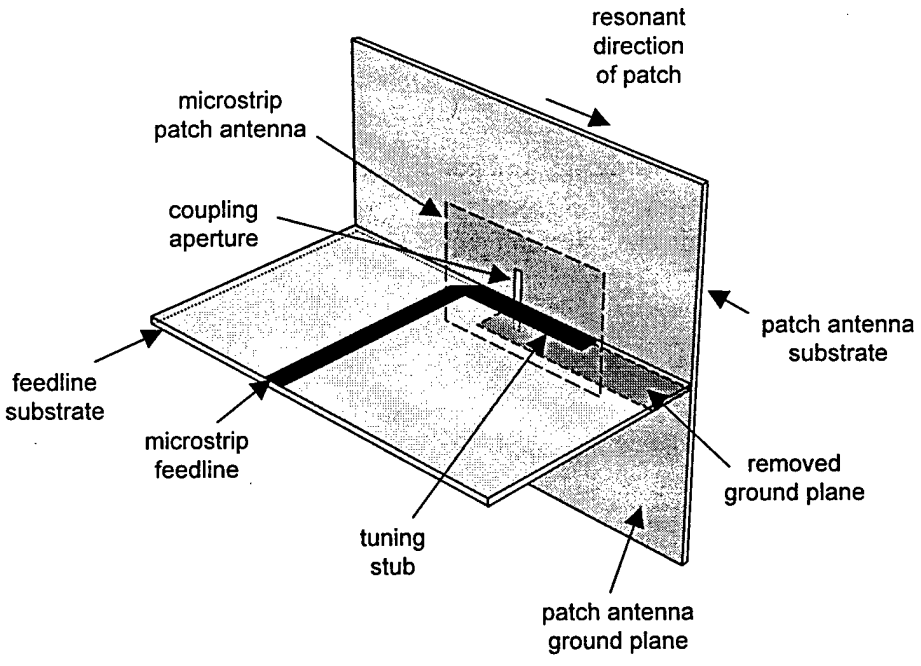

Figure 5. 1

Geometry of a Perpendicular Patch

The second perpendicular patch was designed to operate at the frequency where the brick architecture is to eventually be implemented (30GHz). Note that the portion of the ground plane that was removed is rectangular, while reference [12] seems to indicate an angle smaller than 90° between the edge of the substrate and the ground plane (see Figure 4.4). Simulations showed better return loss performance for rectangular shaped ground plane removal.

Both antennas were simulated and optimized with the Micro-Stripes package, then built and tested. The following sections provide design details and results, both simulated and measured, obtained for each design.

5.2 2GHz PERPENDICULAR PATCH

RT/duroid® 5880 with ½ ounce rolled copper was selected as the material for both substrates; its relative dielectric constant (ε_r) of 2.2 with a thickness of 1.58mm were the closest available match to the substrates used in reference [12]. A 5% shift in resonance frequency between simulated and measured results is expected; therefore, the resonant frequency of the simulated structure was set to 1.9GHz

The open-circuited stub length was then set to 25mm, which is approximately 20.5% of λ_g for the portion of the line where the ground plane has been removed (see Figure 5.1). This value was selected using the results of the critical coupling analysis of section 3.4.3, which showed good performance for a stub length equal to 20% of λ_g with similar substrates around 2GHz. The patch and slot dimensions were then adjusted until an acceptable resonant frequency was achieved.

Appendix D provides the design and geometry details of the 2GHz perpendicular patch, as well as the Micro-Stripes geometry file used to simulate the device. The following sub-sections will discuss simulated and measured results.

5.2.1 SIMULATION RESULTS

Table 5.1 provides a list of the main results obtained with the Micro-Stripes package.

5.2.1.1 S-PARAMETER ANALYSIS

The resonant frequency of the device is located at the point where $|S_{11}|$, the return loss, is minimal. For the Micro-Stripes model the $|S_{11}|$ minimum occurred at a frequency of 1.849GHz (see Figure 5.2 (a)). Its magnitude of –18.37dB indicates efficient coupling

to the patch, with less than 1.5% of the incident power being reflected. Using the complex S_{11} value at resonance the input impedance (Z_{in} = 53.85 + j12.01 Ω) was evaluated, showing a good match to the 50Ω input.

Parameter	Value
resonant frequency	1.849GHz
$\|S_{11}\|$ at resonant frequency	–18.37dB
Z_{in} at resonant frequency	53.85 + j12.01 Ω
SWR < 2 impedance bandwidth	2.67%
maximum forward cross-polarized radiation	–12.36dB
front/back power ratio	11.92dB
directive co-polarized gain	7.179 dBi

Table 5. 1

2GHz Perpendicular Patch Tabled Simulation Results

The impedance bandwidth of a device generally indicates the frequency range over which it performs well. The microstrip patch, the feedline, the aperture, the distance between the feedline and the perpendicular ground plane, and the coaxial-to-microstrip

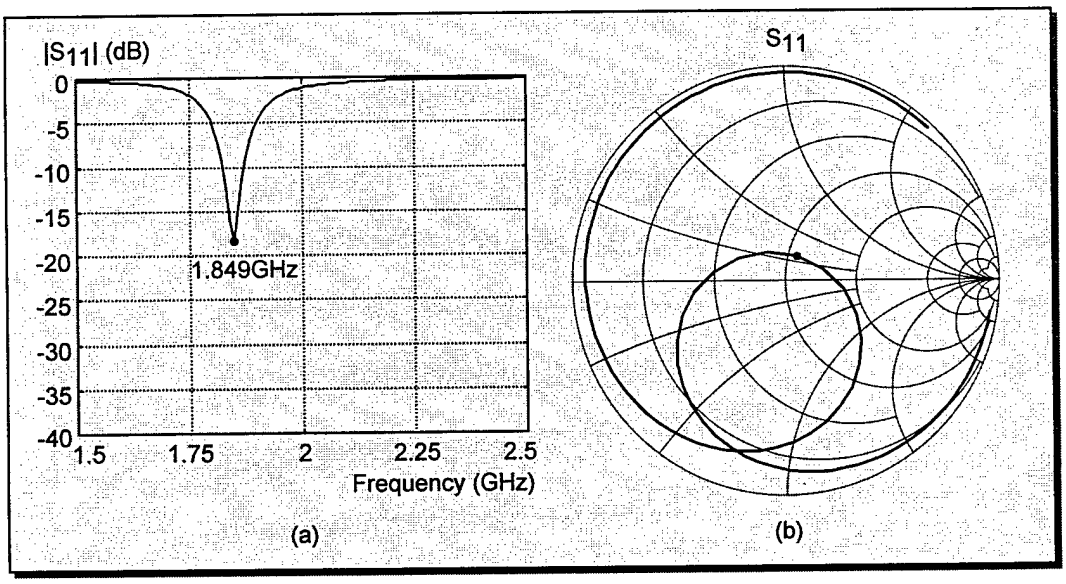

Figure 5. 2

2GHz Perpendicular Patch Simulation S_{11} Results

connector (for the prototype) all affect the frequency response of this device. Throughout this report the bandwidth is defined as the frequency range over which the standing wave ratio (SWR) at the input of the device is lower than 2 (corresponds to $|S_{11}| < 9.55dB$), expressed in percentage of the range's center frequency. Within this range less than 11.1% of the input power is reflected back to the source. For this simulation model the impedance bandwidth was 2.67%.

Figure 5.2 (b) shows the Smith chart plot of S_{11}, which indicates that the antenna would be slightly overcoupled (because the loop formed by the locus near resonance extends beyond the center of the chart).

5.2.1.2 RADIATION PATTERN ANALYSIS

The Micro-Stripes *Near->Far Field* module was used to evaluate the antenna radiation patterns. The far field transformation uses an equivalent surface positioned around the radiating structure being modeled. Equivalent electric and magnetic surface currents are calculated on this surface at specified frequencies, these surface currents are then used to calculate the far field radiation patterns. A more detailed explanation of this method is contained in the user's guide provided with the Micro-Stripes software package.

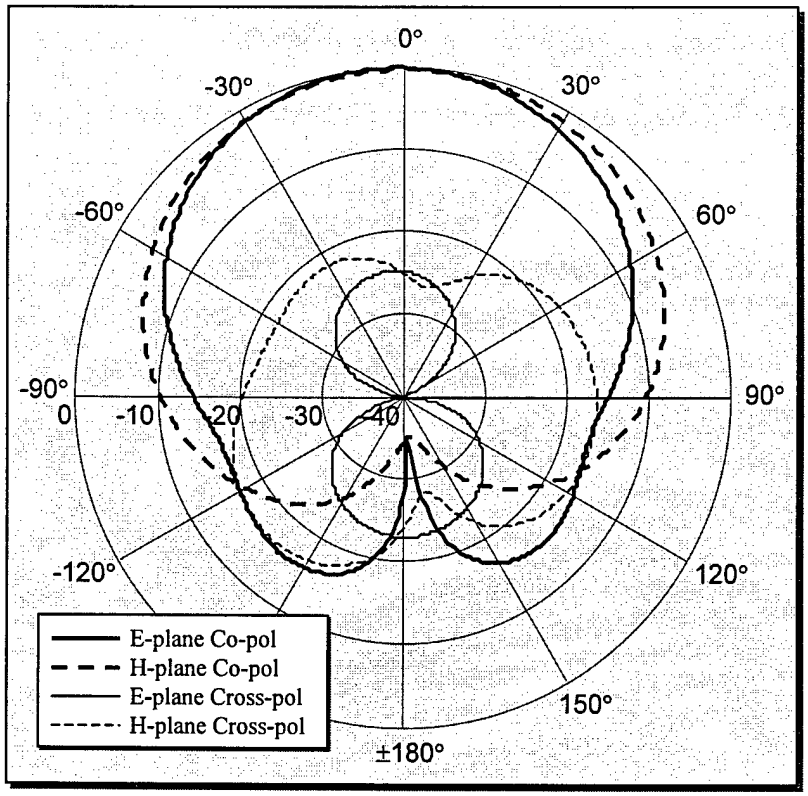

Figure 5. 3

2GHz Perpendicular Patch Simulated Radiation Patterns at 1.849GHz

Figure 5.3 shows the normalized E-plane and H-plane, co-polarized and cross-polarized, simulated radiation patterns at 1.849GHz. See Figure 5.4 for the orientation of the E- and H-planes. The polar representation is used to represent the patterns with 0° corresponding to the antenna's boresight direction, while the magnitude circles range from 0dB at the outer edge of the plot to –40dB at its center. The asymmetry of the back lobes could be due to radiation from the open-circuited stub with the feed substrate ground plane removed in the $-90° < \theta < -180°$ quadrant.

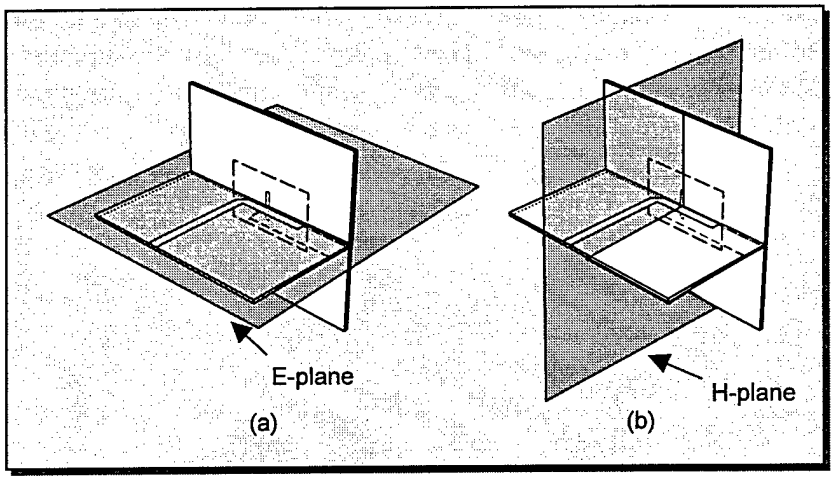

Figure 5. 4

Perpendicular Patch E-plane and H-plane

The maximum forward cross-polarized radiation of Table 5.1 (–12.36dB) represents the worst case cross-polarization for the forward hemisphere ($-90° < \theta < 90°$) found over the eight normalized radiation pattern cuts that were analyzed. Note that cross-polarization in the back hemisphere was not taken into consideration since the feed mechanism is to be used for a planar array radiating in the boresight direction. The worst case cross-polarization occurred for θ of approximately –75° of the $\phi = 135°$ cut, the E-plane corresponding to $\phi = 0°$ and the H-plane to $\phi = 90°$. The maximum cross-polarization in the E-plane was –24.76dB, and –13.78dB in the H-plane (at $\theta = -90°$).

The front/back ratio of 11.92dB was evaluated to get an estimate of how much power was radiated in the back hemisphere with the perpendicular feeding method. The total co-polarized power radiated in the front and back hemispheres were evaluated by surface integration, using the method described in appendix A (section A.2.5.2.3), then the ratio was calculated. In this case the result indicates that close to 94% of the power is radiated forward.

The directive co-polarized gain of the device (7.179dBi) was evaluated with a Matlab routine that follows the same algorithm, as described in appendix A. Note that the cross-polarization was left out so that simulated directive gain results could be compared to measured directive gain, as it would have been extremely difficult to accurately record the relative phase of cross- and co-polarized patterns so their powers could be added.

5.2.2 MEASURED RESULTS

The prototype was constructed using a coaxial-to-microstrip connector attached to the circuit with a brass mounting block (Figure 5.5). The two perpendicular substrates were soldered together at the junction between their ground planes, with the soldering line running from the edge of the substrates to approximately 1mm of the coupling aperture. An "L"-shaped bracket, made of low dielectric constant material (ε_r of approximately 2.5), was then glued on both substrates to add rigidity to the structure.

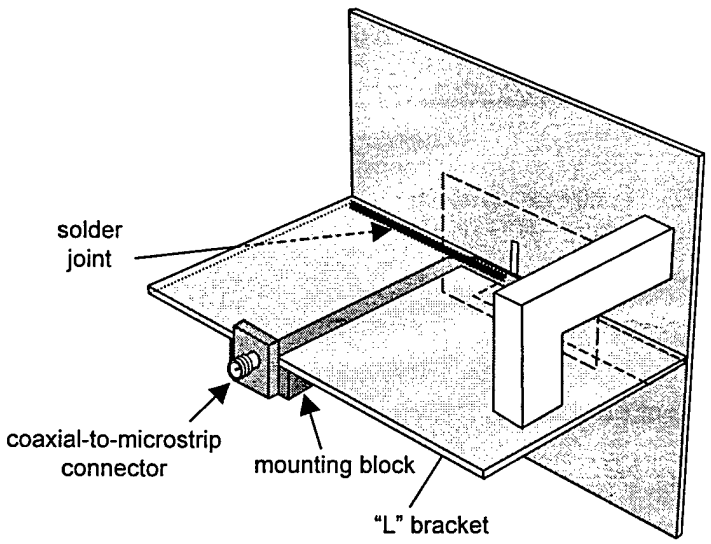

Figure 5. 5

2GHz Perpendicular Patch Prototype Fabrication

Table 5.2 lists the key results obtained through measurement of the 2GHz perpendicular patch prototype.

Parameter	Value
resonant frequency	2.02GHz
$\|S_{11}\|$ at resonant frequency	–40.285dB
Z_{in} at resonant frequency	(48.436 – j0.197) Ω
SWR < 2 impedance bandwidth	1.088%
maximum forward cross-polarized radiation	–12.13dB
front/back ratio	11.14dB
directive co-polarized gain	7.611dBi
gain at resonant frequency	5.89 ± 0.5dB

Table 5. 2

2GHz Perpendicular Patch Measured Results

5.2.2.1 S-PARAMETER ANALYSIS

S_{11} measurements were made with the Wiltron® 360B vector network analyzer located in the DREO/DFL Antenna Research Laboratory (DDARL). Prior to any set of measurements being taken the network analyzer was calibrated for a 50Ω standard over the frequency range of interest, the reference plane being set at the end of the test cable.

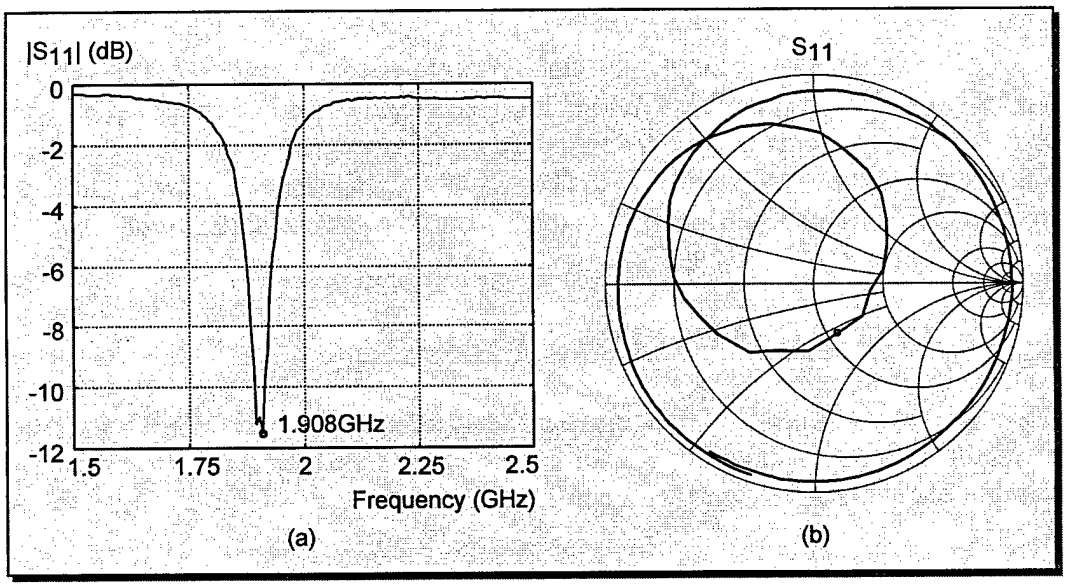

Figure 5. 6

2GHz Perpendicular Patch Measured S_{11} Results

Measurements of S_{11} for the fabricated prototype are shown at Figure 5.6. The relatively high $|S_{11}|_{min}$ (–11.376dB) and the loop formed by the antenna's locus extending over the center of the Smith chart indicated that the antenna was over-coupled. The aperture length was then reduced, using copper tape, until critical coupling was achieved. This occurred for a length of approximately 12mm. All subsequent measurements were done with this setup.

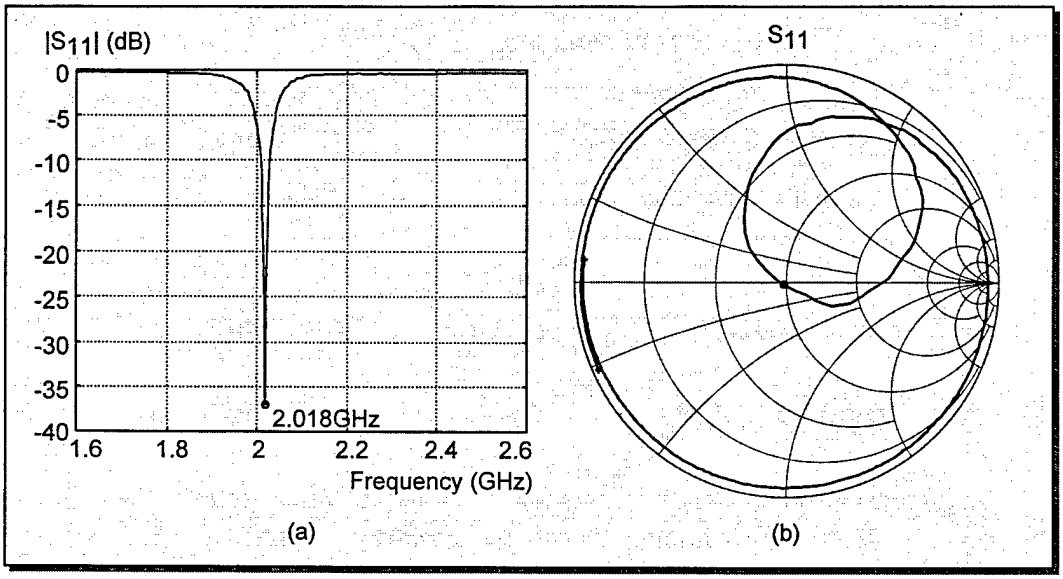

Figure 5. 7

"Tuned" 2GHz Perpendicular Patch Measured S_{11} Results

The resonant frequency of the "tuned" prototype was found at 2.018GHz, with a $|S_{11}|$ of –40.285dB (Figure 5.7 (a)). The Smith chart shows critical coupling, with the locus crossing its center (Figure 5.7 (b)). The input impedance at the resonant frequency is also very good at 48.436 – j0.197 Ω. The SWR < 2 impedance bandwidth of the device was evaluated at 1.088%, which is less than half of the simulated bandwidth.

5.2.2.2 RADIATION PATTERN ANALYSIS

Radiation pattern and gain measurements were done at the DDARL far-field measurement range, which uses a 5.8m x 3.3m x 3.3m shielded anechoic chamber. The chamber's operating frequency range is 2.0-62.5GHz.

To study the efficiency of the perpendicular substrates coupling mechanism both the forward (towards boresight) and backward radiation should be analyzed, to determine if most of the energy is actually radiated in the boresight direction. But, because of physical layout of the positioning equipment full 360° patterns cannot be easily

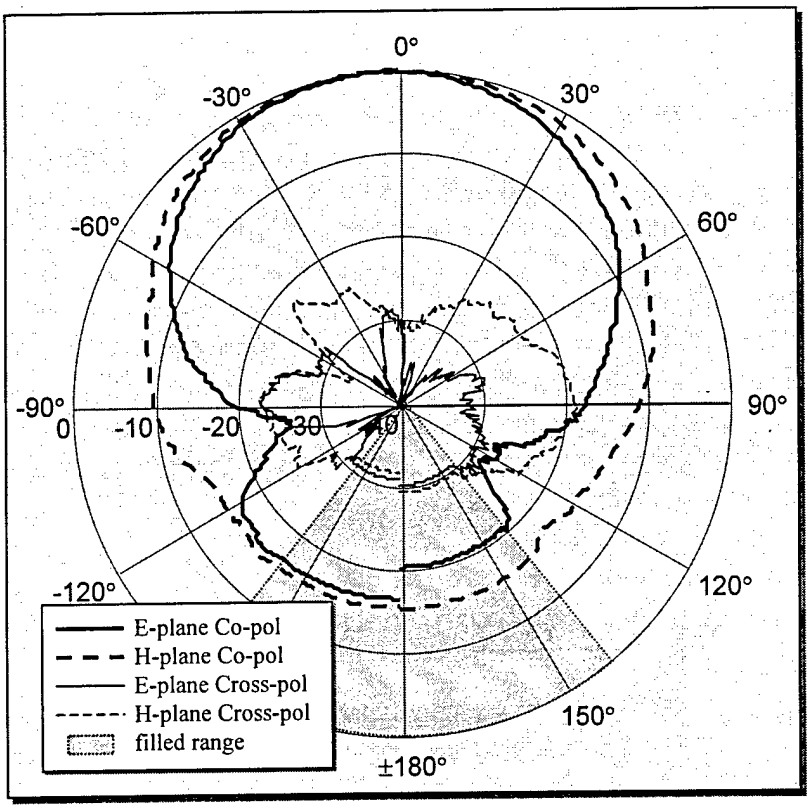

Figure 5. 8

2GHz Perpendicular Patch Measured Radiation Patterns at 2.02GHz

measured. For large angles from boresight, which vary depending on the geometry of the antenna under test (AUT) and its supporting hardware, the AUT positioner cuts through the direct path between the probe and the AUT. For the perpendicular patch, measurements were limited to the $-140° < \theta < 140°$ range.

Figure 5.8 shows the normalized E-plane and H-plane, co-polarized and cross-polarized, radiation pattern measurements of the "tuned" prototype at 2.02GHz. Note that for directivity and front/back calculation purposes the pattern values at $\theta = 140°$ and $\theta = -140°$ were used to fill the remaining portions of the pattern ($140° < \theta < 180°$ and $-180° < \theta < -140°$, respectively). The back radiation asymmetry caused by radiation from the open-circuited stub can again be seen in the $-90° < \theta < -180°$ quadrant, especially for the E-plane co-polarized pattern.

The measured value of –12.13dB maximum forward cross-polarized radiation represents the worst case cross-polarization for the forward hemisphere ($-90° < \theta < 90°$) found over the eight radiation pattern cuts that were analyzed. The worst case cross-polarization occurred for a θ angle of approximately 90° of the $\phi = 135°$ cut, the E-plane

corresponding to $\phi = 0°$ and the H-plane to $\phi = 90°$. The maximum cross-polarization in the E-plane was –23.25dB, and –18.44dB in the H-plane (at $\theta = 90°$).

A front/back ratio of 11.14dB was evaluated indicating over 92% of the radiated power was being transmitted in the forward direction. The directive co-polarized gain (G_d) of the device was evaluated to be 7.611dBi. The cross-polarization was left out of the calculation, since as mentioned before, it would have been nearly impossible to accurately record the relative phase of cross- and co-polarized patterns so their radiated powers could be added. Note that, because the back hemisphere was filled with a constant value beyond the $-140° < \theta < 140°$ range, the front/back ratio and directive gain are not accurate evaluations. However, they provide a good approximation since, based on simulation results, there should be no radiation beyond the level of the values used to fill the ranges for which there were no measured data. In fact, the exact front/back ratio and directive gain values should be slightly higher because simulations show radiation nulls, or minima, in the filled areas.

5.2.2.3 GAIN EVALUATION

The gain (G) of the device was evaluated with the three-antenna method. An EMCO Model 3160-03 (1.7-2.6GHz) standard gain horn (SGH) and a Rhode & Schwarz Model HL040 (0.4-3.0GHz) log periodic dipole array (LPDA) were used as the other antennas. To get an idea about the accuracy of the measurements, evaluated gains of the SGH and LPDA antennas were compared to their theoretical values over the frequency range of interest (Figure 5.9). The evaluated gain of both antennas was slightly lower than the theoretical data by an average of 0.21dB and 0.30dB, respectively. These results give a high degree of confidence in the gain results of the 2GHz perpendicular patch of Figure 5.9, which can conservatively be considered accurate within ± 0.5dB. At 2.02GHz the gain of the antenna is 5.89 ± 0.5dB.

The radiation efficiency (η) can be estimated using the following relation:

$$G = \eta D$$

where G is the gain, and D is the directivity (equivalent to the directive gain (G_d)) of the antenna.

Using the estimated 7.61dBi as the directivity, a value of $\eta = 0.673 \pm 0.08$ is calculated, meaning that 60 to 75 percent of the power fed to the device is radiated in the forward direction. However, it should be noted that this estimate includes all losses within the device (resistive losses in the feedline, coaxial-to-microstrip connector induced losses, mismatches of feed circuit impedance or of polarization, etc...) in addition to the losses incurred by the perpendicular feed mechanism.

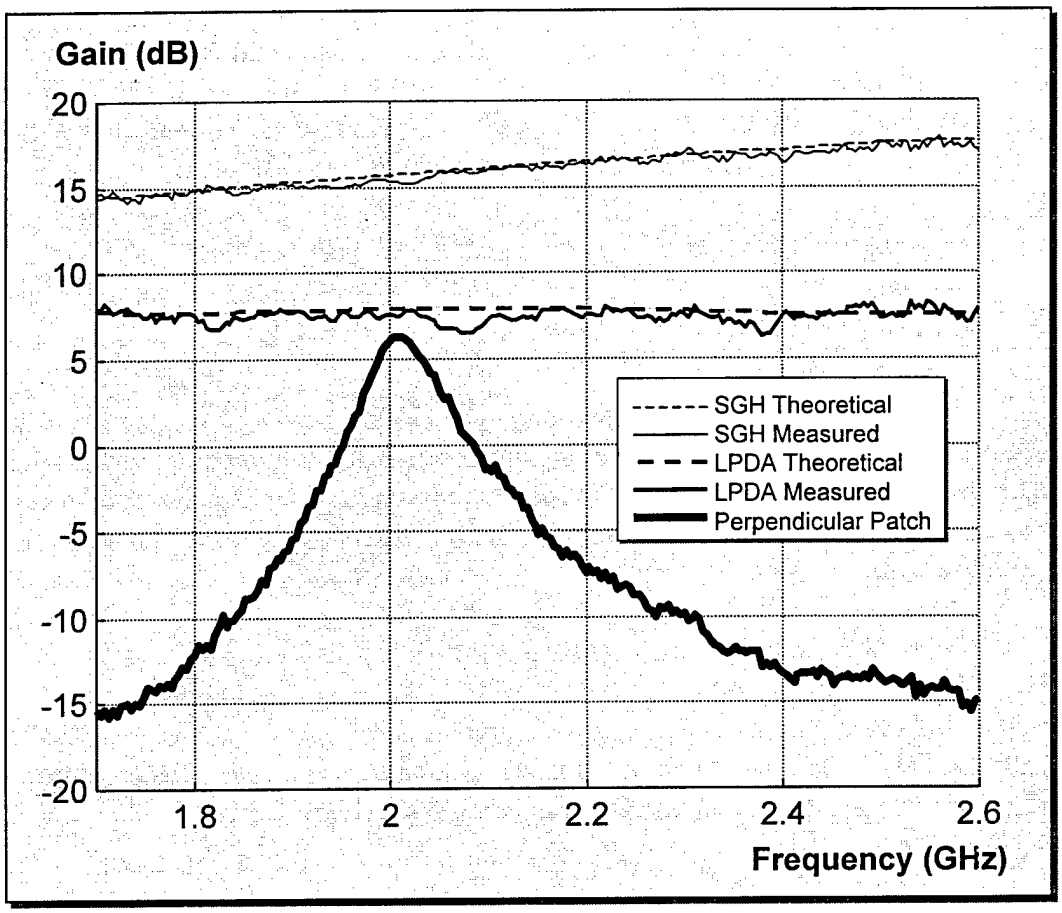

Figure 5. 9

2GHz Perpendicular Patch Gain Measurement Results

5.2.3 RESULTS COMPARISON

Prototype measurement and simulation results are fairly close, with some exceptions. As expected, the resonant frequency of the prototype was higher than predicted by the simulation (2.018GHz vs 1.925GHz), which is a shift of 4.8%. Another difference is the amount of coupling between the feedline and the radiating microstrip patch, which was greater for the measured prototype. As a result the aperture had to be reduced to 12mm to achieve critical coupling, while in simulations critical coupling was achieved with a 16mm aperture. The reason for this difference is unknown. Also, the impedance bandwidth was significantly narrower for the prototype (1.088%) than expected from simulation results (2.426% at critical coupling). Simulated and measured radiation pattern analysis results were similar (Figures 5.3 and 5.8).

The prototype results should also be compared to those of reference [12], Figure 5. That model was built with both substrates having a dielectric constant (ε_r) of 2.55 and a

thickness of 1.58mm. The substrate dimensions were comparable in both cases. The SWR < 2 bandwidth obtained by Pozar and Jackson[12] was stated to be about 1.3%, which is slightly larger than the 1.088% obtained here. However, their results indicated much larger back radiation levels (approximately –5.5dB in the E-plane and –11dB in the H-plane), than was measured here (–16.38dB and –15.58dB respectively). Unfortunately, the reference makes no mention of gain or cross-polarization results.

5.3 30GHz PERPENDICULAR PATCH

RT/duroid® 5880 ($\varepsilon_r = 2.2$) with ½ ounce rolled copper was again selected as the material for both substrates. The feed substrate was 0.254mm thick, while the patch substrate thickness was 0.787mm. The resonant frequency goal for the simulated model was chosen around 28.5GHz, expecting to achieve approximately 30GHz with the prototype measurements.

The open-circuited stub length was then set to 1.098mm, which is approximately 13.34% of λ_g for the portion of the line where the ground plane has been removed (Figure 5.10). The critical coupling analysis of section 3.3.3 indicates that good results should be achieved for this stub length around 30GHz. The patch and slot dimensions were then adjusted until an acceptable resonant frequency was achieved.

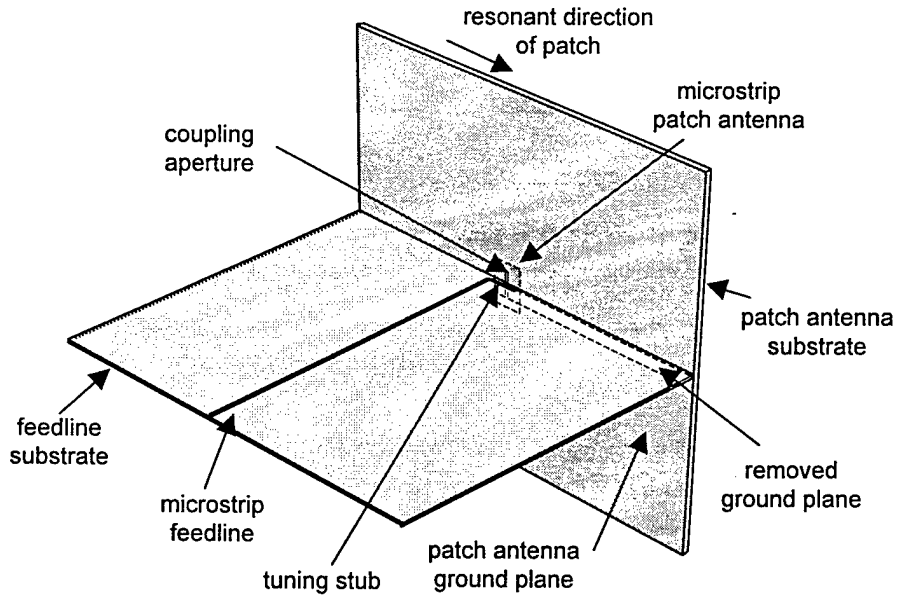

Figure 5. 10

Geometry of 30GHz Perpendicular Patch

Appendix E provides the design and geometry details of the 30GHz perpendicular patch, as well as the Micro-Stripes geometry file used to simulate the device. The following sub-sections will discuss simulated and measured results.

5.3.1 SIMULATION RESULTS

Table 5.3 lists the key simulation results obtained with the Micro-Stripes software package.

Parameter	Value
resonant frequency	28.406GHz
$\|S_{11}\|$ at resonant frequency	–45.397dB
Z_{in} at resonant frequency	49.60 + j0.36 Ω
SWR < 2 impedance bandwidth	17.35%
maximum forward cross-polarized radiation	–6.60dB
front/back power ratio	9.96dB
directive co-polarized gain	7.44dBi

Table 5. 3

30GHz Perpendicular Patch Tabled Simulation Results

5.3.1.1 S-PARAMETER ANALYSIS

The resonant frequency of the simulation model was 28.406GHz, which is close to the 28.5GHz simulation design goal. The $|S_{11}|$ of –45.397dB and input impedance of 49.60 + j0.36 Ω at that frequency indicate critical coupling. This can also be seen on the Smith chart of Figure 5.11 (a), with the locus almost passing through the center of the chart.

The simulation impedance bandwidth of 17.35% is uncharacteristically large for this type of antenna, therefore prototype measurements are expected to produce a lower bandwidth value.

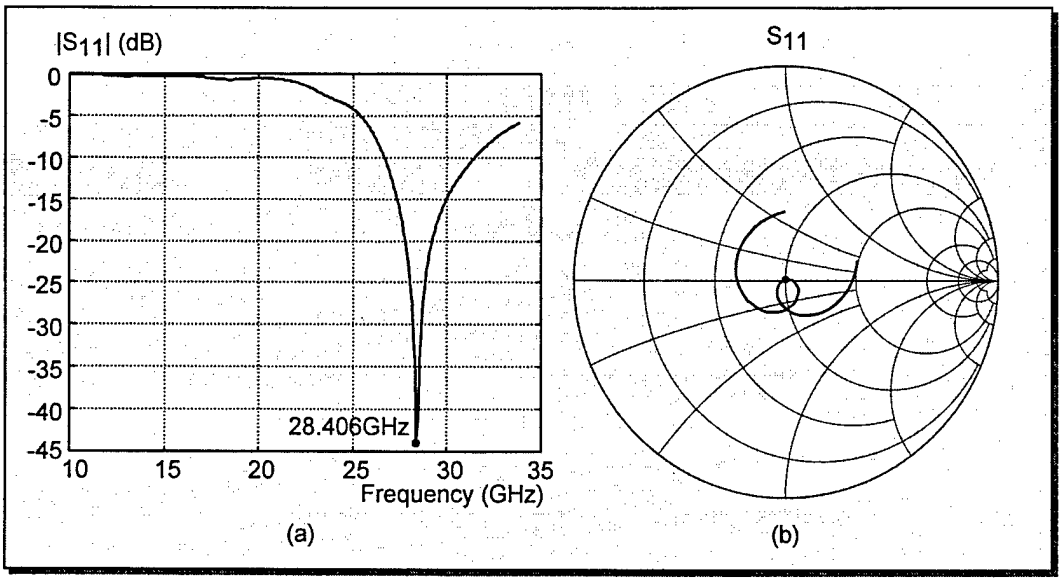

Figure 5. 11

30GHz Perpendicular Patch Simulation S_{11} Results

5.3.1.2 RADIATION PATTERN ANALYSIS

Figure 5.12 shows the normalized E-plane and H-plane, co-polarized and cross-polarized, simulated radiation patterns at 28.406GHz. See Figure 5.4 for the orientation of the E- and H-planes. Again, the asymmetry in the back lobes is probably caused by radiation from the open-circuited stub with the feed substrate ground plane removed in the $-90° < \theta < -180°$ quadrant.

The maximum forward cross-polarized radiation of –6.6dB is the worst case cross-polarization for the forward hemisphere ($-90° < \theta < 90°$). Note that cross-polarization in the back hemisphere was not taken into consideration since the feed mechanism is to be used for a planar array radiating in the boresight direction. The worst case cross-polarization occurred for θ of approximately –75° of the $\phi = 22.5°$ cut, the E-plane corresponding to $\phi = 0°$ and the H-plane to $\phi = 90°$. The maximum cross-polarization in the E-plane was –26.28dB, and –19.49dB in the H-plane.

The front/back co-polarization ratio of 9.962dB indicates that approximately 91% of the power is radiated in the forward direction. The directive co-polarized gain of the device was evaluated at 7.44dBi.

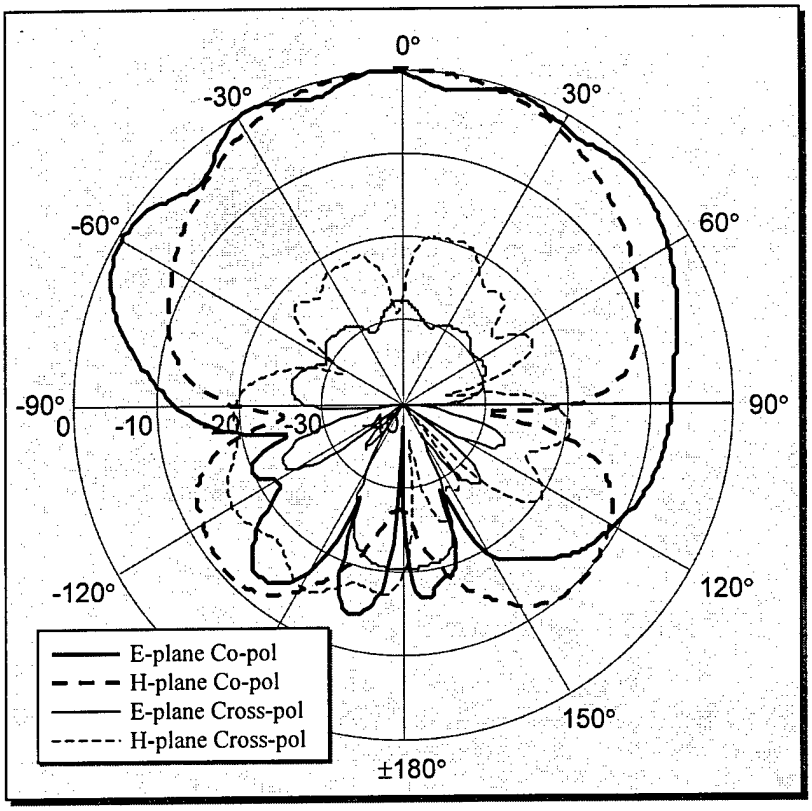

Figure 5. 12

30GHz Perpendicular Patch Simulated Radiation Patterns at 28.406GHz

5.3.2 MEASURED RESULTS

For the 30GHz perpendicular patch prototype a large plastic support had to be fabricated to keep both substrates at right angles, and to provide enough physical strength to mount the coaxial-to-microstrip connector (Figure 5.13). With a thickness of only 0.254mm, the feed substrate was not strong enough to support it. The coaxial-to-microstrip connector was therefore attached to the circuit with a brass mounting block, which was screwed through the plastic support. The two perpendicular substrates were soldered together at the junction between their ground planes, with the solder joint running from the edge of the substrates right to the edge of the coupling aperture. The plastic support, made of low dielectric constant material (ε_r of approximately 2.5),was attached to the patch substrate with plastic screws. A straight plastic bracket was used to clamp the feed substrate to the plastic support, it was also secured with plastic screws. The plastic support was hollowed-out above the feedline and at the junction of the two substrates to limit the effect of the support on the electromagnetic performance of the device.

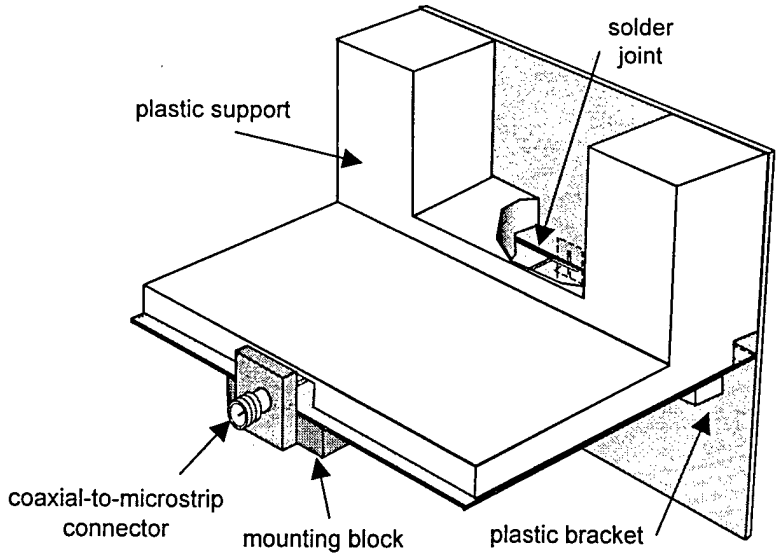

Figure 5. 13

30GHz Perpendicular Patch Prototype Fabrication

It is important to note at this point that the prototype's performance was very sensitive to the coaxial-to-microstrip connector. Loosening or tightening of the screws holding the brass mounting block onto the device affected its performance, to the point where contact may be lost between the connector and the feedline. The connector was also sensitive to the manipulations required to connect the device to the network analyzer for S_{11} measurements, or to the positioner for pattern and gain measurements.

Table 5.4 lists the key results obtained through measurement of the 30GHz perpendicular patch prototype.

Parameter	Value
resonant frequency	30.564GHz
$\|S_{11}\|$ at resonant frequency	–75.477dB
Z_{in} at resonant frequency	$49.985 - j0.0079\ \Omega$
SWR < 2 impedance bandwidth	> 5.08%
maximum forward cross-polarized radiation	–11.30dB
front/back power ratio	7.512dB
directive co-polarized gain	7.015dBi
gain at resonant frequency	5.82 ± 0.5dB

Table 5. 4

30GHz Perpendicular Patch Tabled Prototype Results

5.3.2.1 S-PARAMETER ANALYSIS

As was done before, S_{11} measurements were made with the Wiltron® 360B vector network analyzer located in the DREO/DFL Antenna Research Laboratory (DDARL). Prior to any set of measurements being taken the network analyzer was calibrated for a 50Ω standard over the frequency range of interest, the reference plane being set at the end of the test cable.

Figure 5.14 shows a 25-40GHz plot of $|S_{11}|$. Local $|S_{11}|_{min}$ are spaced 1.68, 2.94, 1.44, 2.25, 1.56, 1.83 and 1.92GHz apart, from left to right. The plot indicates some sort of *unexpected* resonances, the source of which is unknown. After adjusting the coaxial-to-microstrip connector the ripple was reduced, but it could not be eliminated as can be seen in Figure 5.15 (a).

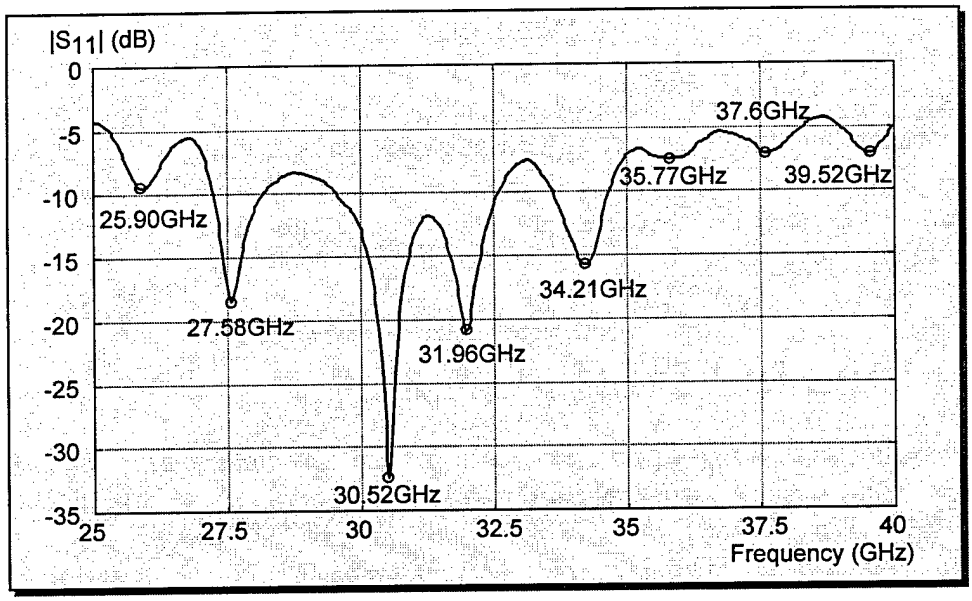

Figure 5. 14

25-40GHz |S11| Measurement of 30GHz Perpendicular Patch Prototype

After adjustments to the connector the 30GHz perpendicular patch prototype's resonant frequency was found at 30.564GHz, which is slightly above the design goal of 30GHz. The $|S_{11}|_{min}$ of –75.48dB and input impedance of 49.985 – j0.0079 Ω indicate a nearly perfect match, as shown by the critical coupling of the Smith chart plot at Figure 5.15. Note that while "tuning" the coaxial-to-microstrip connector $|S_{11}|_{min}$ values ranging from approximately –32dB to –80dB were measured.

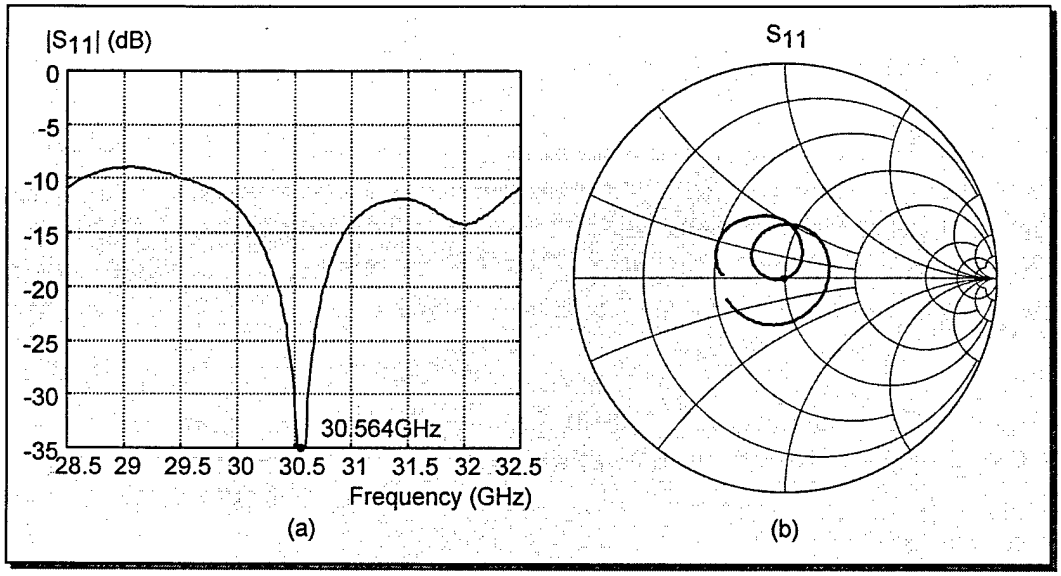

Figure 5. 15

30GHz Perpendicular Patch Prototype Measured S_{11} Results

In this case, since the $|S_{11}|$ plot remains below the SWR < 2 line (-9.55dB) over a wide range because of the *unexpected* resonances. Using SWR < 2 to would give an impedance bandwidth in excess of 17%, which may not be a true reflection of the antenna's performance. Therefore, a lower bound of 5.08% was evaluated over the $|S_{11}| < -11.85$dB range (–11.85dB is the level of the first maximum to the right of the resonant frequency).

5.3.2.2 RADIATION PATTERN ANALYSIS

Radiation pattern and gain measurements were done in the CRC anechoic chamber, which runs the Flam & Russell FR959 software package to control the positioners and to evaluate the pattern gain measurements. For these pattern measurements the available data range went from $\theta = -175°$ to $\theta = 175°$ range.

Figure 5.16 shows the normalized E-plane and H-plane, co-polarized and cross-polarized, radiation pattern measurements of the prototype at 30.30GHz. Note that for directivity and front/back calculation purposes the pattern values at $\theta = 175°$ and $\theta = -175°$ were used to fill the remaining portions of the pattern ($175° < \theta < 180°$ and $-180° < \theta < -175°$, respectively). It is unclear why the radiation patterns are so "bumpy", but multi-path propagation, surface waves or radiation from the patch substrate's edge are possible causes. Noise was ruled-out of the possible causes because separate measurements produce the same variations. For this reason, the back radiation asymmetry caused by radiation from the open-circuited stub is not as easily identifiable as in the 2GHz case.

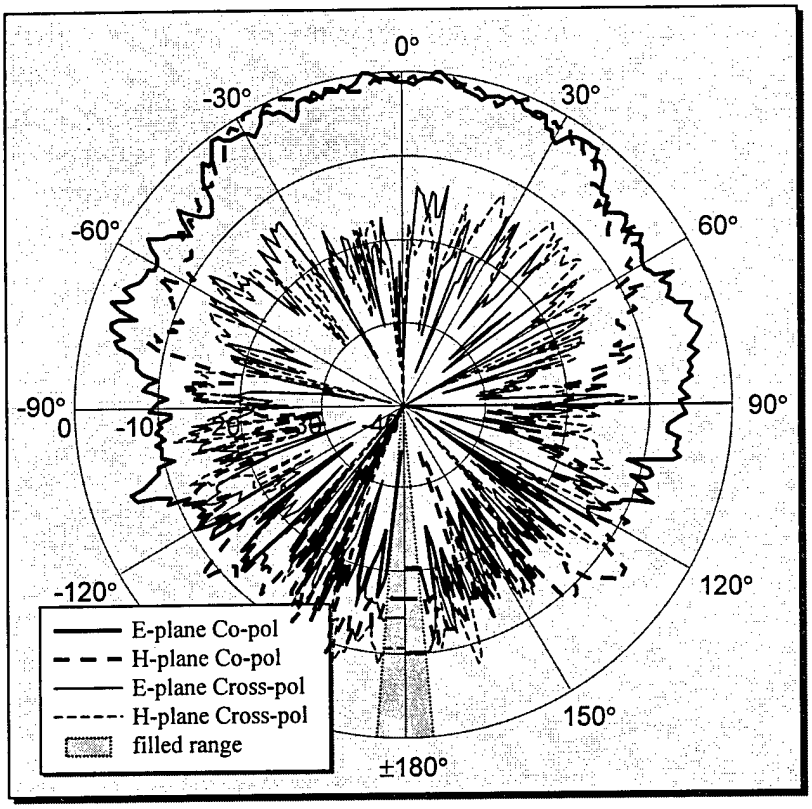

Figure 5. 16

30GHz Perpendicular Patch Measured Radiation Patterns at 30.30GHz

The –11.30dB maximum forward cross-polarized radiation represents the worst case cross-polarization for the forward hemisphere ($-90° < \theta < 90°$) found over the two radiation pattern cuts that were analyzed. The worst case cross-polarization occurred for a θ angle of approximately 40° of the H-plane cut. The maximum cross-polarization in the E-plane was –11.56dB (at $\theta = -56°$).

A front/back ratio of 7.512dB was evaluated indicating almost 85% of the radiated power going in the forward direction. The directive co-polarized gain of the device was evaluated at 7.015dBi. The back hemisphere was filled with a constant value for a very small range ($-175° < \theta < 175°$), but only two cuts were available. Therefore the front/back ratio and directive gain are not accurate evaluations. They provide the best approximation available.

5.3.2.3 GAIN EVALUATION

The gain of the 30GHz perpendicular patch was evaluated with the gain transfer method. A Hughes 26.5-40GHz standard gain horn was used as the reference antenna. The results are shown at Figure 5.17, which are considered accurate within ± 0.5dB. At 30.3GHz the gain of the antenna is 5.82 ± 0.5dB. Note that it is unknown why the gain is higher around 29.5GHz (up to 6.84 ± 0.5dB). Like the radiation pattern bumpiness, this could be due to frequency sensitive multi-path propagation, surface waves, or radiation from the patch substrate's edge.

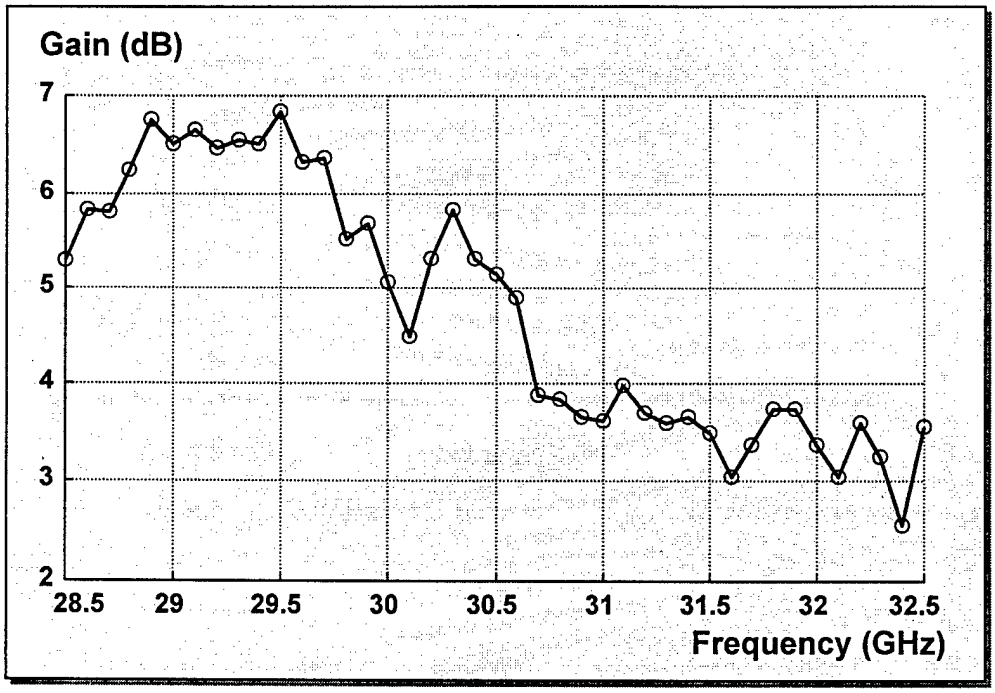

Figure 5. 17

30GHz Perpendicular Patch Gain Measurement Results

Using the estimated 7.015dBi as the directivity, a value of $\eta = 0.76 \pm 0.08$ is calculated, meaning that 68 to 84 percent of the power fed to the device is radiated in the forward direction. However, it should be noted that this estimate includes all losses within the device (resistive losses in the feedline, coaxial-to-microstrip connector induced losses, mismatches of feed circuit impedance or of polarization, etc...) in addition to the losses incurred by the perpendicular feed mechanism.

5.3.3 RESULTS COMPARISON

Prototype measurement and simulation S-parameter result comparisons are complicated by the *unexpected* resonances discussed in section 5.3.2.1. The resonant frequency of the prototype was higher than for the simulation (~30.4GHz vs 28.406GHz), as expected. In this case the critical coupling was achieved between the feedline and the patch as predicted by the simulation, showing better correlation between simulation and measured results than for the 2GHz perpendicular patch. The impedance bandwidth results seemed to be significantly narrower for the prototype (above 5.08%) than for the simulated model (17.35%); however, the measured bandwidth calculation is strongly affected by the *unexpected* resonances.

The maximum measured cross-polarization level of the prototype was better than that of the simulation (–11.3dB vs –6.6dB), but in the E- and H-planes simulation results were far better (–26.28 and –19.49dB vs –11.56 and –11.3dB, respectively). Co-polarization directive gain evaluations are very similar, but there is almost a 2.5dB difference between the two front/back power ratios. Exactly what caused this latter difference is unknown.

CHAPTER 6

CONCLUSION

6.1 ACCOMPLISHMENTS

The three main objectives to be achieved for the report, as stated in section 1.5, were: the development of a 30GHz antenna array configuration for a fixed-beam portable communications terminal, the study of some microstrip patch antenna design parameters, and the development of a microstrip patch antenna perpendicular feeding method. The following paragraphs will provide a short description of what was achieved with regards to these objectives.

6.1.1 ARRAY CONFIGURATION STUDY

6.1.1.1 ARRAY PATTERNS PROGRAM

The Array Patterns Program, developed with Matlab version 4.2c.1, is a versatile tool that can be used to predict planar array radiation patterns for design and illustration purposes. It inputs calculated or measured radiation pattern cuts from a text file as radiating element data. For each element the x-y coordinates corresponding to the location of the element in the plane of the array and the element's input signal amplitude and phase are entered in another text file, called the array specification file. Two- and three-dimensional radiation patterns can be evaluated and displayed in rectangular or polar/spherical format. Being well documented and written in a widely known programming language, the program can easily be upgraded or modified to suit specific user requirements.

6.1.1.2 ARRAY CONFIGURATION

In chapter 2 an array configuration suitable for fixed-beam portable communication applications at 30GHz was developed. Its small dimension (only 16cm in diameter) makes it ideal for integration in a briefcase size unit. 128 quad electromagnetically coupled (EMC) patch antenna elements arranged in 32 identical linear modules make-up the array. Sidelobe levels of –17.42dB below the main beam and a directivity of 30.07dB were achieved with the array.

6.1.2 DESIGN PARAMETERS

Chapter 3 shows the results of a critical coupling analysis for aperture-fed microstrip patch antennas where the feedline and patch were on parallel substrates. For open-circuited stub lengths varying between 6% and 50% of the feedline's guide wavelength (λ_g) the aperture length was adjusted until critical coupling was achieved. Simulation results were then analyzed to determine various characteristics (impedance bandwidth, frequency variations, directive gain, front-to-back ratio and relative cross-polarization) of the critically coupled antennas. The resulting charts provided a helpful guide for the design of perpendicular substrates microstrip patch antennas at 2GHz and 30GHz.

6.1.3 PERPENDICULARLY-FED PATCH ANTENNAS

6.1.3.1 PERPENDICULAR COUPLER

A microstrip line-to-line coupler, with the two transmission lines on perpendicular substrates, was successfully built and tested to verify the proximity feeding technique. The microstrip feedline, after a 90° mitered bend, ran parallel to the ground plane of the perpendicular substrate where another microstrip transmission line was located. A rectangular aperture was etched in the perpendicular substrate's ground plane to provide coupling between the two lines. Both microstrip lines were terminated with $\lambda_g/4$ open-circuited stubs.

6.1.3.2 2GHz PERPENDICULAR PATCH ANTENNA

A microstrip patch antenna fed from a perpendicular substrate was designed to operate in the 2GHz range. Excellent results were achieved, with the resonant frequency at 2.018GHz and an impedance bandwidth of 1.09%. The gain of the device was measured to be 5.89 ± 0.5dB. Results are comparable with reference [11]. The main differences are the bandwidth (reference states 1.3%) and the back lobe levels, which were much higher for the E-plane in the reference.

6.1.3.3 30GHz PERPENDICULAR PATCH ANTENNA

Another perpendicularly fed microstrip patch antenna was designed to operate in the 30GHz range. The resonant frequency of the patch was 30.48GHz, but $|S_{11}|$ data showed *unexpected* resonances occurring at approximately 1.8GHz intervals. The source of those resonances could not be determined, and measurements were done without this issue being rectified. The antenna's impedance bandwidth is greater than 5.1%; an exact value could not be evaluated because of the *unexpected* resonances.

The measured radiation patterns were very bumpy, with very high cross-polarization levels (up to –8.32dB in the forward hemisphere). A gain of 6.35 ± 0.5dB was evaluated for the perpendicular patch. Although some problems were encountered with the prototype, which could not be resolved within the short period of time that was available, it served to prove the perpendicular substrates aperture coupling feed concept at 30GHz.

6.2 FUTURE WORK

6.2.1 ARRAY PATTERNS PROGRAM

Some improvements could be made to the program, such as a module to calculate theoretical element radiation patterns for common antenna types. The inclusion of mutual coupling effects between array elements could also be considered. Another useful addition would be to develop an automated procedure to vary the amplitude and phase of the signal fed to array elements, to simplify beam steering analysis.

6.2.2 CRITICAL COUPLING ANALYSIS

The critical coupling analysis of chapter 4 was done with Micro-Stripes simulation results. If time and resources are available, these results should be verified by building, testing and analyzing a number of aperture-fed microstrip patch antenna prototypes.

6.2.3 30GHz PERPENDICULAR PATCH ELEMENT

Before an array using the perpendicular proximity feeding technique can be built, follow-on work needs to be done on 30GHz perpendicular patch devices. First, the source of the unexpected resonances must be identified and eliminated. This may possibly be achieved by designing a different way of assembling the antenna. The plastic support could be installed on the ground side of the feed substrate, or replaced with some other type of supporting structure. Another aspect that needs further investigation is the poor polarization purity of the perpendicular patch; cross-polarization levels must be reduced for it to become a viable radiating element. Additional work could then be carried-out to tune the various design parameters until the desired results are achieved.

6.2.4 30GHZ PERPENDICULARLY FED QUAD EMC PATCH

Exactly how the performance of the 30GHz perpendicular patch would translate to a perpendicularly fed quad EMC patch element is unknown at this time. However, the analysis of a few simulated models should provide some good insight into its potential. A prototype can then be designed, built and tested.

6.2.5 128 ELEMENT ARRAY DEVELOPMENT

The eventual development of an array of 128 perpendicularly fed quad EMC patch elements in the rounded grid configuration of chapter 3 would then likely take the following route:

- selection and development of the connection method to be used between the feed network and the modules;
- development of a passive (no amplifiers or other electronic devices) four element module, including the support arrangement required to integrate the modules into the array;
- development of the four element module with amplifier and other required electronic devices, if any; and
- development of the required feed network

REFERENCES

Number	Bibliography
[1]	D.J. Roscoe, J. Carrie, M. Cuhaci, A. Ittipiboon, L. Shafai, and A. Sebak, "A 30 GHz Transmit Array for Portable Communications Terminals", IEEE Antenna and Propagation Society International Symposium 1996, pp. 1116-1119, July 1996.
[2]	D. Roscoe, L. Shafai, A. Ittipiboon, M. Cuhaci, and H.Moheb, "Novel Low Profile Antenna Candidates for EHF Portable Terminals", 1995 IMSC Symposium, Ottawa, Canada, pp. 318-323, June 1995.
[3]	P. Bhartia, K.V.S. Rao, R.S. Tomar, "Millimiter-Wave Microstrip and Printed Circuit Antennas", Artec House, Norwood, MA, 1991.
[4]	R.J. Mailloux, "Phased Array Antenna Handbok", Artec House, Norwood, MA, 1994.
[5]	S. Sanzgiri, D. Bostrom, W. Pottenger, and R.Q. Lee, "A Hybrid Tile Approach for Ka Band Subarray Modules", IEEE Transactions on Antennas and Propagation, vol. 43, no. 9, pp. 953-959, Sep. 1995.
[6]	D.W. Griffin and A.J. Parfitt, "Electromagnetic Design Aspects of Packages for MMIC-Based Arrays w/ Integrated Antenna Elements", IEEE Transactions on Antennas and Propagation, vol. 43, no. 9, pp. 927-931, Sep. 1995.
[7]	D.E. Riemer, "Packaging Design of Wide-Angle Phased-Array Antenna for Frequencies Above 20 GHz", IEEE Transactions on Antennas and Propagation, vol. 43, no. 9, pp. 915-920, Sep. 1995.
[8]	R.J. Mailloux, "Array Elements and Architecture of Printed Circuit Antenna Arrays", IEEE MTT-S Newsletter, pp. 29-32, Summer 1988.
[9]	J.A.Kinzel, B.J. Edward, and D. Rees, "V-Band, Space-Based Phased Arrays", Microwave Journal, pp.89-102, Jan. 1987.
[10]	Antenna Radiation Patterns Software Version 2.1, Far Field, 1995.

[11] P.L. Sullivan, and D.H. Schaubert, "Analysis of an Aperture Coupled Microstrip Antenna", IEEE Transactions on Antennas and Propagation, vol. AP-34, no. 8, pp. 977-984, August 1986.

[12] D.M. Pozar and R.W. Jackson, "An Aperture Coupled Microstrip Antenna with a Proximity Feed on a Perpendicular Substrate", IEEE Transactions on Antennas and Propagation, vol. AP-35, no. 6, pp. 728-731, June 1987.

[13] T. Kitsuregawa, Advanced Technology in Satellite Communication Antennas Electrical & Mechanical Design, Artech House, Norwood MA, 1990.

[14] Microwave Antenna Theory and Design, Edited by S. Silver, Dover Publications Inc., New York, 1965.

[15] http://www.sonnetusa.com/ms/msintro.html

[16] A.C. Buck, and D.M. Pozar, "Aperture Coupled Microstrip Antenna with a Perpendicular Feed", Electronic Letters, Vol. 22, No. 3, pp. 125-126, 30 January 1986.

[17] D.M. Pozar, Microwave Engineering, Addison-Wesley, 1990.

APPENDIX A

ARRAY PATTERNS PROGRAM USER'S GUIDE

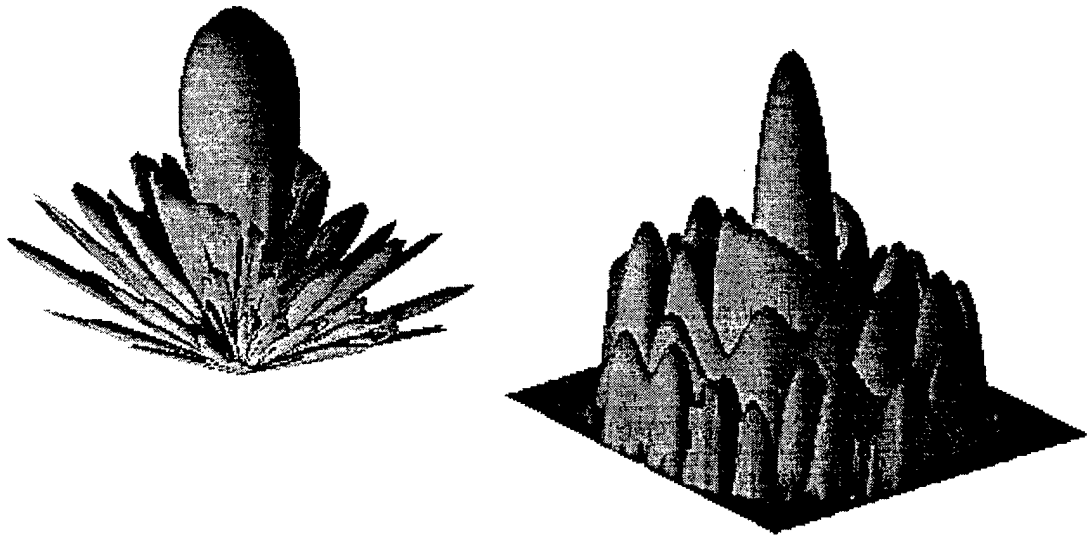

A.1 PROGRAM DESCRIPTION

The Array Patterns Program was written as a design and educational tool to help users in the prediction of antenna array radiation patterns. The program uses array specification and experimental (or calculated) element radiation pattern tabled data files to calculate the array's radiation pattern. It is important to note that mutual coupling effects are not taken into account in radiation pattern calculations. Patterns can then either be displayed in 2-dimensional rectangular and polar constant phi-angle cuts, or in 3-dimensional rectangular and spherical views.

The program was written using the Matlab Version 4.2c.1 for Windows software (some figure management commands will cause error messages to be displayed in the command window if earlier versions are used). The Matlab environment was selected for its ease of programming and readily available graphics display functions. It also has the advantage of being widely used throughout the academic and scientific communities. The program can be easily adapted to suit user specific requirements. Matlab is not a compiled language, therefore the use of function m-files for the computationally intensive

parts of the program is used extensively. This greatly speeds up program execution since function files are compiled when first called, and retained in memory for future use.

Please note that all attempts have been made to make the program "crash proof", but sometimes Matlab itself causes memory protection errors which cannot be prevented. These errors are not due to the Array Patterns Program, but to Matlab/Windows memory management problems.

A.2 USER'S GUIDE

Throughout this guide, actual Matlab programming lines will be written using the `courier font`. Please note that a working knowledge of the Matlab software, and its programming language will be assumed throughout this document.

The Array Patterns Program consists of a main program window (Matlab *figure*) offering five menu options (*Workspace, Parameters, 2-D Display, 3-D Display* and *Help*), each with a number of related sub-menu options. Each menu and sub-menu can be accessed either by clicking on the item with the left mouse button, or by pressing the "Alt" key and holding it while pressing the underlined letter of the desired menu item. Note that the figure must be the active one for the Alt-key selection to work.

Once an item has been selected from the main program window, another window will be opened to carry out the requested action (except for the *Workspace/Save* option). On completion of the action this window will either be closed automatically by the program (when loading or saving the *workspace*), or by the user when selecting the appropriate button (*Cancel*, *Clear*, Close, *Exit* or *Ok*).

A.2.1 Main Program Window

The Array Patterns Program's main program window (figure A.1) is a Matlab *figure* run by *pattern.m*, a script m-file.

Figure A. 1

Main Program Window

Following is a brief description of the *pattern.m* m-file provided to give the reader an idea of how Matlab figures are managed by the program. The other m-files used by the program will not be listed in of this document (a list of all m-files is included at the end

of this document). The comments written as part of the m-files should be sufficient for experienced Matlab programmers.

A.2.1.1 *pattern.m* M-File Description

The *clear* command is used to remove all current variables from the Matlab workspace. *global* variables are used to pass data to and from the program's functions without having to declare them as input or output arguments.

```
clear variables;        % clear old data
clear global;           %

global freq wavenum root1 elemtxt spect programdir workingdir ...
       afrecalc aprecalc eprecalc comment1 comment2 curveres
```

The default parameters are used to establish initial values for variables that could cause execution errors if they were not set.

```
%%%%%%%%%%%%%%%%%%%%%%%%%%%%%%%
% setting default parameters %
%%%%%%%%%%%%%%%%%%%%%%%%%%%%%%%

freq = 30e9;                    % frequency
wavenum = 2*pi*freq/3e8;        % wavenumber
root1 = sqrt(-1);               % complex "j"
elemtxt = 'none loaded';        %
spect = 'none loaded';          %
afrecalc = 'y';                 %
aprecalc = 'y';                 %
eprecalc = 'y';                 %
curveres = 361;                 %
comment1 = '';                  %
comment2 = '';                  %
```

The program files directory (*programdir*), current working directory (*workingdir*) and workspace saving directory (*wksppath*) are initially set to the directory where the program files are located.

```
programdir = cd;        % program files directory
workingdir = cd;        % current working directory
wksppath = cd;          % workspace saving path
wkspcheck = 0;          % workspace saving check variable
```

Windows (Matlab *figures*) are opened in the same manner throughout the program. The opening of the main program window will be used to briefly explain this process.

First, the title to be displayed at the top of the window is set in the *namestr* variable, then the *figflag* function is used to verify if a figure with that name is already open. If it already exists, it is made the active window. If the figure does not already exist, it is created using the *figure* command. The figure's handle is stored in a variable, *mainfig* in this case. The menu items are then set using the *uimenu* command (*callback* is used to set the command(s) to be executed when the menu item is selected). In cases

where graphics are to be displayed in the window the *axes* command is also used to set the portion of the window that will be used by the plotting commands, and to set initial axes properties.

```
%%%%%%%%%%%%%%%%%%%%%%%%%%%%%
% setup main program figure %
%%%%%%%%%%%%%%%%%%%%%%%%%%%%%

namestr = 'Array_Patterns_Program';
[fexist,mainfig] = figflag(namestr);

% create figure if does not already exist
if ~fexist;
  mainfig = figure('MenuBar','none','NumberTitle','off',...
    'Name',namestr,'Resize','on','Units','points',...
    'Position',[5,326,468,1],'BackingStore','on');

% workspace menu
  workspmenu = uimenu(gcf,'Label','&Workspace','Position',1);
  uimenu(workspmenu,'Label','&New...',...
  'Callback','newws');
  uimenu(workspmenu,'Label','&Save',...
  'Callback','savews','Separator','on');
  uimenu(workspmenu,'Label','Save &As...',...
  'Callback','savewsas');
  uimenu(workspmenu,'Label','&Load...',...
  'Callback','loadws','Separator','on');
  uimenu(workspmenu,'Label','&Printer Setup...',...
  'Callback','print -dsetup','Separator','on');
  uimenu(workspmenu,'Label','&Exit','Separator','on',...
  'Callback','exitpgm');

% Parameters menu
  paramenu = uimenu('Label','&Parameters','Position',2);
  uimenu(paramenu,'Label','Operating &Frequency...',...
  'Callback','opfreq');
  uimenu(paramenu,'Label','Load &Data Files...',...
  'Callback','ldfiles');
  uimenu(paramenu,'Label','&Edit Array Element Specifications...',...
  'separator','on','Callback','edelspec');

% 2-D display menu
  display2d = uimenu(gcf,'Label','&2-D Display','Position',3);
  uimenu(display2d,'Label','&Element Pattern Cut...',...
  'Callback','ep2d;');
  uimenu(display2d,'Label','Array &Factor Cut...',...
  'Callback','af2d');
  uimenu(display2d,'Label','Array &Pattern Cut...',...
  'Callback','ap2d');
  uimenu(display2d,'Label','Array Elements &Layout',...
  'Callback','arylyout');

% 3-D display menu
  display3d = uimenu(gcf,'Label','&3-D Display','Position',4);
  uimenu(display3d,'Label','&Element Pattern...',...
  'Callback','ep3d');
  uimenu(display3d,'Label','Array &Factor...','Callback','af3d');
  uimenu(display3d,'Label','Array &Pattern...','Callback','ap3d');

% Help menu
  helpmenu = uimenu(gcf,'Label','&Help','Position',5);
  uimenu(helpmenu,'Label','&About','Callback','about');

% Set flag for active window
  set(mainfig,'visible','on');

end
```

A.2.2 Workspace Menu

The *Workspace* menu (figure A.2) is used for clearing, saving and loading Matlab's workspace, and for exiting the program. The workspace is where Matlab stores all variables used by m-files and by the command window.

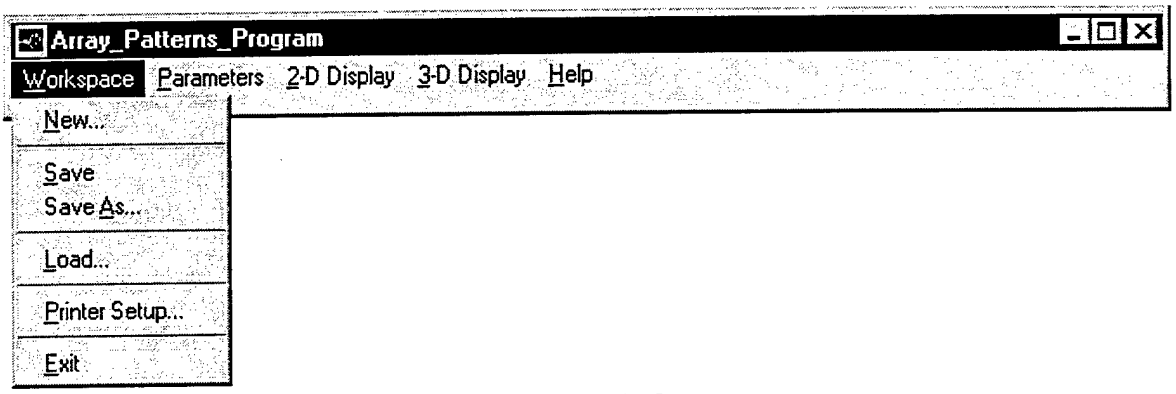

Figure A. 2

Workspace Menu

A.2.2.1 New

Pressing the *Clear* button after selecting *New* from the *Workspace* menu closes all program windows, removes all current data from memory and then restarts the program. The *New_Workspace* window (figure A.3) is run by *newws.m*, a script m-file.

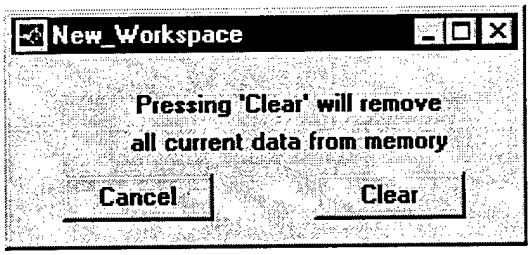

Figure A. 3

New Workspace Window

A.2.2.2 Save

When the *Save* option is selected all current variables (including array specifications, element pattern cuts, and calculated element pattern, array factor and array pattern data) are saved to the file name and path specified in the last *Save As* operation. If a name and path have not been previously set, the program will default to the *Save As*

option. Note that if 3-D patterns with high mesh resolutions have been calculated, saving the workspace will require a large amount of disk space. The *Save* option is run by *savews.m*, a script m-file.

A.2.2.3 Save As

The *Save As* option enables the user to select a file name and path where all current variables will be saved. The *Save_Workspace_As* window is run by *savewsas.m*, a script m-file.

A.2.2.4 Load

Load enables you to bring back into the workspace previously saved data. The *Load_Workspace* window is run by *loadws.m*, a script m-file.

A.2.2.5 Printer Setup

Printer Setup enables the user to select the printer to be used, and to set its properties.

A.2.2.6 Exit

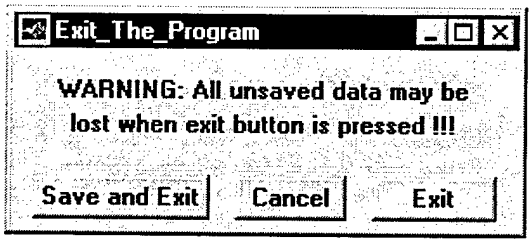

Figure A. 4

Exit Window

Selecting *Exit* brings up a dialog box offering three choices to the user: to save the current data before leaving the program, to cancel the operation, or to exit the program. Note that he *Exit* option will close the program, and all unsaved data will be lost. When either *Save and Exit* or *Exit* is selected, all program windows will be closed. The *Exit_The_Program* window (figure A.4) is run by *exitpgm.m*, a script m-file.

A.2.3 Parameters Menu

The *Parameters* menu (figure A.5) is used for setting the operating frequency used by the program, for loading element pattern and array specification files, and for editing (or creating) array specification files.

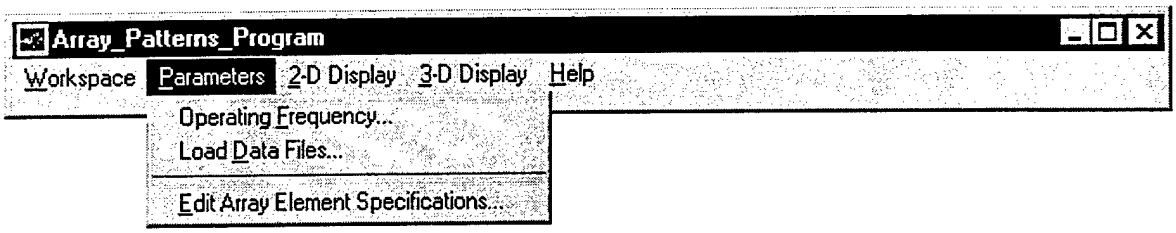

Figure A. 5

Parameters Menu

A.2.3.1 Operating Frequency

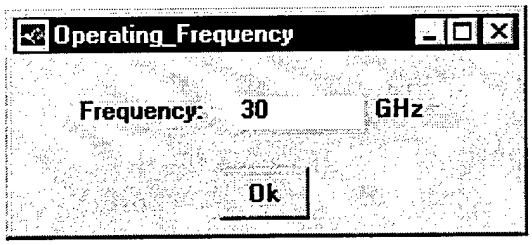

Figure A. 6

Operating Frequency Window

The operating frequency is used in the evaluation of the array factor and array radiation pattern data. The user only needs to change the value in the editable text box to the desired frequency then press the *Ok* button to continue. The default value is set at 30 GHz. The *Operating_Frequency* window (figure A.6) is run by *opfreq.m*, a script m-file.

A.2.3.2 Load Data Files

The *Load Data Files* option is used to select and load the element radiation pattern and array specification files. The *Element Pattern* file contains the constant-ϕ cuts, while the array specification file details the array elements location, respective signal amplitude and relative phase. They are simple text files that must follow the formats detailed in the next two paragraphs. Any text editor can be used to build the files. Either *tabs* or *spaces* can be used to separate data columns. The *Load_Data_Files* window (figure A.7) is run by *ldfiles.m*, a script m-file. The *loaddata.m* function is then used to select and load the appropriate data files.

Note: The element pattern file names must be terminated with a ***.dat*** extension and the array specification file must have a ***.spc*** extension.

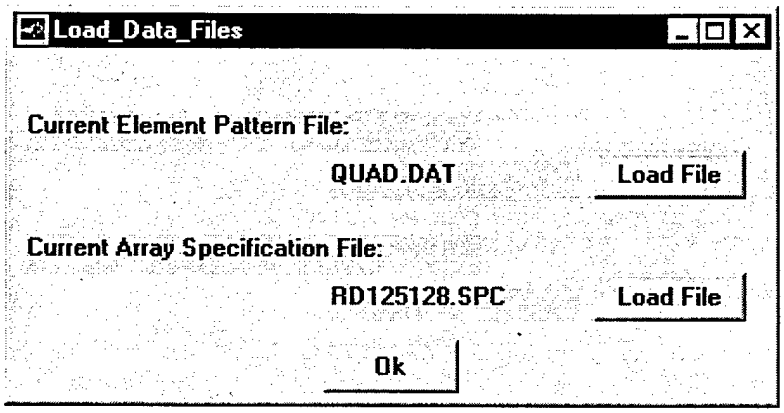

Figure A. 7

Load Data Files Window

A.2.3.2.1 Element Pattern Files

The element pattern file (see figures A.8 and A.9) contains a variable number of columns per line. The first column represents the angle (θ) in degrees of the data points forming the cuts, while subsequent columns contain pattern power magnitude in Decibels (dBs) for the constant-ϕ cuts. The ϕ angles of the cuts must cover the 0 to 180 degrees range (the $\phi = 180°$ cut is not included since it is the same as the $\phi = 0°$ cut). The $\phi = 0°$ cut must be in the second column, and the other cuts must be in order of monotonically increasing ϕ angle. Note that the accuracy of the array radiation patterns generated by the program will generally increase with the number of constant-ϕ cuts used, and the program does not limit the number of constant-ϕ cuts.

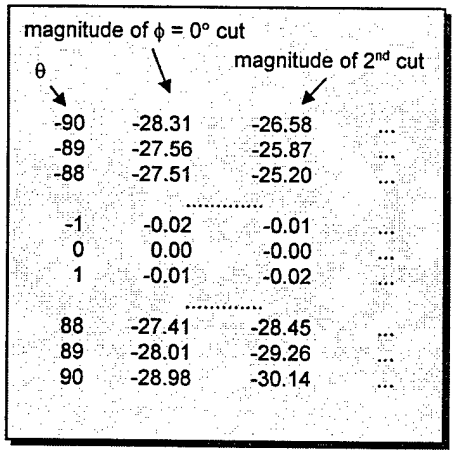

Figure A. 8
Sample Element Pattern File Data

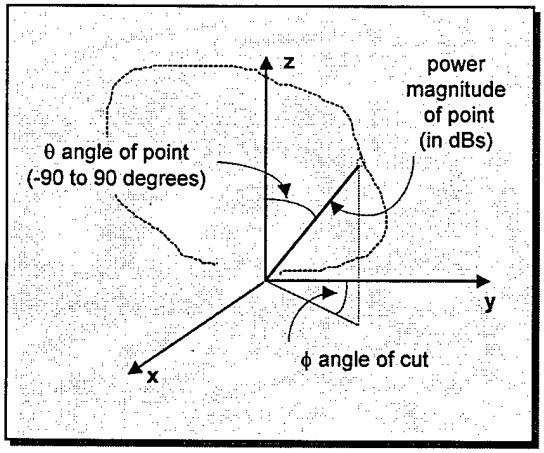

Figure A. 9
Element Pattern Data Geometry

Upon loading the element pattern file an m-file function (*normelem.m*) will be called to normalize the pattern files, so that the overall maximum value of the pattern is set to 0dB. It will then convert the pattern magnitude values into volts, as program pattern evaluations are carried-out in voltage. As well, *normelem.m* will ensure the pattern cuts go from $\theta = -90°$ to $\theta = 90°$ by increments of 1 degree. This is accomplished by removing magnitude data outside the $-90° < \theta < 90°$ range, by padding it with 0.0001V if the file's cuts do not cover the full $-90° < \theta < 90°$ range, and by using linear interpolation to fill-in the 1° increments.

A.2.3.2.2 Array Specification Files

The array specification file (see figures A.10 and A.11) must contain four columns per line. The first two columns represent the *x* and *y* coordinates of the element's location in meters. The third column contains the element's excitation amplitude in volts, and the last column is for the element's relative phase in degrees. Only planar arrays made of identical elements (with the same x-y orientation) can be simulated by the program, and they are assumed to be located in the $z = 0$ plane. The number of elements forming the array is not limited by the program.

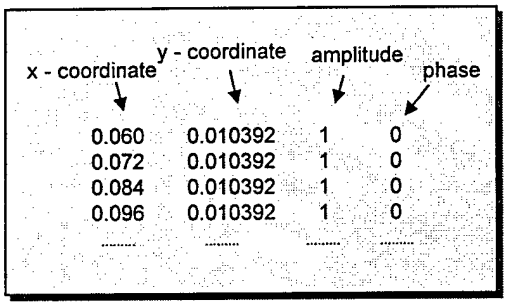

Figure A. 10
Sample Array Specification Data

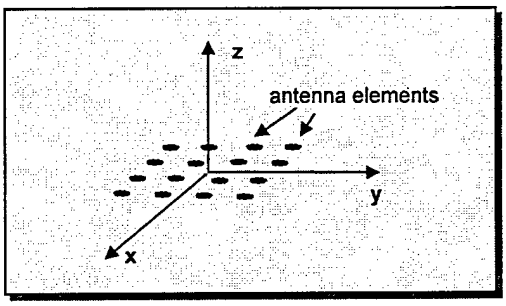

Figure A. 11
Array Specification Data Geometry

A.2.3.3 Edit Array Element Specifications

This module can be used either to modify an existing array specification file, or to create a new file. The window (figure A.12) displays the name of the file currently loaded into the workspace, or creates a *no_name.spc* file if there is no array specification file loaded into the workspace. The *Load file* button enables the user to load a file from disk.

The data fields show the element number, the x and y coordinates, the voltage amplitude, and relative phase for the element. These fields can be edited simply by clicking on the editable text box with the mouse, then using the keyboard to change the field to the desired value. Changing the value of the element number box and pressing

Enter moves the display to the specified element number, or to the first or last elements if the number entered is out of the valid range of element numbers. The << and >> buttons move the display to the previous or next element, respectively. The *<Add* and *Add>* buttons are used to insert a new element before or after the element currently being displayed. *Remove* deletes the displayed element and *Save new file* saves the edited file to a user specified file name and location. The *Ok* button closes the window. *edelspec.m*, a script m-file, runs the *Edit_Array_Element_Specifications* window.

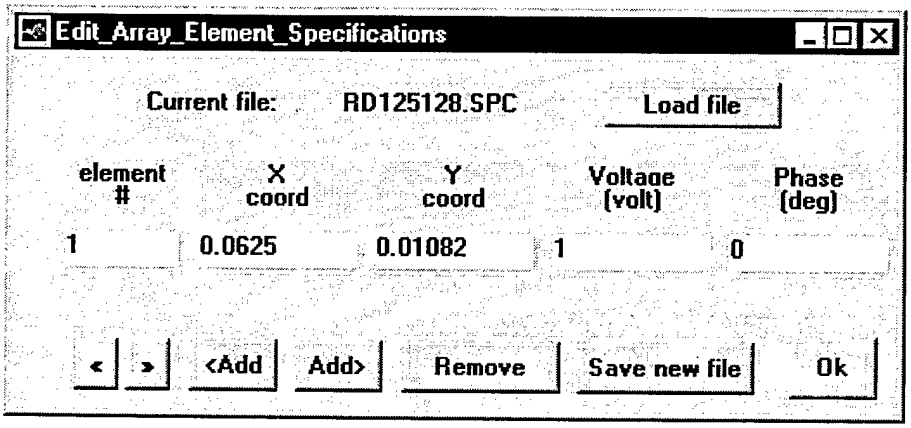

Figure A. 12

Edit Array Element Specifications Window

Note: The workspace array specification file is modified "on-the-fly" as changes are made to the element data fields. Therefore, changes made to the file currently loaded into the workspace could be lost, if they are not saved to disk.

A.2.4 2-D Display Menu

The *2-D Display* menu (figure A.13) is used for calculating and displaying two-dimensional element radiation pattern, array factor and array radiation pattern cuts, and to display the array elements layout.

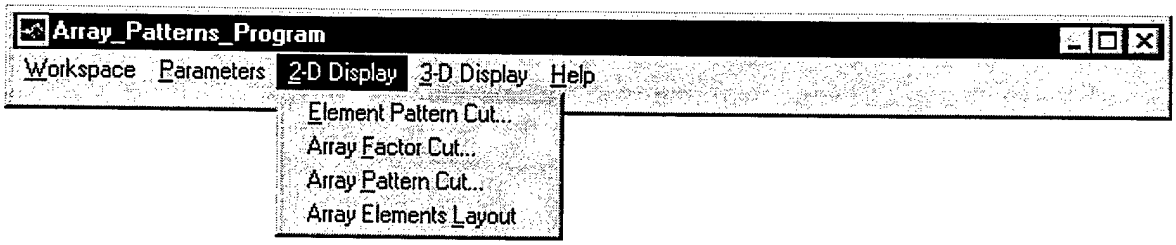

Figure A. 13

2-D Display Menu

A.2.4.1 2-D Element Pattern

This module is used to calculate and display 2-D element radiation pattern constant-ϕ angle cuts. Note that if the user attempts to enter the module without *an element pattern* data file being loaded into the workspace, a dialog box advising that this file must be loaded will appear instead of the module's window. *ep2d.m*, a script m-file, runs the *2-D_Element_Pattern* window (figure A.14). The figure at the top of next page shows an example of an element pattern cut, with rectangular coordinates display.

Once into the module, the user can specify the ϕ-angle of the cut and the θ range over which the pattern will be evaluated. Two comment lines can also be entered; these comments will be displayed below the pattern plot after *Display* has been pressed.

Pressing the *Display* button calls on the *ep2dcl.m* function m-file to evaluate the element pattern. The function uses linear interpolation to evaluate the pattern magnitude within the desired θ range for the specified constant-ϕ cut.

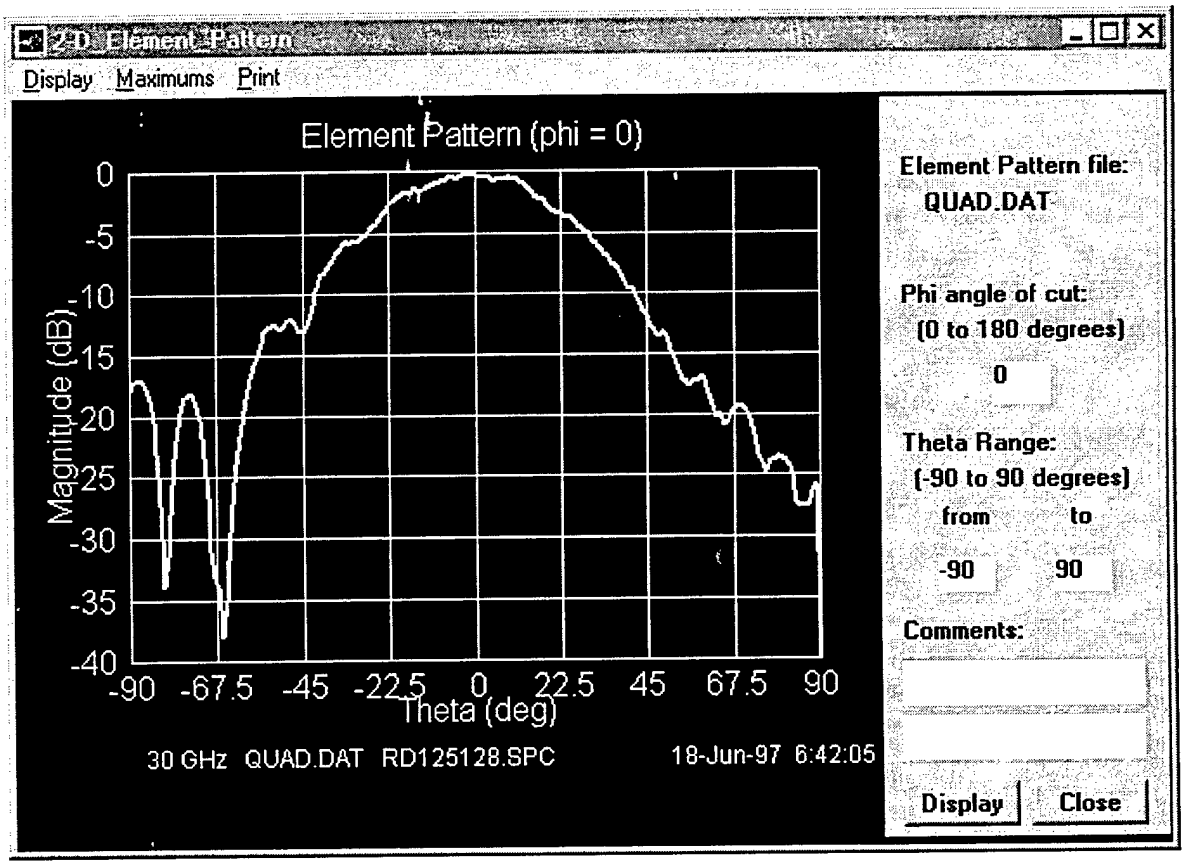

Figure A. 14

2-D Element Pattern Window

A.2.4.2 2-D Element Pattern Window Menus

Three menus are located at the top of the *2-D_Element_Pattern* window: *Display*, *Maximums* and *Print*.

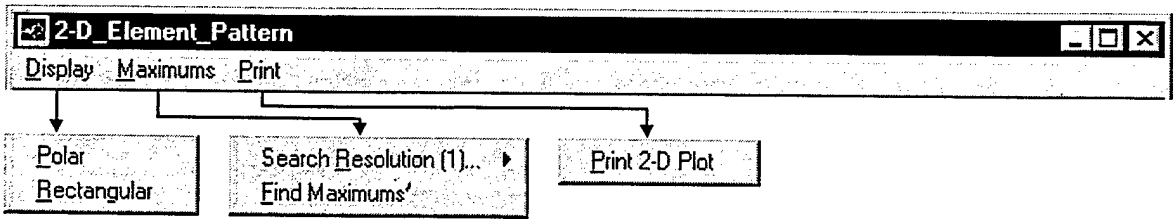

Figure A. 15

2-D Element Pattern Window Menus

A.2.4.2.1 Display Menu

The *Display* menu offers a choice between polar and rectangular representations of the element pattern. In the rectangular representation (see figure A.14) the element pattern magnitude in dBs is shown on the vertical axis, while the theta angle is represented on the horizontal axis. The *rect2d.m* function is used to produce the display. For an example of the polar representation, see the 2-D Array Factor section.

A.2.4.2.2 Maximums Menu

The *Maximums* menu is used to set the maximums search resolution and to find the maximums of the currently displayed element pattern cut. The maximums search algorithm sequentially looks at each of the 361 points making up the displayed curve to see if, within the search range, there are any points with a higher magnitude than the point currently being considered. The search range includes the number of points set by the

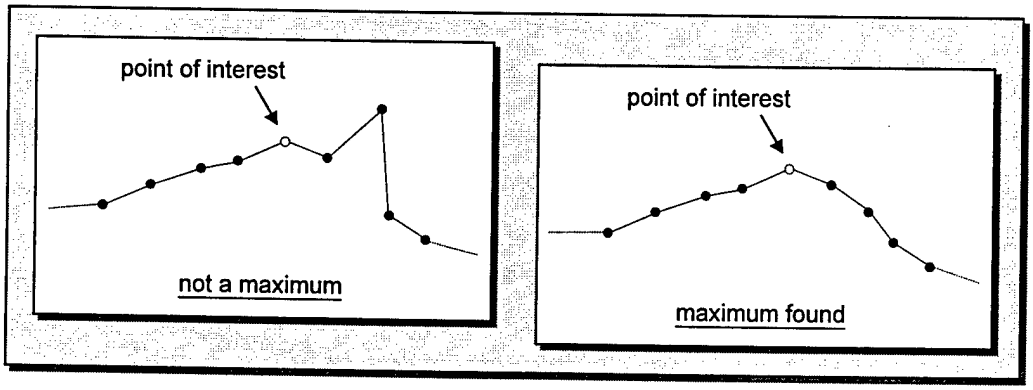

Figure A. 16

Maximums Search

search resolution option on both sides of the point of interest (the number in parenthesis next to the *Search Resolution* menu option is the current search resolution). For example (see figure A.16), if the search resolution is set to 4: the range will include 4 points to the left and 4 to the right of the point of interest. If any of those is higher than the point of interest, then it is not a maximum. However, if none are higher than the point of interest a maximum has been found. By selecting a higher search resolution, the user can "filter-out" some of the minor spikes showing on the pattern plot.

The 2-D Pattern Maximum(s) window (figure A.17) is run by *maxfnct2.m*, a script m-file. After searching for maximums, it displays how many maximums were found and an evaluation of the 3dB beamwidth of the pattern. The theta locations and magnitude of the maximums are displayed in the window's white background areas. All of the maximums are sorted by order of magnitude, from the highest to the lowest, and can be cycled through using the << and >> buttons. The *Save to file* button enables the user to save the tabled results to a text file for future use, or for printing. The *Ok* button closes the window.

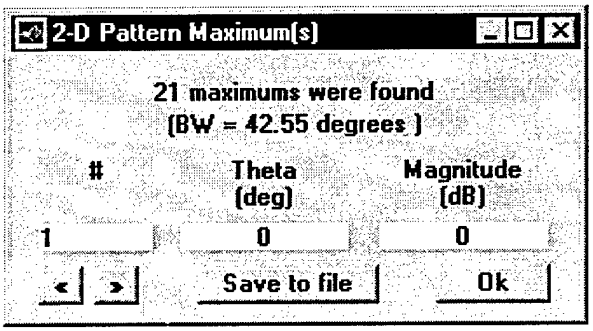

Figure A. 17

2-D Patterns Maximum(s) Window

A.2.4.2.3 Print Menu

The *Print* menu is used to print the curve, grid lines, comments and other details shown in the display area of the window to the current Windows default printer.

A.2.4.3 2-D Array Factor

This module is used to calculate and display 2-D array factor constant-ϕ angle cuts. The array factor is the radiation pattern of an array of isotropic elements. Note that if the user attempts to enter the module without an array specification data file being loaded into the workspace, a dialog box advising that this file must be loaded will appear instead of the module's window. The *2-D_Array_Factor* window (figure A.18) is run by *af2d.m*, a script m-file. The module's menus and buttons are the same as for the *2-D_Element_Pattern* window.

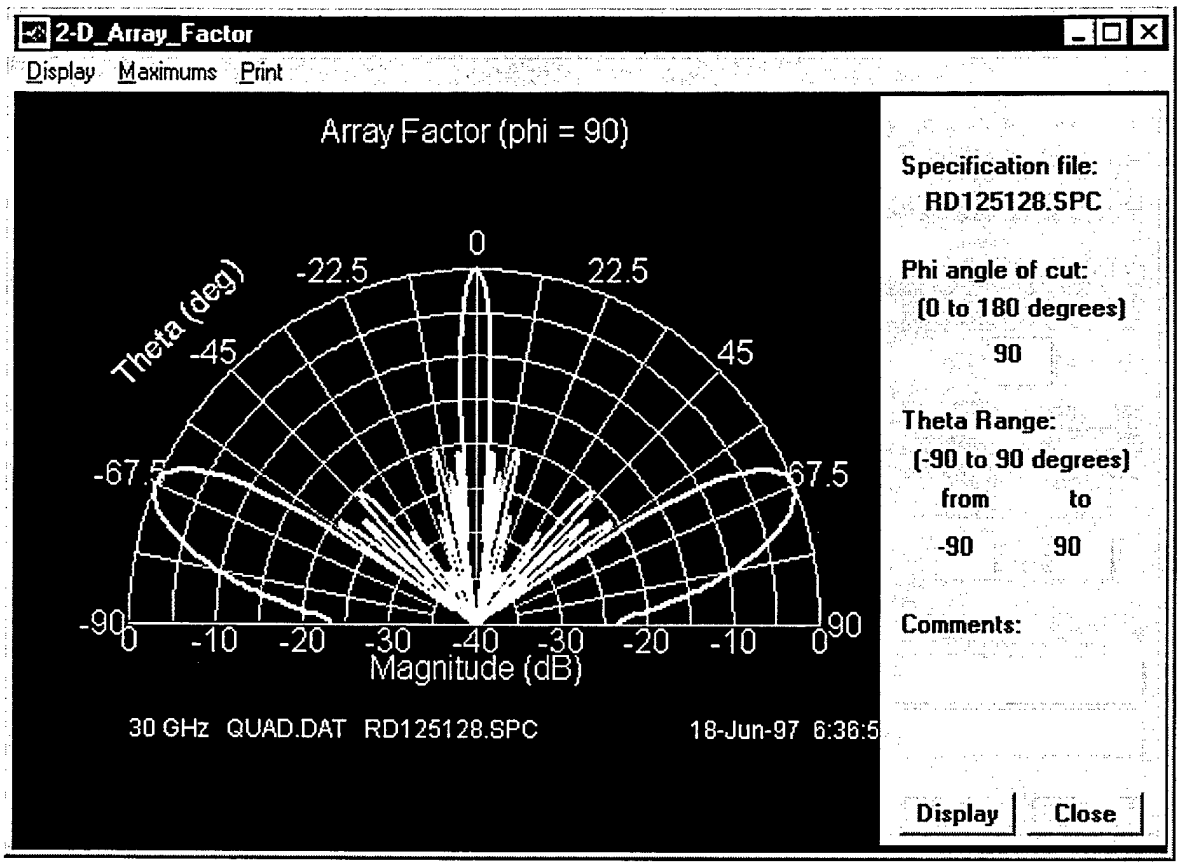

Figure A. 18

2-D Array Factor Window

Figure A.18 shows a polar representation where the semi-circular grid lines represent constant array factor magnitudes in dBs, while the straight grid lines represent constant theta angles. The *polar2d.m* function m-file is used to produce the display.

Pressing the *Display* button calls on the *af2dcl.m* function m-file to evaluate the array factor. The following equation is used to calculate the array factor *(AF)* for each point of the cut, in dBs:

$$AF = 20\log_{10}\left(\sum_{i=1}^{N} V_i \cdot e^{j\varphi_i}\right)$$

where:

N is the total number of elements

V_i is the voltage amplitude of the element

$\varphi_i = k\,x_i \sin(\theta)\cos(\phi) + k\,y_i \sin(\theta)\sin(\phi) + \beta_i$

$k = 2\pi/\lambda$ is the wavenumber

(x_i, y_i) is the position of the element in the $z = 0$ plane

β_i is the relative phase of the element

A.2.4.4 2-D Array Pattern

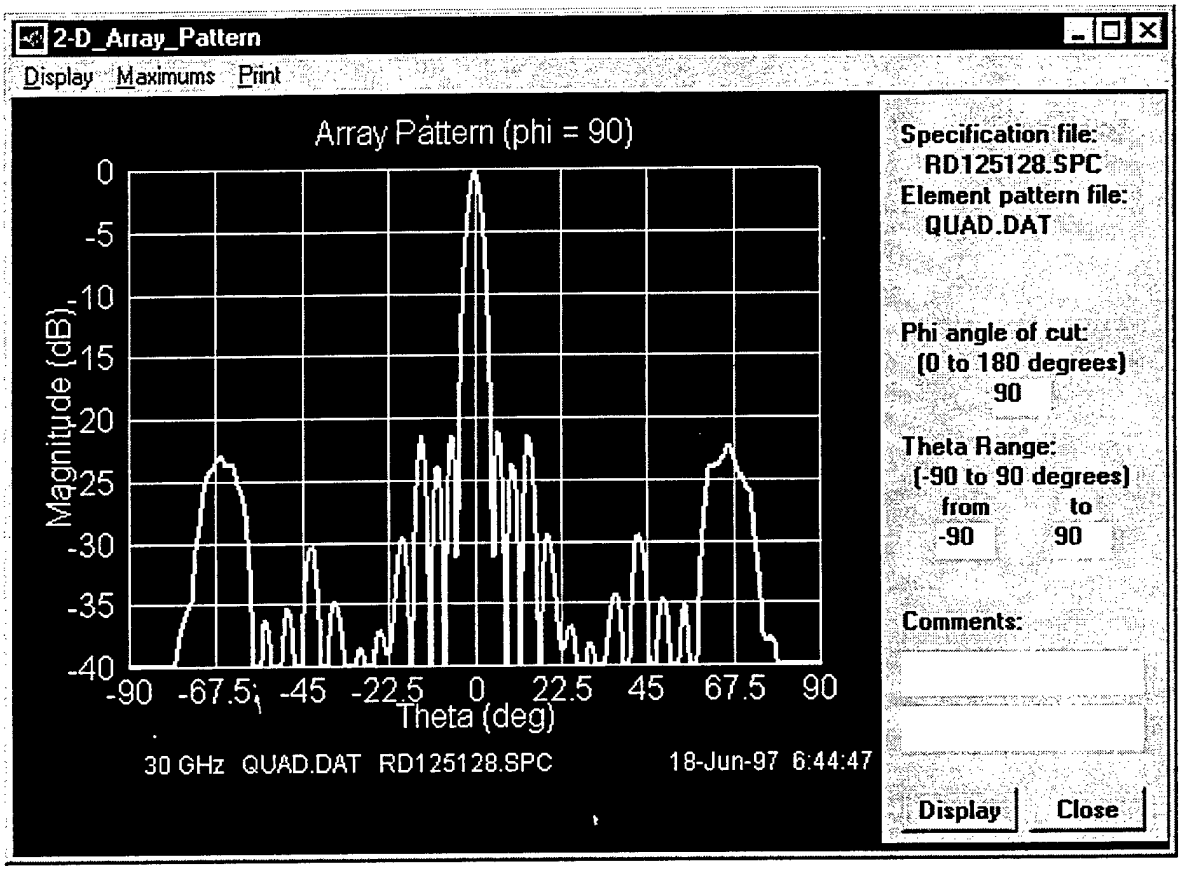

Figure A. 19

2-D Array Pattern Window

This module is used to calculate and display 2-D array radiation pattern constant phi angle cuts. Note that if the user attempts to enter the module without the array specification, and element pattern data files being loaded into the workspace, a dialog box advising that they must be loaded will appear instead of the module's window. The *2-D_Array_Pattern* window (figure A.19) is run by *ap2d.m*, a script m-file. The module's menus and buttons are the same as for the *2-D_Element_Pattern* window.

Pressing the *Display* button calls on the *ap2dcl.m* function m-file to evaluate the array pattern. The following equation is used to calculate the array pattern *(AP)* for each point of the cut, in dBs:

$$AP = 20 \log_{10} \ (EP \times AF)$$

where

EP is the radiation pattern of an array element

AF is the array factor (radiation pattern of a planar array of isotropic elements)

A.2.4.5 Array Elements Layout

The array element layout module is used to display the array lattice. Note that if the user attempts to enter the module without the array specification data file being loaded into the workspace, a dialog box advising that it must be loaded will appear instead of the module's window. The *Array_Elements_Layout* window (figure A.20) is run by *arylyout.m*, a script m-file.

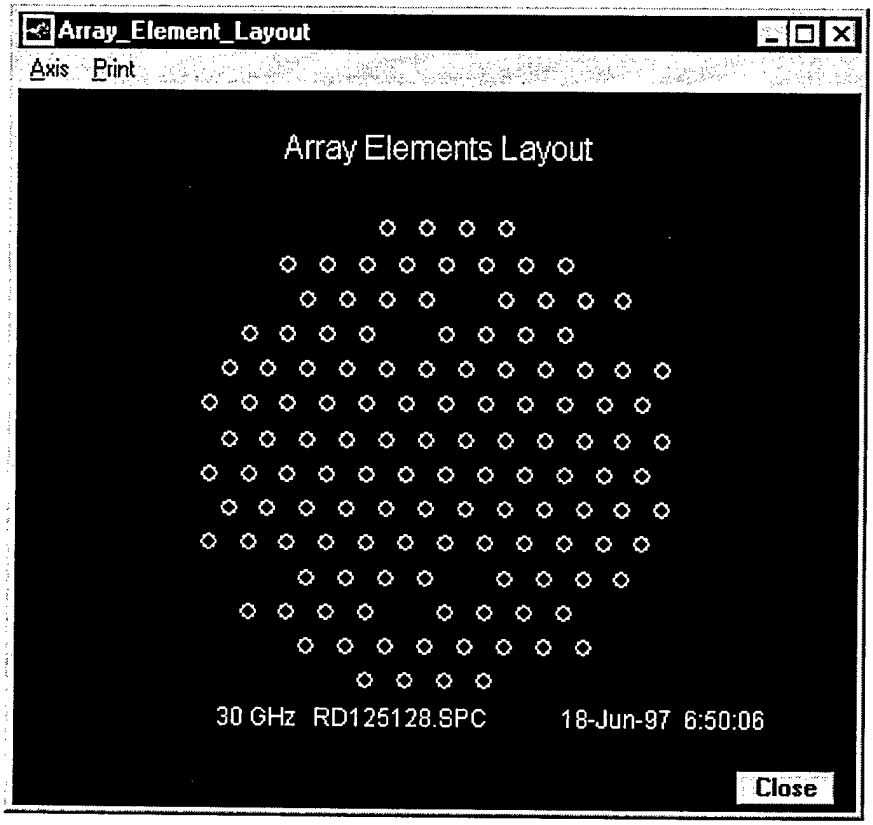

Figure A. 20

Array Elements Layout Window

Figure A.20 shows an example of a planar array made of 128 elements in a partially filled hexagonal grid. The *Axis* menu is used to toggle between the *Axis on* and *Axis off* options (** indicates which option is currently selected). The *Print* menu is used to print the array elements layout currently being displayed. The *Close* button exits the module.

A.2.5 3-D Display Menu

The *3-D Display* menu (figure A.21) is used for calculating and displaying three-dimensional element radiation pattern, array factor and array radiation patterns.

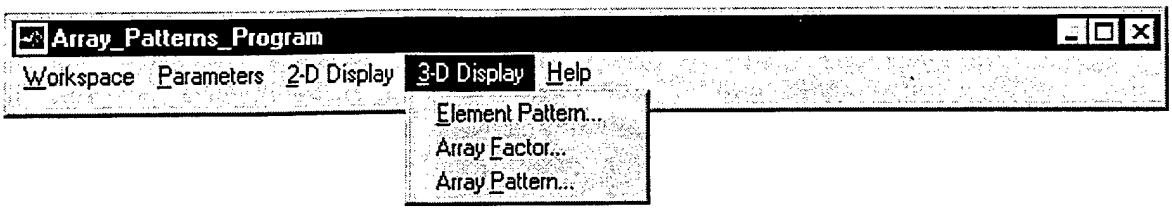

Figure A. 21

3-D Display Menu

A.2.5.1 3-D Element Pattern

This module is used to calculate and display 3-D element radiation patterns. Note that if the user attempts to enter the module without the element pattern data file being loaded into the workspace, a dialog box advising that it must be loaded will appear instead of the module's window. The *3-D_Element_Pattern* window (figure A.22) is run by *ep3d.m*, a script m-file.

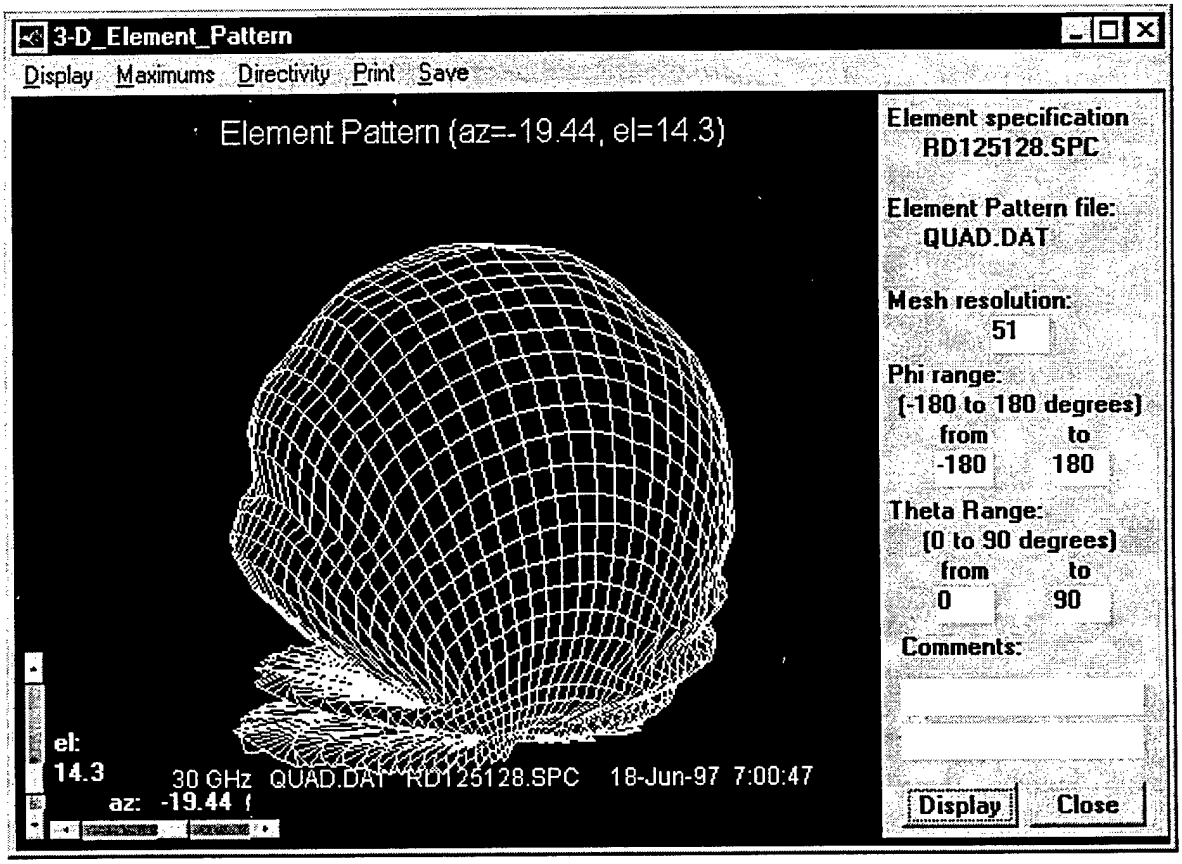

Figure A. 22

3-D Element Pattern Window

Pressing the *Display* button calls on the *ep3dcl.m* function m-file to evaluate the element pattern. The first part of the function evaluates the rectangular coordinate (*x* and *y*) limits corresponding to the specified *phi* and *theta* ranges, so that only the portion of the pattern which is included in this area can be evaluated. This area is then subdivided into a rectangular grid with the number of points in each direction set equal to the specified mesh resolution. For each point of this grid the phi and theta angles are evaluated, then linear interpolation is used to evaluate the pattern magnitude in the same manner as for the 2-D element pattern. The 3-D spherical pattern is then calculated using the rectangular coordinate values. Note that the phi angle range is defined counter-clockwise.

A.2.5.2 3-D Element Pattern Window Menus

Five menus are located at the top of the *3-D_Element_Pattern* window (figure A.23): *Display*, *Maximums, Directivity, Print,* and *Save*.

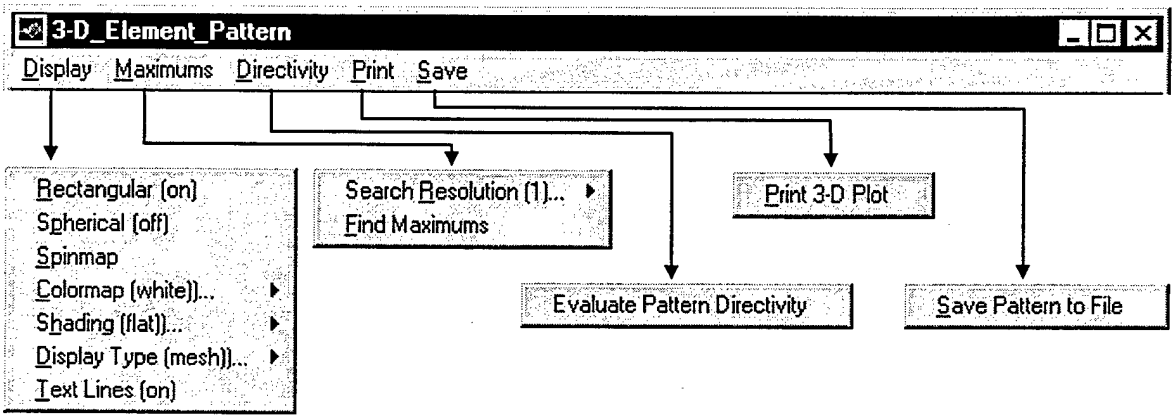

Figure A. 23

3-D Element Pattern Window Menus

A.2.5.2.1 Display Menu

The *Display* menu offers a choice between rectangular (default) and spherical representations of the element pattern. The *3-D_Element_Pattern* of figure A.22 shows an example of a spherical representation. The distance of each point from the origin of the coordinate system represents the element pattern magnitude in dBs, and the phi and theta angles are as in figure A.24. The *polar3d.m* function is used to produce the display. For an example of the rectangular representation, see the 3-D Array Factor section.

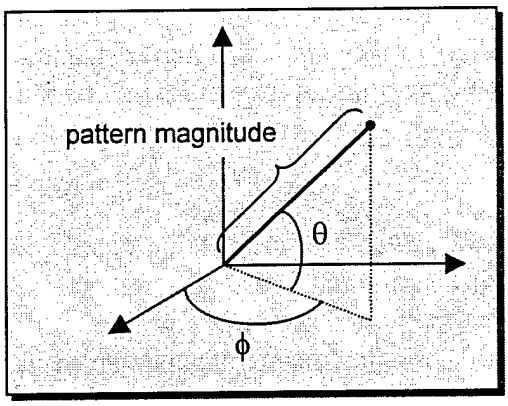

Figure A. 24

Spherical Representation

The *Spinmap* option cyclically rotates the color map for about five seconds. This provides the user with a better view of the pattern surface characteristics (works best with the following settings: *colormap-jet, shading-interp, display type-surf*). Note that *Spinmap* may not work on certain systems, or when the screen's color resolution is too high (try with 256 colors). The *Text Lines* option selects whether the comments, filenames, date and time information is shown or not. The two sliders in the display area are used to set the graph's viewpoint (see Matlab's *view* command).

Note that changes made using the *Display* menu options and the viewpoint sliders will not take effect until the display button is pressed, except for *Spinmap*. Users should refer to the Matlab Reference Guide for more information on the 3-D display settings.

A.2.5.2.2 Maximums Menu

The *Maximums* menu is used to set the maximums search resolution and to find the maximums of the currently displayed element pattern. The maximums search algorithm sequentially looks at each of the points making up the displayed surface to see if, within the search area, there are any points with a higher magnitude than the point currently being considered. The search area includes the number of points set by the

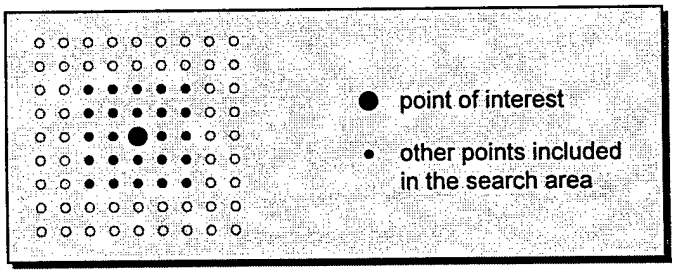

Figure A. 25

3-D Maximums Search

search resolution option around the point of interest. Figure A.25 shows an example for a search resolution of 2, if any of those points is higher than the point of interest it is not a maximum, but if none are higher then a maximum has been found. By selecting a higher search resolution, the user can "filter-out" some of the minor spikes showing on the pattern plot.

The *3-D Pattern Maximum(s)* window (figure A.26) is run by *maxfnct3.m*, a script m-file. After searching for maximums, it displays how many were found and an evaluates the 3 dB beamwidth of the pattern along the *x* and *y* axes. The phi and theta locations, as well as the magnitude of the maximums are then displayed in the white background areas. The maximums are sorted by order of magnitude, from the highest to the lowest, and can be cycled through using the << and >> buttons. The *Save to file* button enables the user to save the tabled results to a text file for future use, or for printing. The *Ok* button closes the window.

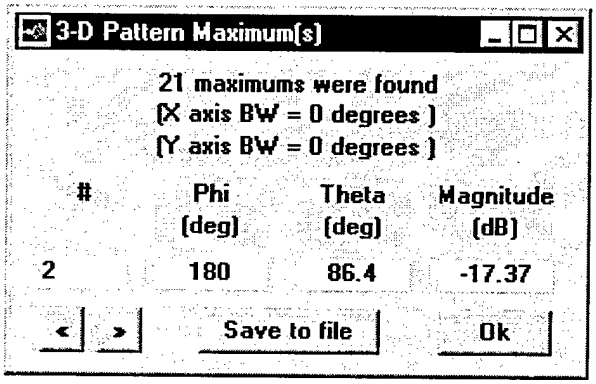

Figure A. 26

3-D Pattern Maximum(s) Window

A.2.5.2.3 Directivity Menu

This menu item is used to estimate the currently displayed pattern's directivity (also called directive gain). The general equation for evaluating the directivity of an antenna array in the (θ_O, ϕ_O) direction is defined as:

$$D(\theta,\phi) = \frac{4\pi P(\theta_0,\phi_0)}{\int_0^{360°}\int_0^{180°} P(\theta,\phi)\sin\theta\, d\theta\, d\phi}$$

where $P(\theta,\phi)$ is the power pattern of the array.

In this application the surface integration is evaluated numerically over the $0 < \theta < 90°$ and $-180° < \phi < 180°$ ranges since we are only looking at planar arrays'

radiation above the $z = 0$ plane. The directivity is evaluated in the direction, (θ_O, ϕ_O), of the pattern's maximum power value. The algorithm follows these steps (see figure A.27):

a. evaluate power pattern constant-ϕ cuts at one degree increments (360 half-cuts), each half-cut having $\theta = 1°$ increments;

b. normalize the cuts so that the maximum value is 0dB;

c. convert back to power ($10^{dB/10}$);

d. for each point of the cuts: evaluate the surface of the corresponding projection on a unit radius half-sphere;

e. evaluate the total power radiated by the array by summing the product of the surface corresponding to each point by its power magnitude; and

f. the directivity in dB is then equal to $10 \log_{10}\left(\frac{2\pi}{\text{total radiated power}}\right)$.

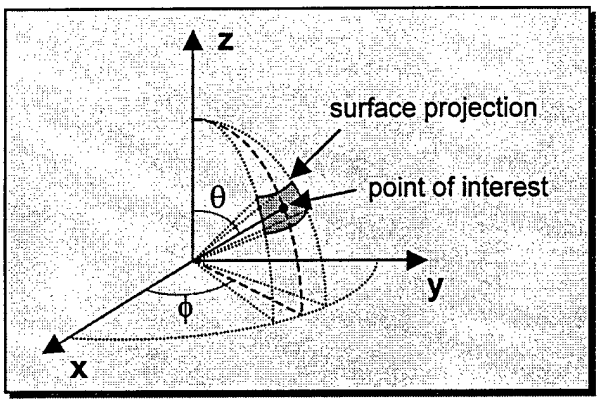

Figure A. 27

Directivity Integration

The *Pattern_Directivity* window is run by *directiv.m*, a script m-file. Note that three different functions are used to evaluate the directivity for element patterns (*epdirect.m*), array factors (*afdirect.m*) and array radiation patterns (*apdirect.m*).

A.2.5.2.4 Print Menu

The *Print* menu is used to print the pattern, comments and other details shown in the display area of the window to the current Windows default printer.

A.2.5.2.5 Save Menu

With this option the user can save the desired number of element radiation pattern, array factor and array radiation pattern cuts (dB) to a file. The format of this data is as described in section A.2.3.2.1 (element pattern files). This feature is especially useful

when designing arrays made of identical sub-arrays (or modules) since the array radiation pattern of a sub-array can be saved to disk and used as the element pattern file to simulate the full array.

The *Saving_Pattern_Cuts* window is run by *savecuts.m*, a script m-file. Note that three different functions are used to save the pattern cuts for element patterns (*selptrn.m*), array factors (*safptrn.m*) and array radiation patterns (*saryptrnt.m*).

A.2.5.3 3-D Array Factor Pattern

This module is used to calculate and display 3-D array factor patterns. The array factor is the radiation pattern of an array of isotropic elements. Note that if the user attempts to enter the module without an array specification data file being loaded into the workspace, a dialog box advising that this file must be loaded will appear instead of the module's window. The *3-D_Array_Factor* window (figure A.28) is run by *af3d.m*, a script m-file. The module's menus and buttons are the same as for the *3-D_Element_Pattern* window.

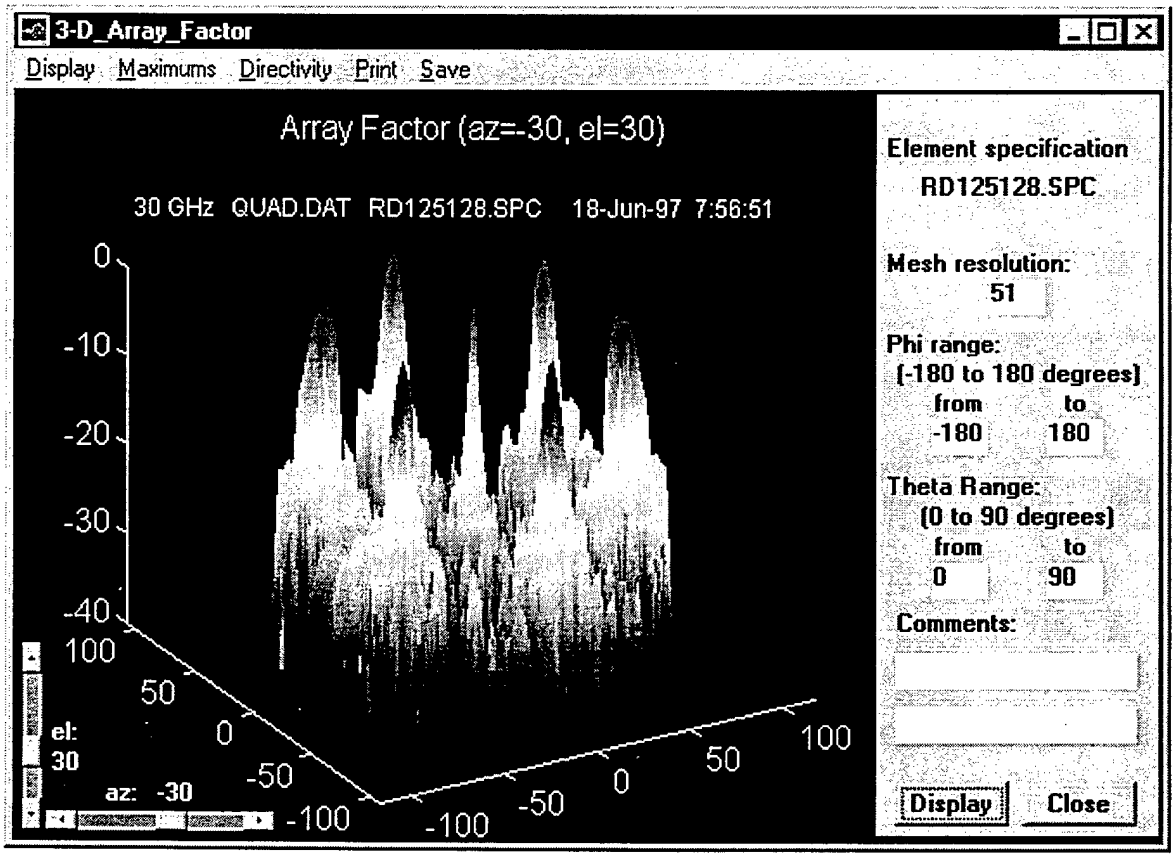

Figure A. 28

3-D Array Factor Window

Figure A.28 shows an example of a rectangular representation where the vertical axis represents the array factor magnitude in dBs, while the other two axes are scaled in degrees See figure A.29 for a graphical representation of the coordinate system. The *rect3d.m* function m-file is used to produce the display.

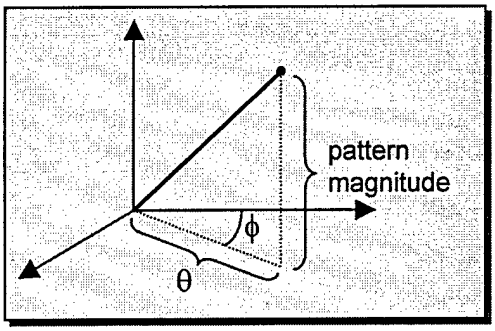

Figure A. 29

3-D Rectangular Representation

Pressing the *Display* button calls on the *af3dcl.m* function m-file to evaluate the array factor. The following equation is used to calculate the array factor *(AF)* for each point of the pattern, in dBs:

$$AF = 20\log_{10}\left(\sum_{i=1}^{N} V_i \cdot e^{j\varphi_i}\right)$$

where:

N is the total number of elements
V_i is the voltage amplitude of the element
$\varphi_i = k\,x_i \sin(\theta)\cos(\phi) + k\,y_i \sin(\theta)\sin(\phi) + \beta_i$
$k = 2\pi/\lambda$ is the wavenumber
(x_i, y_i) is the position of the element in the $z = 0$ plane
β_i is the relative phase of the element

A.2.5.4 3-D Array Pattern

This module is used to calculate and display 3-D array radiation patterns. Note that if the user attempts to enter the module without the array specification and element pattern data files being loaded into the workspace, a dialog box advising that they must be loaded will appear instead of the module's window.

Figure A.30 shows an example of the rectangular representation of an array radiation pattern. In this example the *phi* and *theta* ranges were set to zoom-in on a portion of the pattern, to have a closer look at a particular lobe. Notice that, because the program normalizes all patterns, the lobe's main peak now appears to be at 0 dB.

The *3-D_Array_Pattern* window (figure A.30) is run by *ap3d.m*, a script m-file. The module's menus and buttons are the same as for the *3-D_Element_Pattern* window.

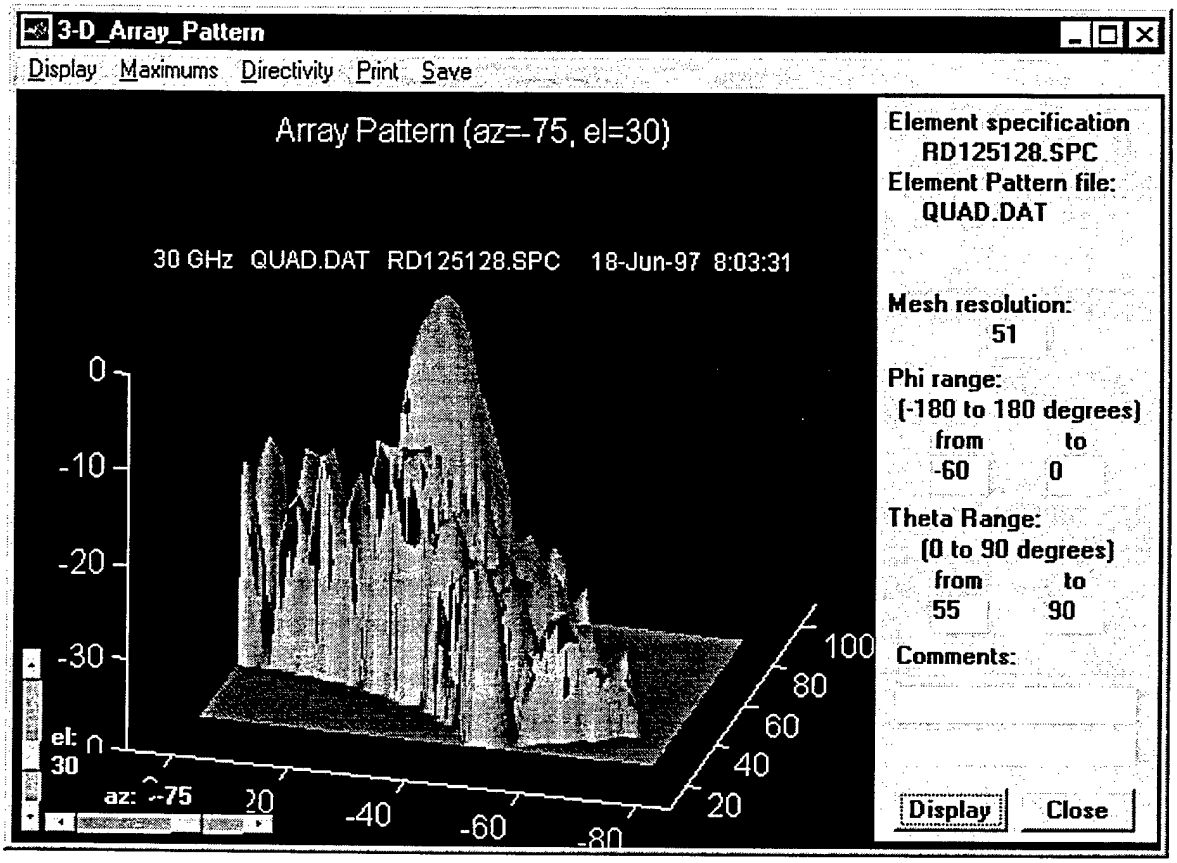

Figure A. 30

3-D Array Pattern Window

Pressing the *Display* button calls on the *ap3dcl.m* function m-file to evaluate the array pattern. The following equation is used to calculate the array pattern *(AP)* for each point of the pattern, in dBs:

$$AP = 20 \log_{10} \ (EP \times AF)$$

where

EP is the radiation pattern of an array element

AF is the array factor (radiation pattern of a planar array of isotropic elements)

A.2.6 Help Menu

The *Help* menu (figure A.31) contains only one option, which gives information about the program.

Figure A. 31

Help Menu

A.2.6.1 About

About (figure A.32), run by the *about.m* script m-file provides information on the program version, date, and author.

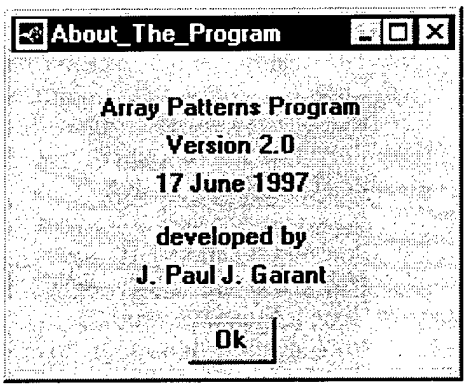

Figure A. 32

About Window

A.2.7 Program Files List

Table A.1 lists all the files used by the program, along with a very brief description of what it does. The letter included in square brackets at the beginning of the description indicates whether the file is a script [S] or a function [F] m-file.

A.2.8 References

The following documents were consulted during the program's development phase:

- Antenna Radiation Patterns Software Version 2.1 User's Guide, Far Field, 1995
- Matlab Reference Guide, The MathWorks, Inc., Natik, Mass., 1995

File Name	Description
about.m	Version, date and author information. [S]
af2d.m	2-D array factor window control. [S]
af2dcl.m	2-D array factor calculation. [F]
af3d.m	3-D array factor window control. [S]
af3dcl.m	3-D array factor calculation. [F]
afdirect.m	Array factor directivity calculation. [F]
ap2d.m	2-D array radiation pattern window control. [S]
ap2dcl.m	2-D array radiation pattern calculation. [F]
ap3d.m	3-D array radiation pattern window control. [S]
ap3dcl.m	3-D array radiation pattern calculation. [F]
apdirect.m	Array radiation pattern directivity calculation. [F]
arylyout.m	Array elements configuration layout. [S]
directiv.m	Pattern directivity window control. [S]
edelspec.m	Array element specification file editing window. [S]
ep2d.m	2-D element radiation pattern window control. [S]
ep2dcl.m	2-D element radiation pattern calculation. [F]
ep3d.m	3-D element radiation pattern window control. [S]
ep3dcl.m	3-D element radiation pattern calculation. [F]
epdirect.m	Element radiation pattern directivity calculation. [F]
exitpgm.m	Exit program and close all windows. [S]
ldfiles.m	Load data files control window. [S]
loaddata.m	Read data files from disk. [F]
loadws.m	Load previously saved workspace. [S]
maxfnct2.m	Find maximums of 2-D pattern. [S]
maxfnct3.m	Find maximums of 3-D pattern. [S]
newws.m	Clear all current workspace data. [S]
normelem.m	Normalize the element pattern file. [F]
opfreq.m	Set array operating frequency. [S]
pattern.m	Main program window control. [S]
polar2d.m	Display 2-D polar coordinate plots. [F]
polar3d.m	Display 3-D spherical coordinate plots. [F]
rect2d.m	Display 2-D rectangular coordinate plots. [F]
rect3d.m	Display 3-D rectangular coordinate plots. [F]
safptrn.m	Save array factor pattern cuts to file. [F]
saryptrn.m	Save array radiation pattern cuts to file. [F]
savecuts.m	Save pattern cuts window control. [S]
savews.m	Save current workspace to current file. [S]
savewsas.m	Save current workspace to specific file. [S]
selptrn.m	Save element radiation pattern cuts to file. [F]

Table A.1

Program Files List

APPENDIX B

DETAILED CRITICAL COUPLING ANALYSIS RESULTS

Tables B.1 and B.2 contain the results of the Micro-Stripes simulations conducted for the critical coupling analysis of chapter 4. The model naming convention used for the first column is as follows:

For model SL$$ST##:

- $$ represents the slot length expressed in percentage of λ_d, and
- ## represents the open-circuited stub length in percentage of λ_g.

Examples:

- SL15ST20 means the slot is 15% of λ_d and the stub is 20% of λ_g, and
- SL29ST125 means the slot is 29% of λ_d and the stub is 12.5% of λ_g.

Parameters in the last four columns of the table were only evaluated for models that were determined to be critically coupled, except for some values in the bandwidth column.

Model	Resonant Frequency (GHz)	$\|S_{11}\|$ at Resonant Frequency (dB)	Over, Critical or Under Coupling (O/C/U)	VSWR<2 Bandwidth (%)	Antenna Directive Gain (dBi)	Relative Cross-Polarization Gain (dB)	Front/ Back Ratio (dB)
SL25ST00	1.755	-0.64	U				
SL30ST00	1.548	-0.66	U				
SL40ST00	1.184	-0.55	U				
SL20ST05	1.912	-10.55	U				
SL25ST05	1.724	-14.15	U				
SL30ST05	1.514	-13.7	U				
SL35ST05	1.303	-10.87	U				
SL25ST06	**1.718**	**-27.5**	**C**	**2.078**	**5.225**	**-17.06**	**6.050**

SL30ST06	1.508	-19.3	U	2.275			
SL20ST07	**1.905**	**-24.25**	**C**	**2.017**	**5.833**	**-15.97**	**7.998**
SL25ST07	1.711	-19.8	O	2.264			
SL29ST07	1.547	-20.2	O				
SL30ST07	1.498	-22.2	O				
SL15ST10	**2.062**	**-25.3**	**C**	**1.961**	**6.232**	**-14.49**	**9.518**
SL20ST10	1.898	-10.7	O				
SL25ST10	1.697	-8.15	O				
SL13ST15	**2.12**	**-30.7**	**C**	**2.017**	**6.329**	**-13.35**	**9.832**
SL15ST15	2.073	-13.6	O				
SL20ST15	1.915	-5.8	O				
SL10ST20	2.182	-8.55	U	0			
SL13ST20	**2.134**	**-28.5**	**C**	**2.055**	**6.319**	**-12.55**	**9.769**
SL15ST20	2.091	-12.9	O	1.981			
SL20ST20	1.956	-5.25	O				
SL10ST25	2.185	-6.68	U				
SL13ST25	2.141	-19.6	U				
SL14ST25	**2.121**	**-25.3**	**C**	**2.049**	**6.299**	**-12.22**	**9.724**
SL15ST25	2.103	-18.97	O				
SL20ST25	1.986	-6.35	O				
SL10ST30	2.186	-4.33	U				
SL13ST30	2.142	-10.8	U				
SL15ST30	2.106	-20.5	U				
SL16ST30	**2.087**	**-31.15**	**C**	**2.037**	**6.28**	**-12.14**	**9.671**
SL20ST30	1.995	-9.2	O				
SL13ST35	2.14	-5.08	U				
SL15ST35	2.103	-8.7	U				
SL187ST35	**2.024**	**-31.15**	**C**	**1.942**	**6.23**	**-12.15**	**9.669**
SL20ST35	1.993	-18.6	O				
SL15ST40	2.094	-2.68	U				
SL20ST40	1.98	-11.3	U				
SL228ST40	**1.904**	**-22.6**	**C**	**1.976**	**6.143**	**-12.5**	**9.607**
SL25ST40	1.838	-12.55	O				
SL25ST45	1.817	-13.9	U				
SL268ST45	**1.759**	**-23.7**	**C**	**1.978**	**6**	**-13.07**	**9.225**
SL30ST45	1.66	-9.15	O				
SL30ST50	**1.632**	**-36.5**	**C**	**1.938**	**5.824**	**-13.5**	**8.606**

Table B.1

2GHz Simulation Results

Model	Resonant Frequency (GHz)	$\|S_{11}\|$ at Resonant Frequency (dB)	Over, Critical or Under Coupling (O/C/U)	VSWR<2 Bandwidth (%)	Antenna Directive Gain (dBi)	Relative Cross-Polarization Gain (dB)	Front/ Back Ratio (dB)
SL35ST05	24.368	-11.1	U	3.276			
SL40ST05	22.747	-16.5	U	5.328			
SL45ST05	21.275	-20	U	5.546			
SL50ST05	20.084	-17.8	U	5.163			
SL40ST06	**22.475**	**-42.75**	**C**	**6.766**	**5.872**	**-11.81**	**5.633**
SL33ST075	24.732	-36	U	8.298			
SL335ST75	**24.572**	**-44**	**C**	**8.366**	**6.335**	**-11.73**	**6.778**
SL35ST075	24.069	-24	O	8.325			
SL295ST10	**26.073**	**-38**	**C**	**10.55**	**6.567**	**-11.68**	**7.508**
SL30ST10	25.953	-35	O	10.96	6.548	-11.66	
SL35ST10	24.326	-11.1	O	7.747			
SL28ST125	26.911	-22.6	U	10.13			
SL29ST125	**26.783**	**-52.5**	**C**	**11.57**	**6.594**	**-11.65**	**7.820**
SL28ST15	27.278	-19	U	9.301			
SL30ST15	**27.167**	**-46**	**C**	**11.5**	**6.596**	**-11.66**	**8.045**
SL33ST15	27.263	-17.45	O	13.05			
SL30ST20	27.394	-16	U				
SL33ST20	27.373	-27.3	U				
SL34ST20	**27.322**	**-50.8**	**C**	**10.45**	**6.588**	**-11.74**	**8.342**
SL35ST20	27.316	-29.6	O	10.79			
SL35ST25	27.126	-19.2	U	8.293			
SL385ST25	**26.995**	**-52.2**	**C**	**9.74**	**6.586**	**-11.78**	**8.540**
SL40ST25	26.945	-26	O	10.09			
SL40ST30	26.613	-23.2	U	8.394			
SL42ST30	**26.533**	**-38.5**	**C**	**9.045**	**6.581**	**-11.79**	**8.658**
SL45ST35	25.907	-27.8	U	8.153			
SL465ST35	**25.699**	**-38.2**	**C**	**8.533**	**6.517**	**-11.69**	**8.711**
SL47ST35	25.664	-32.1	O	8.609			
SL50ST40	**25.1**	**-34.2**	**C**	**7.744**	**6.39**	**-11.55**	**8.637**

Table B.2

30GHz Simulation Results

APPENDIX C

2GHz PERPENDICULAR COUPLER DESIGN DETAILS

C.1 DESIGN DATA

Parameter	Dimension
Substrate:	
- dielectric constant	2.2
- thickness	1.58mm
- size	120mm x 60mm
Feed Line:	
- characteristic impedance (with ground plane)	50Ω
- width	4.868mm
- open circuited stub length (from center of slot)	30mm
- distance from perpendicular substrate	1mm
Ground Plane:	
- width of area removed	12mm
- removal angle from edge of substrate	21.8°

Table C.1

Feed Substrate

Parameter	Dimension
Substrate:	
- dielectric constant	2.2
- thickness	1.58mm
- size	120mm x 90mm
Coupled Line:	
- characteristic impedance	50Ω
- width	4.868mm
- open circuited stub length (from center of slot)	27.375mm
Ground Plane:	
- slot length	55mm
- slot width	1.1mm

Table C.2

Aperture Substrate

C.2 DETAILED GEOMETRY

The detailed geometry of both substrates follows, with the data points marked by small circles and their locations are given by the corresponding *(x,y)* pairs. Dimensions are given in millimeters.

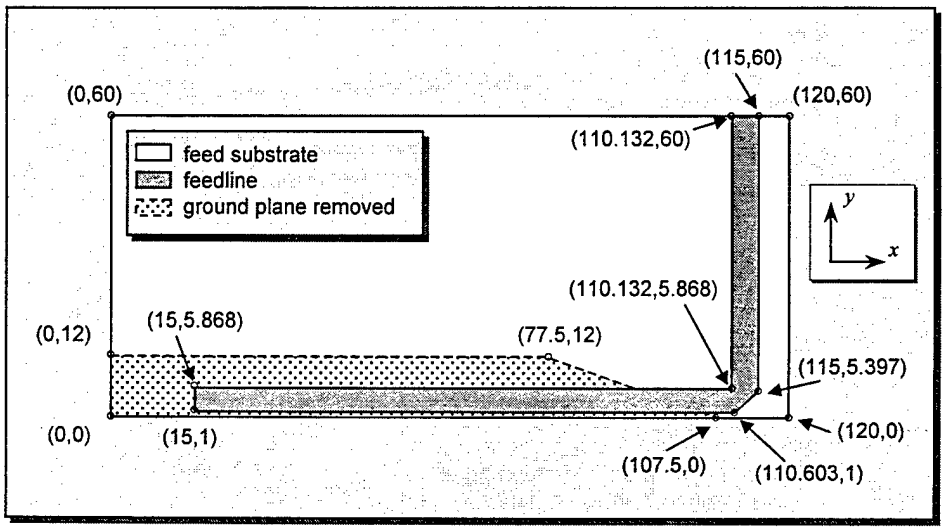

Figure C.1

Feed Substrate

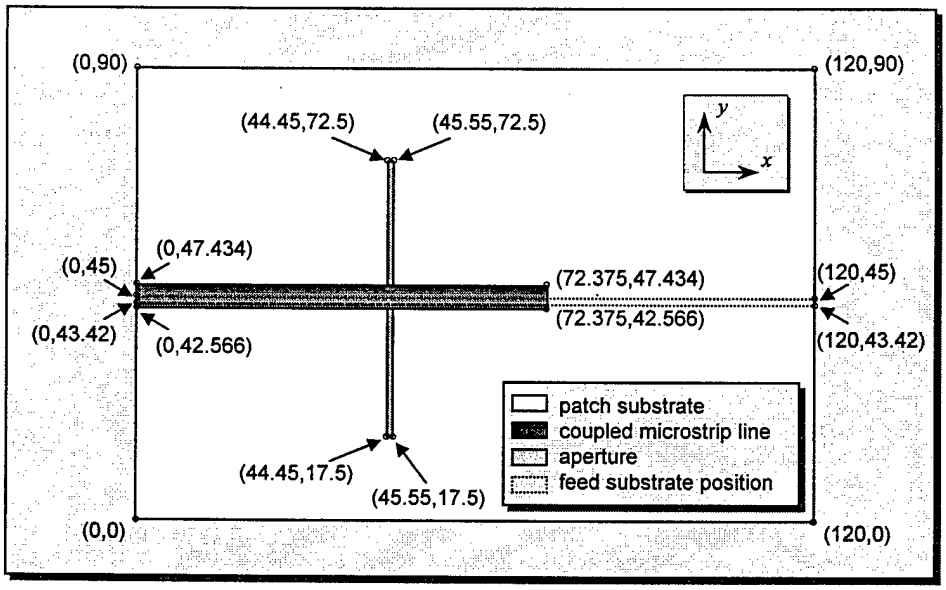

Figure C.2

Aperture Substrate

C.3 MICRO-STRIPES GEOMETRY FILE LISTING

```
data_id  Part 5 v13_12 - 21.8deg, **conn.**, slot 55mm long, FULL MODEL

work_space
  brick
    corner; coords        -10m        -50m        -45m
    corner; coords         60m         50m         80m

#PERPENDICULAR DIELECTRIC SUBSTRATE
medium
  epsr  2.2
  colour  60 230  60
  brick
    corner; coords     -1.596m        -45m        -45m
    corner; coords       -16u         45m         75m

#perpendicular dielectric groundplane
metal
  colour 139  34  34
  #shape
  intersectnot
    #metal sheet
    brick
      corner; coords       -16u        -45m        -45m
      corner; coords         0         45m         75m
    #less aperture
    brick
      corner; coords       -16u      -27.5m       -550u
      corner; coords         0       27.5m        550u

#perpendicular microstrip line
metal
  brick
    corner; coords     -1.612m     -2.434m        -45m
    corner; coords     -1.596m      2.434m     27.375m

#FEED DIELECTRIC SUBSTRATE
medium
  epsr  2.2
  colour  34 139  34
  brick
    corner; coords         0      -1.58m        -45m
    corner; coords       60m           0         75m

#feed dielectric groundplane
metal
  colour 139  34  34
  intersection
    prism
      axis;   comps          0           1           0
      point;  coords       12m           0        -45m
      point;  coords       12m           0       32.5m
      point;  coords         0           0       62.5m
      point;  coords         0           0         75m
      point;  coords       60m           0         75m
      point;  coords       60m           0        -45m
    slice
      point;  coords         0     -1.596m           0
      point;  coords         0      -1.58m           0

#feed microstrip line
metal
  intersection
    prism
      axis;   comps          0           1           0
      point;  coords        1m           0        -30m
      point;  coords        1m           0     65.603m
      point;  coords     5.397m           0        70m
      point;  coords       60m           0        70m
      point;  coords       60m           0     65.132m
      point;  coords     5.868m           0     65.132m
      point;  coords     5.868m           0        -30m
```

```
    slice
      point;  coords          0          0          0
      point;  coords          0        16u          0

output
  time_domain
    # port 1
    point
      coords        53m      -790u      67.8m
      field Ey Hz
    point
      coords        29m      -790u      67.8m
      field Ey Hz
    # port 2
    point
      coords      -796u          0       -37m
      field Ex Hy
    point
      coords      -796u          0       -13m
      field Ex Hy
  space_domain
    frequency 2G
    brick
      corner; coords      -7.5m     -47.5m    -43.75m
      corner; coords     58.75m      47.5m      77.5m
      field Er Ei Hr Hi Kr Ki partial_equivalent_surface

#port 1
initial_mode
  brick
    corner; coords      59.9m       -50m       -45m
    corner; coords        60m        50m        80m

  initial
    brick
      corner; coords      59.9m          0    65.132m
      corner; coords        60m     -1.58m        70m
    E          0          1          0
  frequency 0

mesh
rectangular
    cell_size 2.5m
    work_space
      brick
        corner; coords       -10m       -50m       -45m
        corner; coords        60m        50m        80m
    boundaries
      xmin  absorbing
      xmax  absorbing
      ymin  absorbing
      ymax  absorbing
      zmin  absorbing
      zmax  absorbing
      space_truncation  unchecked
    duration_times_c 5
    x
      cell_face -10m
      cells     2
      cell_face -5m
      cells     4
      cell_face -1.596m
      cells     4
      cell_face 0
      cells     1
      cell_face 300u
      cells     2
      cell_face 1m
      cells     5
      cell_face 5.397m
      cells     1
      cell_face 5.868m
      cells     4
      cell_face 9m
      cells     3
      cell_face 12m
      cells     2
```

```
  cell_face 15m
  cells     17
  cell_face 57.5m
  cells     2
  cell_face 60m
y
  cell_face -50m
  cells     2
  cell_face -45m
  cells     5
  cell_face -32.5m
  cells     4
  cell_face -27.5m
  cells     4
  cell_face -22.5m
  cells     10
  cell_face -5m
  cells     3
  cell_face -2.434m
  cells     2
  cell_face -1.58m
  cells     4
  cell_face 0
  cells     3
  cell_face 2.434m
  cells     3
  cell_face 5m
  cells     10
  cell_face 22.5m
  cells     4
  cell_face 27.5m
  cells     4
  cell_face 32.5m
  cells     5
  cell_face 45m
  cells     2
  cell_face 50m
z
  cell_face -45m
  cells     2
  cell_face -42.5m
  cells     4
  cell_face -32.5m
  cells     2
  cell_face -30m
  cells     2
  cell_face -27.5m
  cells     10
  cell_face -2.5m
  cells     3
  cell_face -550u
  cells     4
  cell_face 550u
  cells     3
  cell_face 2.5m
  cells     9
  cell_face 25m
  cells     2
  cell_face 27.375m
  cells     2
  cell_face 30m
  cells     1
  cell_face 32.5m
  cells     20
  cell_face 61.5m
  cells     1
  cell_face 62.5m
  cells     3
  cell_face 65.132m
  cells     1
  cell_face 65.603m
  cells     5
  cell_face 70m
  cells     4
  cell_face 75m
  cells     2
  cell_face 80m
```

```
lumped_cells
  brick
    corner; coords      17.5m          0      -42.5m
    corner; coords      57.5m          5m      -2.5m
  cells_per_lump 2 6 2
lumped_cells
  brick
    corner; coords      17.5m          0       -2.5m
    corner; coords      57.5m          5m       2.5m
  cells_per_lump 2 6 5
lumped_cells
  brick
    corner; coords      17.5m          0        2.5m
    corner; coords      57.5m          5m      61.5m
  cells_per_lump 2 6 2
lumped_cells
  brick
    corner; coords      17.5m          5m      -42.5m
    corner; coords      57.5m       42.5m       -2.5m
  cells_per_lump 2 2 2
lumped_cells
  brick
    corner; coords      17.5m          5m       -2.5m
    corner; coords      57.5m       42.5m        2.5m
  cells_per_lump 2 2 5
lumped_cells
  brick
    corner; coords      17.5m          5m        2.5m
    corner; coords      57.5m       42.5m       61.5m
  cells_per_lump 2 2 2
lumped_cells
  brick
    corner; coords      17.5m      -6.75m      -42.5m
    corner; coords      57.5m      -1.58m       -2.5m
  cells_per_lump 2 3 2
lumped_cells
  brick
    corner; coords      17.5m      -6.75m       -2.5m
    corner; coords      57.5m      -1.58m        2.5m
  cells_per_lump 2 3 5
lumped_cells
  brick
    corner; coords      17.5m      -6.75m        2.5m
    corner; coords      57.5m      -1.58m       61.5m
  cells_per_lump 2 3 2
lumped_cells
  brick
    corner; coords      17.5m        -45m      -42.5m
    corner; coords      57.5m      -6.75m       -2.5m
  cells_per_lump 2 2 2
lumped_cells
  brick
    corner; coords      17.5m        -45m       -2.5m
    corner; coords      57.5m      -6.75m        2.5m
  cells_per_lump 2 2 5
lumped_cells
  brick
    corner; coords      17.5m        -45m        2.5m
    corner; coords      57.5m      -6.75m       61.5m
  cells_per_lump 2 2 2
lumped_cells
  brick
    corner; coords      17.5m          5m       61.5m
    corner; coords      57.5m       42.5m         75m
  cells_per_lump 2 2 2
lumped_cells
  brick
    corner; coords      17.5m      -6.75m       61.5m
    corner; coords      57.5m      -1.58m         75m
  cells_per_lump 2 3 2
lumped_cells
  brick
    corner; coords      17.5m        -45m       61.5m
    corner; coords      57.5m      -6.75m         75m
  cells_per_lump 2 2 2
lumped_cells
  brick
```

```
    corner; coords          0          5m      -42.5m
    corner; coords        15m        42.5m       -7.5m
  cells_per_lump 3 2 2
lumped_cells
  brick
    corner; coords          0          5m        7.5m
    corner; coords        15m        42.5m         75m
  cells_per_lump 3 2 2
lumped_cells
  brick
    corner; coords          0         -45m      -42.5m
    corner; coords        15m       -6.75m       -7.5m
  cells_per_lump 3 2 2
lumped_cells
  brick
    corner; coords          0       -42.5m        7.5m
    corner; coords        15m       -6.75m         75m
  cells_per_lump 3 2 2
```

APPENDIX D

2GHz PERPENDICULAR PATCH DESIGN DETAILS

D.1 DESIGN DATA

Parameter	Value
Feed Substrate:	
- dimensions	10.0cm x 6.0cm
- dielectric constant (ε_r)	2.2
- thickness	1.58mm
- microstrip feedline	
- characteristic impedance	50Ω
- width	4.868mm
- extension of stub past center of slot	25mm
- feedline guide wavelength (λ_g):	
- with ground plane	109.58mm @ 2GHz
- where ground plane is removed	122mm @ 2GHz
- ground plane:	
- foil thickness	0.01778mm
- ground plane removal area:	
- length (starts at edge of slot)	50mm
- width	12mm
- angle from patch substrate	90°
Patch Substrate:	
- dimensions	10.0cm x 9.0cm
- dielectric constant (ε_r)	2.2
- thickness	1.58mm
- patch:	
- length (resonant dimension)	46.36mm
- width	30mm
- ground plane:	
- foil thickness	0.01778mm
- aperture:	
- length	15mm
- width	1.55mm
- dielectric wavelength (λ_d)	101.13mm @ 2GHz

Table D.1

Design Data

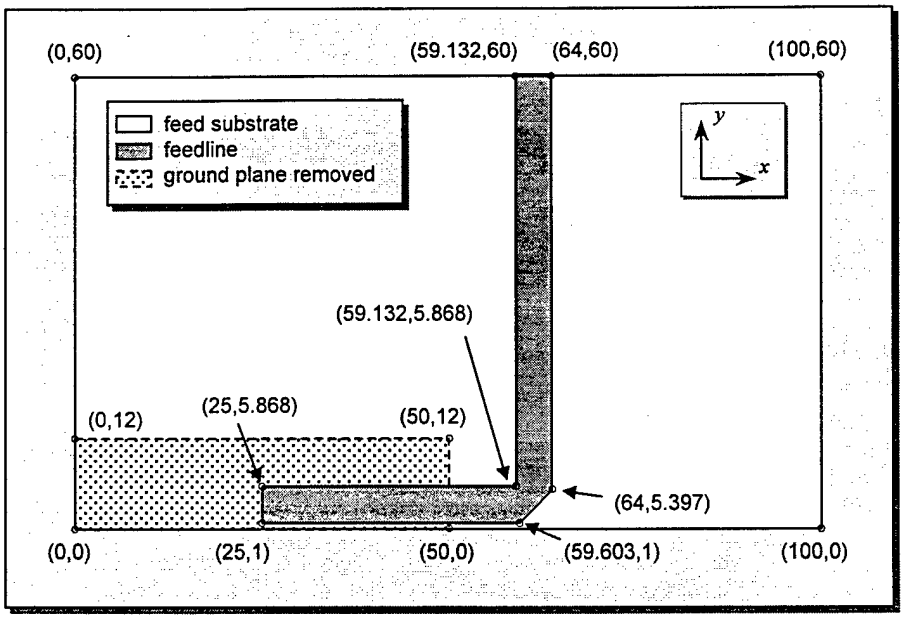

Figure D.1

Feed Substrate

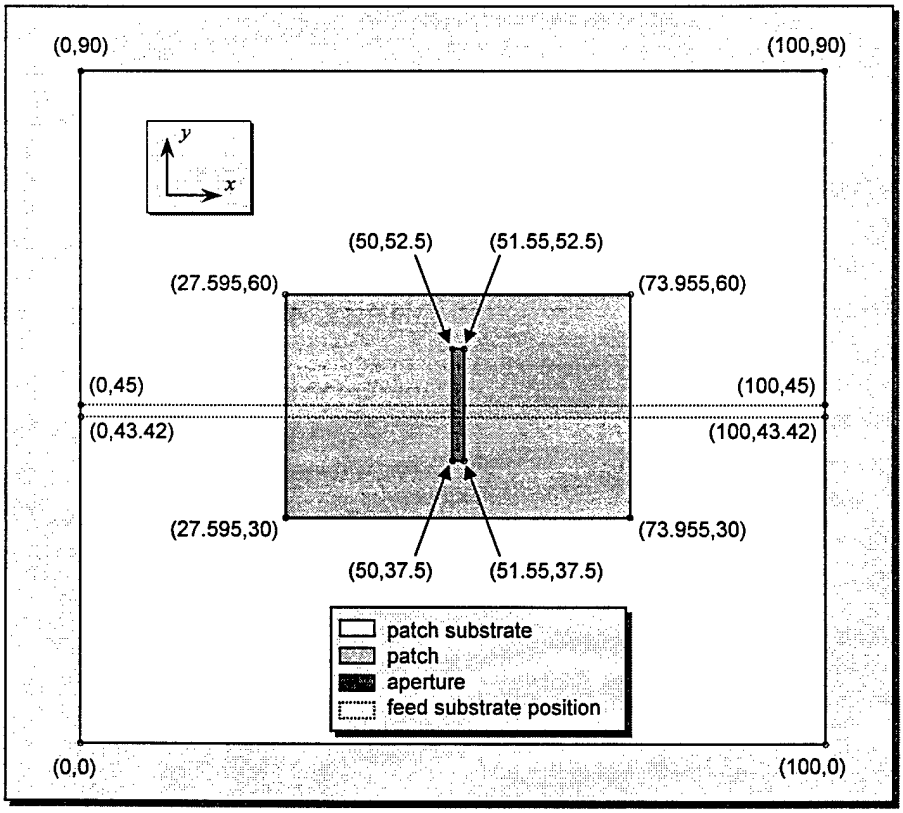

Figure D.2

Patch Substrate

D.2 DETAILED GEOMETRY

The detailed geometry of both substrates is shown at figures D.1 and D.2, with the data points marked by small circles and their locations given by the corresponding *(x,y)* pairs. Dimensions are given in millimeters.

D.3 MICRO-STRIPES GEOMETRY FILE LISTING

```
data_id  Part 9 v1c - DISCONT @slot, stub=25mm, slot=18mm, patch = 46.36x30mm

work_space
  brick
    corner; coords        -10m        -50m        -55m
    corner; coords         60m         50m         55m


#PATCH
metal
  brick
    corner; coords     -1.616m        -15m    -23.955m
    corner; coords     -1.598m         15m     22.405m

#PATCH DIELECTRIC SUBSTRATE
medium
  epsr  2.2
  colour  34 139  34
  brick
    corner; coords     -1.598m        -45m        -50m
    corner; coords        -18u         45m         50m

#PERPENDICULAR GROUND PLANE
metal
  colour 139  34  34
  #shape
  intersectnot
    #metal sheet
    brick
      corner; coords        -18u        -45m        -50m
      corner; coords          0         45m         50m
    #less aperture
    brick
      corner; coords        -18u         -9m      -1.55m
      corner; coords          0          9m          0

#FEED LINE
metal
  intersection
    prism
      axis;   comps           0           1           0
      point;  coords         1m           0        -25m
      point;  coords         1m           0      9.603m
      point;  coords      5.397m           0        14m
      point;  coords        60m           0        14m
      point;  coords        60m           0      9.132m
      point;  coords      5.868m           0      9.132m
      point;  coords      5.868m           0        -25m
    slice
      point;  coords          0           0           0
      point;  coords          0         18u           0
```

```
#FEED DIELECTRIC SUBSTRATE
medium
  epsr  2.2
  colour  34 139  34
  brick
    corner; coords          0      -1.58m        -50m
    corner; coords        60m           0         50m

#FEED GROUND PLANE
metal
  colour 139  34  34
  intersection
    prism
      axis;   comps           0           1           0
      point;  coords        12m           0        -50m
      point;  coords        12m           0          0
      point;  coords          0           0          0
      point;  coords          0           0        50m
      point;  coords        60m           0        50m
      point;  coords        60m           0        -50m
    slice
      point;  coords          0     -1.598m           0
      point;  coords          0      -1.58m           0

output
  time_domain
    # port 1
    point
      coords        52m       -800u      11.79m
      field Ey Hz
    point
      coords      39.9m       -800u      11.79m
      field Ey Hz
  space_domain
    frequency 1.8G 1.847G 1.9G
    brick
      corner; coords       -7.5m        -48m        -53m
      corner; coords         58m         48m         53m
      field Kr Ki partial_equivalent_surface

#port 1
initial_mode
  brick
    corner; coords       59.9m        -50m        -55m
    corner; coords         60m         50m         55m

  initial
    brick
      corner; coords       59.9m      -1.58m      9.132m
      corner; coords         60m           0         14m
    E          0           1           0
  frequency 0

mesh
  cubic
    cell_size 2m
    work_space
      brick
        corner; coords       -10m        -35m        -45m
        corner; coords        60m         35m         55m
    boundaries
      xmin  absorbing
      xmax  absorbing
      ymin  absorbing
      ymax  absorbing
      zmin  absorbing
      zmax  absorbing
    duration_times_c 5
    x
```

```
    cell_face 0
  y
    cell_face 0
  z
    cell_face 0
rectangular
  cell_size 3m
  work_space
    brick
      corner; coords       -10m       -50m       -55m
      corner; coords        60m        50m        55m
  boundaries
    xmin  absorbing
    xmax  absorbing
    ymin  absorbing
    ymax  absorbing
    zmin  absorbing
    zmax  absorbing
    space_truncation  unchecked
  duration_times_c 5
  x
    cell_face -10m
    cells     2
    cell_face -5m
    cells     3
    cell_face -1.598m
    cells     4
    cell_face 0
    cells     3
    cell_face 1m
    cells     5
    cell_face 5.397m
    cells     1
    cell_face 5.868m
    cells     5
    cell_face 12m
    cells     3
    cell_face 16m
    cells     8
    cell_face 40m
    cells     4
    cell_face 52m
    cells     2
    cell_face 58m
    cells     1
    cell_face 59.6m
    cells     1
    cell_face 60m
  y
    cell_face -50m
    cells     2
    cell_face -45m
    cells     10
    cell_face -17.5m
    cells     2
    cell_face -15m
    cells     2
    cell_face -12.5m
    cells     3
    cell_face -9m
    cells     2
    cell_face -7m
    cells     3
    cell_face -2.5m
    cells     1
    cell_face -1.58m
    cells     4
    cell_face 0
    cells     3
```

```
    cell_face 2.5m
    cells     3
    cell_face 7m
    cells     2
    cell_face 9m
    cells     3
    cell_face 12.5m
    cells     2
    cell_face 15m
    cells     2
    cell_face 17.5m
    cells     10
    cell_face 45m
    cells     2
    cell_face 50m
z
    cell_face -55m
    cells     2
    cell_face -50m
    cells     8
    cell_face -27.5m
    cells     2
    cell_face -25m
    cells     1
    cell_face -23.955m
    cells     2
    cell_face -21.455m
    cells     7
    cell_face -3m
    cells     2
    cell_face -1.55m
    cells     4
    cell_face 0
    cells     2
    cell_face 2m
    cells     2
    cell_face 6m
    cells     3
    cell_face 9.132m
    cells     1
    cell_face 9.603m
    cells     5
    cell_face 14m
    cells     3
    cell_face 17m
    cells     4
    cell_face 22.405m
    cells     2
    cell_face 24.905m
    cells     9
    cell_face 50m
    cells     2
    cell_face 55m
  lumped_cells
    brick
      corner; coords        16m       833u        -3m
      corner; coords        56m      17.5m         2m
    cells_per_lump 1 2 4
  lumped_cells
    brick
      corner; coords        16m      17.5m        -3m
      corner; coords        56m        45m         2m
    cells_per_lump 1 1 4
  lumped_cells
    brick
      corner; coords        16m       -45m        -3m
      corner; coords        56m     -17.5m         2m
    cells_per_lump 1 1 4
  lumped_cells
```

```
  brick
    corner; coords          16m      -17.5m         -3m
    corner; coords          56m       -2.5m          2m
  cells_per_lump 1 2 4
lumped_cells
  brick
    corner; coords           0          8m          6m
    corner; coords       5.868m        17.5m     24.905m
  cells_per_lump 3 2 2
lumped_cells
  brick
    corner; coords           0        17.5m          6m
    corner; coords       5.868m          45m     24.905m
  cells_per_lump 3 1 2
lumped_cells
  brick
    corner; coords       5.868m          8m          6m
    corner; coords          16m        17.5m     24.905m
  cells_per_lump 2 2 2
lumped_cells
  brick
    corner; coords       5.868m        17.5m          6m
    corner; coords          16m          45m     24.905m
  cells_per_lump 2 1 2
lumped_cells
  brick
    corner; coords          16m          8m          6m
    corner; coords          56m        17.5m     24.905m
  cells_per_lump 1 2 2
lumped_cells
  brick
    corner; coords          16m        17.5m          6m
    corner; coords          56m          45m     24.905m
  cells_per_lump 1 1 2
lumped_cells
  brick
    corner; coords           0         -45m          6m
    corner; coords       5.868m       -17.5m     24.905m
  cells_per_lump 3 1 2
lumped_cells
  brick
    corner; coords           0       -17.5m          6m
    corner; coords       5.868m        -2.5m     24.905m
  cells_per_lump 3 2 2
lumped_cells
  brick
    corner; coords       5.868m         -45m          6m
    corner; coords          16m       -17.5m     24.905m
  cells_per_lump 2 1 2
lumped_cells
  brick
    corner; coords       5.868m       -17.5m          6m
    corner; coords          16m        -2.5m     24.905m
  cells_per_lump 2 2 2
lumped_cells
  brick
    corner; coords          16m         -45m          6m
    corner; coords          56m       -17.5m     24.905m
  cells_per_lump 1 1 2
lumped_cells
  brick
    corner; coords          16m       -17.5m          6m
    corner; coords          56m        -2.5m     24.905m
  cells_per_lump 1 2 2
lumped_cells
  brick
    corner; coords          -5m       -17.5m     24.905m
    corner; coords           0         17.5m         50m
  cells_per_lump 1 2 1
```

```
lumped_cells
  brick
    corner; coords          -5m      -17.5m        -50m
    corner; coords           0        17.5m     -26.25m
  cells_per_lump 1 2 1
lumped_cells
  brick
    corner; coords          -5m        -45m          6m
    corner; coords           0         45m          17m
  cells_per_lump 1 1 2
lumped_cells
  brick
    corner; coords           0      -17.5m     24.905m
    corner; coords       5.868m       -2.5m         50m
  cells_per_lump 3 2 1
lumped_cells
  brick
    corner; coords           0        833u     24.905m
    corner; coords       5.868m       17.5m         50m
  cells_per_lump 3 2 1
lumped_cells
  brick
    corner; coords       5.868m      -17.5m     24.905m
    corner; coords          16m       -2.5m         50m
  cells_per_lump 2 2 1
lumped_cells
  brick
    corner; coords          16m      -17.5m     24.905m
    corner; coords          56m       -2.5m         50m
  cells_per_lump 1 2 1
lumped_cells
  brick
    corner; coords           0        -45m     24.905m
    corner; coords       5.868m      -17.5m         50m
  cells_per_lump 3 1 1
```

APPENDIX E

30GHz PERPENDICULAR PATCH DESIGN DETAILS

E.1 DESIGN DATA

Parameter	Value
Feed Substrate:	
- dimensions	5.0cm x 5.0cm (5.0cm x 2.0cm for simulation)
- dielectric constant (ε_r)	2.2
- thickness	0.254mm
- microstrip feedline	
- characteristic impedance	50Ω
- width	0.735mm
- extension of stub past center of slot	1.098mm
- feedline guide wavelength (λ_g):	
- with ground plane	7.319mm @ 30GHz
- where ground plane is removed	8mm @ 30GHz
- ground plane:	
- foil thickness	0.0254mm
- ground plane removal area:	
- length (starts at edge of slot)	25.2mm
- width	2.5mm
- angle from patch substrate	90°
Patch Substrate:	
- dimensions	5.0cm x 5.0cm
- dielectric constant (ε_r)	2.2
- thickness	0.787mm
- patch:	
- length (resonant dimension)	2.446mm
- width	3.5mm
- ground plane:	
- foil thickness	0.0254mm
- aperture:	
- length	2.0226mm
- width	0.4mm
- dielectric wavelength (λ_d)	6.742mm @ 30GHz

Table E.1

Design Data

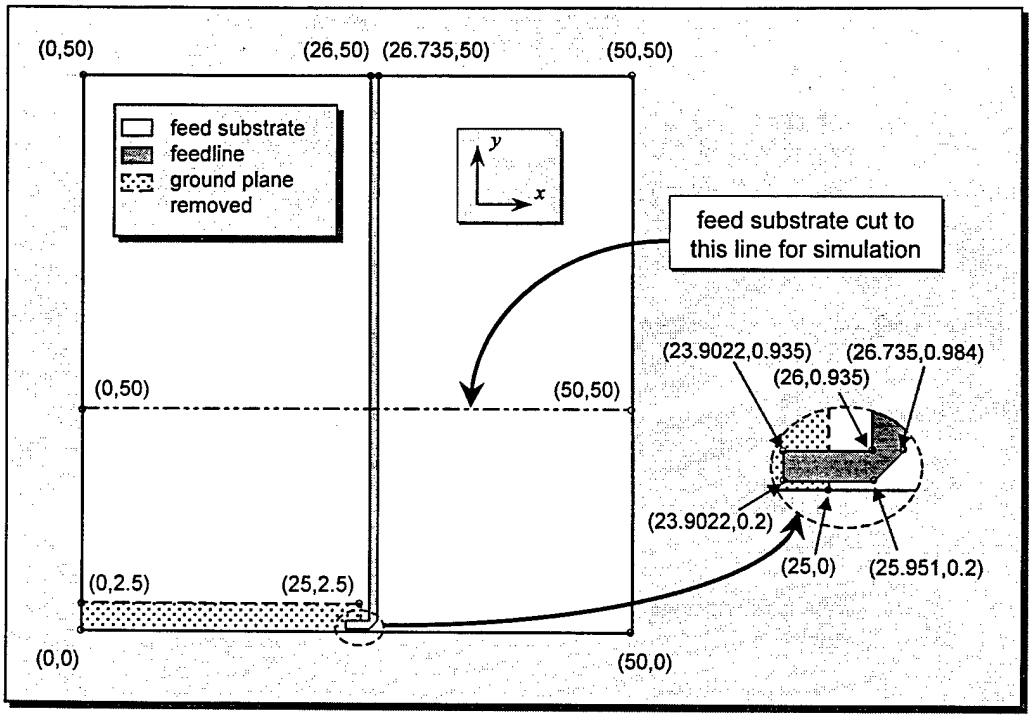

Figure E.1

Feed Substrate

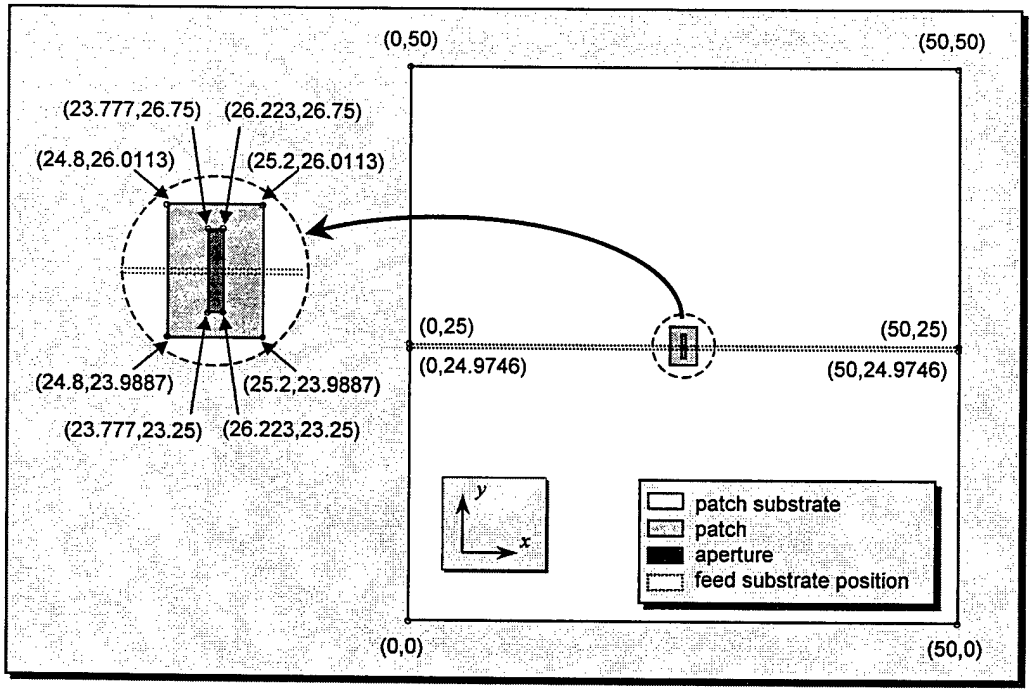

Figure E.2

Patch Substrate

E.2 DETAILED GEOMETRY

The detailed geometry of both substrates is shown at figures E.1 and E.2, with the data points marked by small circles and their locations given by the corresponding *(x,y)* pairs. Dimensions are given in millimeters.

E.3 MICRO-STRIPES GEOMETRY FILE LISTING

```
data_id  Part 10 v4 - 30GHz PERP,st=1.0978mm,sl=2.0226mm,patch=2.446x3.5mm

work_space
  brick
    corner; coords        -10m        -30m        -30m
    corner; coords         50m         30m         30m


#PATCH
metal
  brick
    corner; coords     -837.8u      -1.75m     -1.223m
    corner; coords     -812.4u       1.75m      1.223m

#PATCH DIELECTRIC SUBSTRATE
medium
  epsr  2.2
  colour  34 139  34
  brick
    corner; coords     -812.4u        -25m        -25m
    corner; coords      -25.4u         25m         25m

#PERPENDICULAR GROUND PLANE
metal
  colour 139  34  34
  #shape
  intersectnot
    #metal sheet
    brick
      corner; coords     -25.4u        -25m        -25m
      corner; coords          0         25m         25m
    #less aperture
    brick
      corner; coords     -25.4u    -1.0113m       -200u
      corner; coords          0     1.0113m        200u

#FEED LINE
metal
  intersection
    prism
      axis;   comps            0           1           0
      point;  coords        200u           0   -1.0978m
      point;  coords        200u           0       951u
      point;  coords        984u           0     1.735m
      point;  coords         50m           0     1.735m
      point;  coords         50m           0         1m
      point;  coords        935u           0         1m
      point;  coords        935u           0   -1.0978m
    slice
      point;  coords           0           0           0
      point;  coords           0      25.4u            0

#FEED DIELECTRIC SUBSTRATE
medium
  epsr  2.2
  colour  34 139  34
```

```
  brick
    corner; coords          0       -254u        -25m
    corner; coords        50m           0         25m

#FEED GROUND PLANE
metal
  colour 139  34  34
  intersection
    prism
      axis;   comps           0           1           0
      point;  coords        2.5m          0         -25m
      point;  coords        2.5m          0         200u
      point;  coords          0           0         200u
      point;  coords          0           0          25m
      point;  coords         50m          0          25m
      point;  coords         50m          0         -25m
    slice
      point;  coords          0     -279.4u           0
      point;  coords          0       -254u           0

output
  time_domain
    # port 1
    point
      coords        18m       -125u     1.3675m
      field Ey Hz
    point
      coords        16m       -125u     1.3675m
      field Ey Hz
  space_domain
    frequency 26.559G 27.234G 27.727G 27.998G 28.221G 28.442G 28.67G 28.852G
29.301G 30.065G 31.549G
    brick
      corner; coords       -2.5m        -26m        -26m
      corner; coords       18.6m         26m         26m
      field Kr Ki partial_equivalent_surface

initial_mode
  brick
    corner; coords       19.9m        -26.5m        -26.5m
    corner; coords         20m         26.5m         26.5m

  initial
    brick
      corner; coords       19.9m        -254u          1m
      corner; coords         20m           0      1.735m
    E          0           1           0
  frequency 0

mesh
  cubic
    cell_size 500u
    work_space
      brick
        corner; coords         -5m         -10m         -10m
        corner; coords         15m          10m          10m
    boundaries
      xmin  absorbing
      xmax  absorbing
      ymin  absorbing
      ymax  absorbing
      zmin  absorbing
      zmax  absorbing
    duration_times_c 500m
    x
      cell_face 0
    y
      cell_face 0
    z
      cell_face 0
  rectangular
    cell_size 600u
    work_space
      brick
        corner; coords         -3m       -26.5m       -26.5m
        corner; coords         20m        26.5m        26.5m
    boundaries
```

```
  xmin  absorbing
  xmax  absorbing
  ymin  absorbing
  ymax  absorbing
  zmin  absorbing
  zmax  absorbing
  space_truncation  unchecked
duration_times_c 500m
x
  cell_face -3m
  cells     4
  cell_face -1.5m
  cells     4
  cell_face -812.4u
  cells     5
  cell_face 0
  cells     2
  cell_face 200u
  cells     5
  cell_face 935u
  cells     1
  cell_face 984u
  cells     3
  cell_face 1.5m
  cells     4
  cell_face 2.5m
  cells     4
  cell_face 3.5m
  cells     28
  cell_face 19.9m
  cells     1
  cell_face 20m
y
  cell_face -26.5m
  cells     3
  cell_face -25m
  cells     39
  cell_face -2m
  cells     2
  cell_face -1.75m
  cells     5
  cell_face -1.0113m
  cells     4
  cell_face -254u
  cells     4
  cell_face 0
  cells     6
  cell_face 1.0113m
  cells     4
  cell_face 1.75m
  cells     2
  cell_face 2m
  cells     39
  cell_face 25m
  cells     3
  cell_face 26.5m
z
  cell_face -26.5m
  cells     3
  cell_face -25m
  cells     40
  cell_face -1.473m
  cells     2
  cell_face -1.223m
  cells     1
  cell_face -1.0978m
  cells     2
  cell_face -850u
  cells     2
  cell_face -400u
  cells     2
  cell_face -200u
  cells     4
  cell_face 200u
  cells     2
  cell_face 400u
  cells     3
```

```
  cell_face 951u
  cells     1
  cell_face 1m
  cells     2
  cell_face 1.223m
  cells     4
  cell_face 1.735m
  cells     3
  cell_face 2.3m
  cells     38
  cell_face 25m
  cells     3
  cell_face 26.5m
lumped_cells
  brick
    corner; coords          0          0       2.3m
    corner; coords        18m         2m        25m
  cells_per_lump 1 3 1
lumped_cells
  brick
    corner; coords          0          0       -25m
    corner; coords        18m         2m    -1.473m
  cells_per_lump 1 3 1
lumped_cells
  brick
    corner; coords          0         -2m       2.3m
    corner; coords        18m    -632.5u        25m
  cells_per_lump 1 3 1
lumped_cells
  brick
    corner; coords          0         -2m       -25m
    corner; coords        18m    -632.5u    -1.473m
  cells_per_lump 1 3 1
lumped_cells
  brick
    corner; coords          0          2m      -400u
    corner; coords        18m         25m       400u
  cells_per_lump 1 1 4
lumped_cells
  brick
    corner; coords          0          2m    -1.473m
    corner; coords        18m         25m      -625u
  cells_per_lump 1 1 3
lumped_cells
  brick
    corner; coords          0          2m       400u
    corner; coords        18m         25m       2.3m
  cells_per_lump 1 1 3
lumped_cells
  brick
    corner; coords          0        -25m      -400u
    corner; coords        18m         -2m       400u
  cells_per_lump 1 1 4
lumped_cells
  brick
    corner; coords          0        -25m    -1.473m
    corner; coords        18m         -2m      -625u
  cells_per_lump 1 1 3
lumped_cells
  brick
    corner; coords          0        -25m       400u
    corner; coords        18m         -2m       2.3m
  cells_per_lump 1 1 3
```

UNCLASSIFIED

SECURITY CLASSIFICATION OF FORM
(highest classification of Title, Abstract, Keywords)

DOCUMENT CONTROL DATA

(Security classification of title, body of abstract and indexing annotation must be entered when the overall document is classified)

1. ORIGINATOR (the name and address of the organization preparing the document. Organizations for whom the document was prepared, e.g. Establishment sponsoring a contractor's report, or tasking agency, are entered in section 8.)

Royal Military College of Canada,
Kingston, ON

2. SECURITY CLASSIFICATION (overall security classification of the document including special warning terms if applicable)

UNCLASSIFIED

3. TITLE (the complete document title as indicated on the title page. Its classification should be indicated by the appropriate abbreviation (S,C or U) in parentheses after the title.)

Investigation of a Modular Antenna Array Configuration and a Feeding Technique for Brick Architecture (U)

4. AUTHORS (Last name, first name, middle initial)

J. Paul J. Garant (DND), Gilbert A. Morin (DREO), Yahia M.M. Antar (RMC), David J. Roscoe (CRC)

5. DATE OF PUBLICATION (month and year of publication of document)

Sept. 1997

6a. NO. OF PAGES (total containing information. Include Annexes, Appendices, etc.)

140

6b. NO. OF REFS (total cited in document)

17

7. DESCRIPTIVE NOTES (the category of the document, e.g. technical report, technical note or memorandum. If appropriate, enter the type of report, e.g. interim, progress, summary, annual or final. Give the inclusive dates when a specific reporting period is covered.

DREO Report

8. SPONSORING ACTIVITY (the name of the department project office or laboratory sponsoring the research and development. Include the address.

Defence Research Establishment Ottawa,
3701 Carling Ave., Ottawa, Ont., K1A 0Z4, CANADA

9a. PROJECT OR GRANT NO. (if appropriate, the applicable research and development project or grant number under which the document was written. Please specify whether project or grant)

Thrust 5ca12

9b. CONTRACT NO. (if appropriate, the applicable number under which the document was written)

10a. ORIGINATOR'S DOCUMENT NUMBER (the official document number by which the document is identified by the originating activity. This number must be unique to this document.)

DREO REPORT 1315

10b. OTHER DOCUMENT NOS. (Any other numbers which may be assigned this document either by the originator or by the sponsor)

11. DOCUMENT AVAILABILITY (any limitations on further dissemination of the document, other than those imposed by security classification)

(X) Unlimited distribution
( ) Distribution limited to defence departments and defence contractors; further distribution only as approved
( ) Distribution limited to defence departments and Canadian defence contractors; further distribution only as approved
( ) Distribution limited to government departments and agencies; further distribution only as approved
( ) Distribution limited to defence departments; further distribution only as approved
( ) Other (please specify):

12. DOCUMENT ANNOUNCEMENT (any limitation to the bibliographic announcement of this document. This will normally correspond to the Document Availability (11). however, where further distribution (beyond the audience specified in 11) is possible, a wider announcement audience may be selected.)

Unlimited Announcement

UNCLASSIFIED

SECURITY CLASSIFICATION OF FORM

RA.W (21 Dec 92)

13. **ABSTRACT** (a brief and factual summary of the document. It may also appear elsewhere in the body of the document itself. It is highly desirable that the abstract of classified documents be unclassified. Each paragraph of the abstract shall begin with an indication of the security classification of the information in the paragraph (unless the document itself is unclassified) represented as (S), (C), or (U). It is not necessary to include here abstracts in both official languages unless the text is bilingual).

The satellite communications industry, following the trends seen in personal communications systems, is pursuing the development of smaller and more capable communication terminals. Several antenna technologies and architectures have been studied for a fixed-beam portable communications terminal operating at high frequencies, e.g. 20GHz (receive) and 30GHz (transmit), and capable of providing multiple data links (data, voice, video). However, additional work is required to develop a modular "brick" type of architecture for this application.

This report investigates two aspects of the problem: a modular antenna array configuration, and a suitable feeding scheme involving perpendicular interconnection that is essential to the design of the brick architecture.

An antenna array patterns program was developed within the Matlab environment. This versatile tool can be used to predict planar array radiation patterns for design and general illustration purposes. The program can evaluate, display and analyze two- and three-dimensional radiation patterns, and it can easily be modified to suit specific user requirements. An array configuration suitable for fixed-beam portable satellite applications at 30GHz was developed using this program.

To acquire experience with the design of microstrip patch antennas, and to validate the simulation software that would be used throughout this report, a critical coupling analysis was then conducted for conventional aperture-fed microstrip patch antennas. Simulation results were analyzed to determine the behavior of various parameters for critically coupled antennas, and charts providing a helpful guide for the design of microstrip patch antennas were produced.

The development of the perpendicular interconnection was then initiated with the simulation, fabrication and successful testing of a perpendicular substrate microstrip line-to-line coupler using the proximity feeding technique. A microstrip patch antenna fed from a perpendicular substrate was then designed to operate in the 2GHz range, with excellent results. Following this, a 30GHz perpendicularly fed microstrip patch antenna was developed, generating promising results.

14. **KEYWORDS, DESCRIPTORS or IDENTIFIERS** (technically meaningful terms or short phrases that characterize a document and could be helpful in cataloguing the document. They should be selected so that no security classification is required. Identifiers, such as equipment model designation, trade name, military project code name, geographic location may also be included. If possible keywords should be selected from a published thesaurus. e.g. Thesaurus of Engineering and Scientific Terms (TEST) and that thesaurus-identified. If it is not possible to select indexing terms which are Unclassified, the classification of each should be indicated as with the title.)

antenna, phased array, microstrip antenna, feeding mechanism,
phased array architecture